Vol. 73, Part III, 2003

ISSN 0369-8211

Proceedings of the National Academy of Sciences India

SECTION A — PHYSICAL SCIENCES

National Academy of Sciences, India, Allahabad
राष्ट्रीय विज्ञान अकादमी, भारत, इलाहाबाद

The National Academy of Sciences, India

(Registered under Act XXI of 1860)

Founded 1930

COUNCIL FOR 2003

President

1 Prof Jai Pal Mittal, Ph.D.(Notre Dame), F.N.A., F.A Sc . F N.A Sc . F T W A S., Mumbai

Two Past Presidents (including the Immediate Past President)

2. Prof. S.K. Joshi, D Phil., D.Sc (h.c), F N.A , F.A Sc., F.N.A Sc , F T W A S . New Delhi
3. Dr. V.P. Sharma, D.Phil.,D.Sc.,F.A.M.S.,F.E.S.I , F I.S C.D., F.N A , F.A Sc., F N A Sc., F.R.A.S., New Delhi.

Vice-Presidents

4 Dr. P.K. Seth, Ph.D., F N A., F.N.A.Sc., Lucknow.
5. Prof. M. Vijayan, Ph.D., F.N.A., F A.Sc., F.N.A.Sc., F.T.W.A.S., Bangalore

Treasurer

6. Prof. S.L. Srivastava, D.Phil.,F.I.E.T.E., F.N.A.Sc., Allahabad.

Foreign Secretary

7. Dr. S.E. Hasnain, Ph.D., F.N.A., F.A.Sc., F.N.A.Sc., F.T.W A.S., Hyderabad

General Secretaries

8. Prof. H.C. Khare, M.Sc., Ph.D.(McGill), F.N.A.Sc., Allahabad.
9. Prof. Pramod Tandon, Ph.D., F.N.A.Sc., Shillong.

Members

10. Dr. Premananda Das, Ph.D., F.N.A., F.N.A.A.S, F.N.A.Sc., Bhubaneswar
11. Prof. Asis Datta, Ph.D., D.Sc., F.N.A., F.A.Sc., F.N.A.Sc., F.T.W.A.S., New Delhi
12. Prof. Sushanta Dattagupta, Ph.D., F.N.A., F.A.Sc., F.N.A.Sc., F.T.W.A.S . Kolkata.
13. Dr. Amit Ghosh, Ph.D., F.A.Sc., F.N.A.Sc., Chandigarh.
14. Prof. Girjesh Govil, Ph.D., F.N.A., F.A.Sc., F.N.A.Sc., F.T W.A.S., Mumbai
15. Prof. G.K. Mehta, Ph.D., F.N.A.Sc., Allahabad.
16. Dr. G.C. Mishra, Ph.D., F N.A.Sc., Pune.
17. Dr. Ashok Misra, M.S.(Chem.Engg.), M.S.(Polymer Sc.), Ph.D., F.N.A Sc., Mumbai
18. Prof Kambadur Muralidhar, Ph.D., F.N.A., F A Sc , F.N.A.Sc , Delhi.
19. Prof. Jitendra Nath Pandey, M.D., F.A.M.S., F.N.A.Sc., New Delhi.
20. Dr. Patcha Ramachandra Rao, Ph.D., F.I.E., F.I.M.(London), F.N A.E., F A Sc . F N A., F.N.A Sc., Varanasi.
21. Dr Vijayalakshmi Ravindranath, Ph.D., F.A.Sc , F.N.A.Sc., F T.W.A S., Manesar (Haryana)
22 Prof Khadg Singh Valdiya, Ph D., F.N.A., F.A Sc., F.N.A.Sc., F T W.A.S., Bangalore
23 Vacant

Special Invitees

1 Prof. M.G.K. Menon, Ph.D (Bristol), D.Sc.(h.c.), F.N.A., F A.Sc., F N.A.Sc., F T W.A S . F R S , Mem.Pontifical Acad.Sc., New Delhi.
2. Dr.(Mrs.) Manju Sharma, Ph.D., F.N A.A S., F.A.M.I., F.I.S.A.B., F N.A.Sc , F.T.W.A S , New Delhi
3. Prof. P.N. Tandon, M.S , D.Sc(h c.), F R.C.S., F A.M S., F N A., F A.Sc., F.N.A Sc., F.T W A S. Delhi.

The *Proceedings of the National Academy of Sciences, India,* is published in two Sections: Section A (Physical Sciences) and Section B (Biological Sciences). Four parts of each section are published annually (since 1960).

The Editorial Board in its work of examining papers received for publication is assisted, in an honorary capacity by a large number of distinguished scientists. The Academy assumes no responsibility for the statements and opinions advanced by the authors. The papers must conform strictly to the rules for publication of papers in the *Proceedings*. A total of 25 reprints is supplied free of cost to the author or authors. The authors may ask for a reasonable number of additional reprints at cost price, provided they give prior intimation while returning the proof.

Communication regarding contributions for publication in the *Proceedings*, books for review, subscriptions etc. should be sent to the Managing Editor, The National Academy of Sciences, India, 5 Lajpatrai Road, Allahabad-211 002 (India).

Annual Subscription for both Sections : Rs. 500.00; for each Section Rs. 250.00; Single Copy : Rs. 100.00. Foreign Subscription : (a) for one Section : US $100, (b) for both Sections U.S.$ 200.

(Air-Mail charges included in foreign subscription)

Co-Sponsored by C.S.T., U.P. (Lucknow)

PROCEEDINGS

OF THE

NATIONAL ACADEMY OF SCIENCES, INDIA

2003

VOL LXXIII SECTION–A PART III

Amino acid selective "unlabeling" : A new tool for structural studies of proteins in solution by NMR

H. S. ATREYA*, K. V. R. CHARY and GIRJESH GOVIL

Department of Chemical Sciences, Tata Institute of Fundamental Research, Homi Bhabha Road, Colaba, Mumbai-400 005.

**Author for Correspondence :Email : hsatreya@tifr.res.in; Fax : 0091-22-2152110*

Received August 16, 2001; Accepted January 4, 2002

Abstract

The development of new multidimensional NMR techniques and methodologies, in recent years, has facilitated in obtaining high precision protein structures in solution. However, in the case of large size proteins (M_r > 20 kDa), poor resolution due of severe spectral overlap complicates their analysis. In order to address this problem, we have proposed a novel methodology called amino acid selective "unlabeling" . In this approach, one or more specific amino acid residues in a protein are selectively "unlabeled" while uniformly or fractionally ^{13}C or/and ^{15}N labeling the rest. The cross peaks belonging to the unlabeled amino acid residues are thus absent in various NMR spectra recorded with such a protein sample, leading to significant spectral simplification. Such a methodology has been demonstrated for residuespecific NMR assignments and stereospecific resonance assignments of diastereotopic methyl groups of Val and Leu residues in proteins. Recently, we have used this methodology to obtain pseudocontact shifts (PCS) and residual dipolar coupling (RDC) in a 15 kDa calcium binding protein from *Entamoeba hsitolytica* (*Eh*CaBP). Spectral simplification achieved by simultaneous unlabeling of five amino acid residues selectively, aided in the accurate measurement of several PCS and RDCs in the lanthanide substituted *Eh*CaBP. Outcome of such studies are presented in this paper.

(**Keywords** : isotope labeling/2D NMR/EF-hand proteins/*Eh*CaBP/lanthanide).

Introduction

The development of new experimental techniques and methodologies in the field of nuclear magnetic resonance (NMR) spectroscopy, in recent years, has facilitated in determining the 3D structures of proteins in solution to high precision[1-3]. The size of proteins that are currently being analyzed by NMR is increasing steadily and attempts are on to elucidate structures of proteins as large as 110 kDa[4]. However, application of this technique has been limited, in large molecular weight proteins, by the relaxation properties of various nuclei involved in any experiment and the resolution of spectra. In many cases, severe spectra overlaps hamper analyses even while using multidimensional experiments combined with $^{13}C/^{15}N/^{2}H$ isotopes enrichment of the protein under investigation. Thus, one of the present challenges in protein NMR today is to identify and provide solutions to reduce overlaps in NMR spectra of large proteins.

A novel methodology, which addresses this problem of spectral overlap, is the so called amino acid selective "unlabeling"[5,6]. This is based on selective unlabeling of amino acid residues in a uniformly or fractionally ^{13}C or/and ^{15}N labeled protein, which simplify the multi-dimensional heteronuclear NMR spectra. A particular amino acid in a protein is 'unlabeled' by feeding the host microorganism expressing the protein of interest, with ^{15}N labeled ammonium chloride or/and ^{13}C labeled glucose as the sole source of nitrogen and carbon, respectively, along with the desired amino acids(s) to be unlabeled, in unlabeled form. This renders the desired amino acid residue(s)in the protein unlabeled, as a result of which cross peak due to these residues are not observed in any of the double and triple resonance spectra. A comparison of such a spectrum with that of a control spectrum involving uniformly ^{15}N or/and ^{13}C labeled protein enables one to distinguish peaks, and thereby the corresponding chemical shift of nuclei belonging to the unlabeled amino acid residues(s).

The utility of this methodology has been demonstrated previously for residue specific assignments[5] and stereospecific assignments of diasterotopic methyl groups in Val and Leu residues in large proteins[6]. In the former case, amino acid selective unlabeling combined with an automated approach, TATAPRO[7], was shown to aid in sequence specific resonance assignments, which form the first step towards unraveling 3D structures of proteins by NMR[1]. On the other hand, the second application involved selective unlabeling of amino acid residues in a fractionally (10%) ^{13}C-labeled protein, to obtain unambiguous stereospecific assignments of diastereotopic methyl groups in Val and Leu residues[6]. Such stereospecific assignments provide crucial NMR constraints in computing and refining the 3D structure of proteins[8].

In this paper, we demonstrate yet another utility of this method, namely, the measurement of pseudo-contact shifts (PCS) and residual dipolar couplings (RDC) for proteins with paramagnetic centers. PCS refers to shifts in resonance frequencies (chemical shifts) of nuclei arising due to their hyperfine interaction with an unpaired electron residing on the paramagnetic center. In a metal centered approximation, PCS is given by[9] :

$$\delta^{pc}(\text{ppm}) = \frac{1}{12\pi r^3}\left[\Delta\chi_{ax}\left(3n_i^2 - 1\right) + \frac{3}{2}\Delta\chi_{rh}\left(l_i^2 - m_i^2\right)\right] \qquad (1)$$

where $\Delta\chi_{ax}$ and $\Delta\chi_{rh}$ are the axial and rhombic magnetic susceptibility anisotropy induced by the paramagnetic center and l_i, m_i and n_i refer to the direction cosines of the position vector of atom i (r_i) with respect to the orthogonal system formed by the principle axes of the magnetic susceptibility tensor χ^{para}. As evident from this equation, PCS contains structural information on both the distances and angles in the frame of the magnetic susceptibility tensor. Moreover, the distance dependence is of the $1/r^3$ type, which, when compared to relaxation rate enhancements ($1/r^6$) type, decays more slowly with distance and thus can provide information at a greater distance from the metal ion than those obtained *via* the conventional NOESY experiments.

In addition, the paramagnetic centers, which are characterized by high anisotropy in magnetic susceptibility, induce a partial orientation of the molecules in high magnetic field (B_0). This is owing to the fact that different orientations of the protein (with a paramagnetic center) with respect to B_0 give rise to different interaction energies, resulting in a residual alignment with respect to B_0. Thus, the dipolar coupling between two nuclear spins do not average out to zero, as it usually happens in liquids, giving rise to residual dipolar coupling (RDC). These RDCs contain information on the orientation of the vector connecting the two dipoles with respect to the molecular magnetic susceptibility tensor (χ^{mol}) as given by[9] :

$$\text{RDC(Hz)} = -\frac{1}{4\pi}\frac{B_0^2}{15kT}\frac{\gamma_H\gamma_N h}{4\pi^2 r_{HN}^3}\left[\Delta\chi_{ax}\left(3\cos^2\theta - 1\right) + \frac{3}{2}\Delta\chi_{rh}\left(\sin^2\theta\cos 2\varphi\right)\right] \qquad (2)$$

The strength of such individual RDCs gives an estimate of the degree of alignment, which can then be used as a form of structural constraint in restrained molecular dynamics calculations, for protein structure determination[9].

In the present study, involving a calcium binding protein from *Entamoeba histolytica* (*Eh*CaBP), lanthanum ions were chosen as paramagnetic probes. This is owing to the fact that lanthanide ions have similar ionic radii as calcium and thus can replace the latter in a protein. Further, they posses large anisotropic magnetic susceptibilities, a property very useful for obtaining long range structural information as discussed above. However, in the case of lanthanum loaded *Eh*CaBP, severe spectral overlaps and large resonance line widths prevent accurate measurement of both PCSs, and RDCs. This prompted us to adopt the method of selective amino acid "unlabeling", which resulted in significant spectral simplification and facilitated in accurate measurement of PCSs and RDCs. The following paragraphs describe the outcome of such an endeavor.

Materials and Methods

(i) Sample preparation :

Recombinant proteins are enriched isotopically with ^{13}C and ^{15}N by growing the microbial host in a M9 salt medium, supplemented with a ^{15}N labeled ammonium chloride as the sole source of nitrogen and ^{13}C labeled glucose as the sole source of carbon[10]. *Eh*CaBP was cloned and over-expressed in *E. coli* BL21 (DE3) strain containing pET-3c expression system. Uniformly ^{15}N labeled *Eh*CaBP and amino acid selectively unlabeled-^{15}N labeled *Eh*CaBP samples were obtained using the protocol described earlier[5,7]. In the present study, two samples were prepared : (i) uniformly ^{15}N labeled *Eh*CaBP (hereafter referred to as Sample 1) and (ii) Arg, Phe, Ile, Leu and Lys unlabeled-uniformly ^{15}N labeled *Eh*CaBP (hereafter referred to as Sample 2). The choice of the five amino acids was based on the fact that, these residues are abundant in the protein and at the same time away from the metal binding sites.

(ii) NMR experiments :

NMR experiments were carried out on a Varian Unity + 600 NMR spectrometer equipped with a pulsed-field-gradient unit and triple resonance probe with actively shielded Z-gradients, operating at ^{1}H frequency of 600.051 MHz. All measurements were performed with 0.6 ml samples of approximately 2 mM *Eh*CaBP in 30 mM $CaCl_2$ and 50 mM deuterated TRIS buffer (pH = 6.0) and at a temperature of 35 °C, in

a mixed solvent of 90% H_2O and 10% ^2H_2O. For the measurement of PCS, a 2D sensitivity enhanced [^{15}N-^{1}H]-HSQC[11] was recorded on lanthanide substituted *Eh*CaBP, while RDC measurements were obtained *via* ω_1(^{15}N-^{1}H) coupled 2D [^{15}N-^{1}H]-HSQC. Data transformation and processing were done on Silicon Graphics workstation (R10000 based Indio II Solid Impact Graphics) using the FELIX97 software (*MSI*, U.S.A.)

Dy^{3+} was chosen as the lanthanide ion in the present study. A stock solution containing 20 mM $DyCl_3$ (obtained from SIGMA) was prepared. Addition of the salt to *Eh*CaBP was carried out in the form of titration, wherein 5 µl of the stock solution (corresponding to 0.1:1 metal-protein ratio) was added at every step. PCS and RDCs were measured at 1:1, 2:1, 3:1 and 4:1 metal protein ratio.

Results and Discussion

*Eh*CaBP is a 14.7 kDa monomeric polypeptide (134 amino acid residues) possessing four calcium- binding loops characteristic of EF-hand family of calcium binding proteins. This is evident from its primary sequence shown in Scheme I, where highly homologous Ca^{2+} binding loop segments are highlighted :

MEALFKEI***DVNGDGAVSYEE***VKAFVSKKRAIKNEQ

LLQLIFKSI***DADGNGEIDQNE***FAKFYGSIQGQDLSDDKI

GLKVLYKLM***DVDGDGKLTKEE***VTSFFKKHGIE

KVAEQVMKA***DANGDGYITLEE***FLEFSL

Scheme I

The percentages of various amino acids residues present in *Eh*CaBP are Ala-7.5%, Arg-0.7%, Asn-3.7%, Asp-9.7%, Cys-0%, Gln-4.5%, Glu-9.7%, Gly-9.0%, His-0.7%, Ile-6.7%, Leu-9.7%, Lys-11.9%, Met-2.2%, Phe-6.7%%, Pro-0%, Ser-5.2%, Thr-2.2%, Trp- 0%, Tyr-3.0%, Val-6.7%. Fig. 1a shows the sensitivity-enhanced 2D [^{15}N-^{1}H]HSQC spectrum of uniformly ^{15}N labeled *Eh*CaBP in its Ca^{2+} bound form (Sample 1). Titration of [u-^{15}N] labeled $(Ca^{2+})_4$- *Eh*CaBP (holo) with Dy^{3+} resulted in several changes in the HSQC spectrum due to the binding of Dy^{3+} ions to *Eh*CaBP. Several pseudo-contact shifted peaks were seen in the HSQC spectrum, with some of the cross peaks showing severe line broadening. Such an observation is illustrated in Fig. 1b, which shows a sensitivity enhanced 2D [^{15}N-^{1}H]HSQC spectrum of uniformly ^{15}N labeled *Eh*CaBP at a metal (Dy^{3+}) : protein ratio of 1 : 1. As is

evident from this Fig., it is impossible to assign pseudo-contact shifted peaks, particularly those having ^{1}H chemical shifts between 7.00 ppm and 9.5 ppm, precluding accurate measurements of PCSs and RDCs in this protein.

In principle, it is possible to reduce such spectral overlap by recording 3D NMR experiments, involving one or more heteronuclei. However, it is important to note that in proteins containing paramagnetic centers, resonance lines are considerably broadened owing to strong nuclear-electron dipolar interactions[9]. Thus, due to the fast transverse relaxation of heteronuclei involved, 3D NMR experiments are considerably reduced in sensitivity as compared to 2D experiments. One is then forced to use 2D [$^{13}C/^{15}N$-^{1}H] HSQC spectrum only, to obtain measurements of PCSs and RDCs. In order to simplify this spectrum, we prepared a sample wherein the five amino acid residues, namely Arg, Ile, Leu, Lys and Phe, were selectively unlabeled (Sample 2). The choice of these amino acids was based on two facts. First, these residues are among the most abundant in the protein and do not cross-matabolize to other amino acids during their biosynthesis[10]. Secondly, as evident from Scheme I, these amino acid residues occur less frequently in the four Ca^{2+}-binding loops of *Eh*CaBP as compared to other residues implying that, most of these amino acid residues are away from the Ca^{2+} binding loops. Although, information on these amino acids are lost due to their selective unlabeling, we can measure PCSs and RDCs for the rest of the amino acid residues in the protein that lie in the vicinity of the metal binding sites.

Selective unlabeling of these five residues resulted in the absence of cross peaks belonging to a total of 47 residues. Fig. 1c and 1d show the 2D [^{15}N-^{1}H] HSQC spectrum recorded on Sample 2 in the Ca^{2+}-bound form and at a metal (Dy^{3+}) : protein ratio of 1:1, respectively. A dramatic improvement in the resolution, obtained as a result of selective unlabeling, is evident from these figures, as compared to that of Sample 1 (Fig. 1a and 1b). Cross peaks belonging to several residues in the vicinity of the metal binding sites are now amenable for accurate measurement of PCSs and RDCs as discussed in detail below.

Fig. 2 A-C show selected regions of an uncoupled and coupled 2D [^{15}N-^{1}H] HSQC spectrum recorded on Sample 1 and 2 at a Dy^{3+}-protein ratio of 1:1. Each of the Fig. 2 A-C is divided into five panels (A_i, B_i and C_i, where i = 1-5). Panels 1 and 2, show a selected region of spectrum extracted from an uncoupled 2D [^{15}N-^{1}H] HSQC spectrum of Sample 1, while panels 3 and 4 show the same region for sample 2. Panel 5, extracted from a 2D coupled [^{15}N-^{1}H] HSQC spectrum corresponds, in each case, to the region shown in panel 4 and is used in measuring RDCs for pseudo-contact shifted cross peaks. These regions serve as illustrative examples of

unambiguous measurements of PCSs and RDCs that are facilitated as a result of selective unlabeling. All the assignments shown in these figures are based on sequence specific resonance assignments of ^{1}H and ^{15}N spins in *Eh*CaBP that have been reported earlier[12].

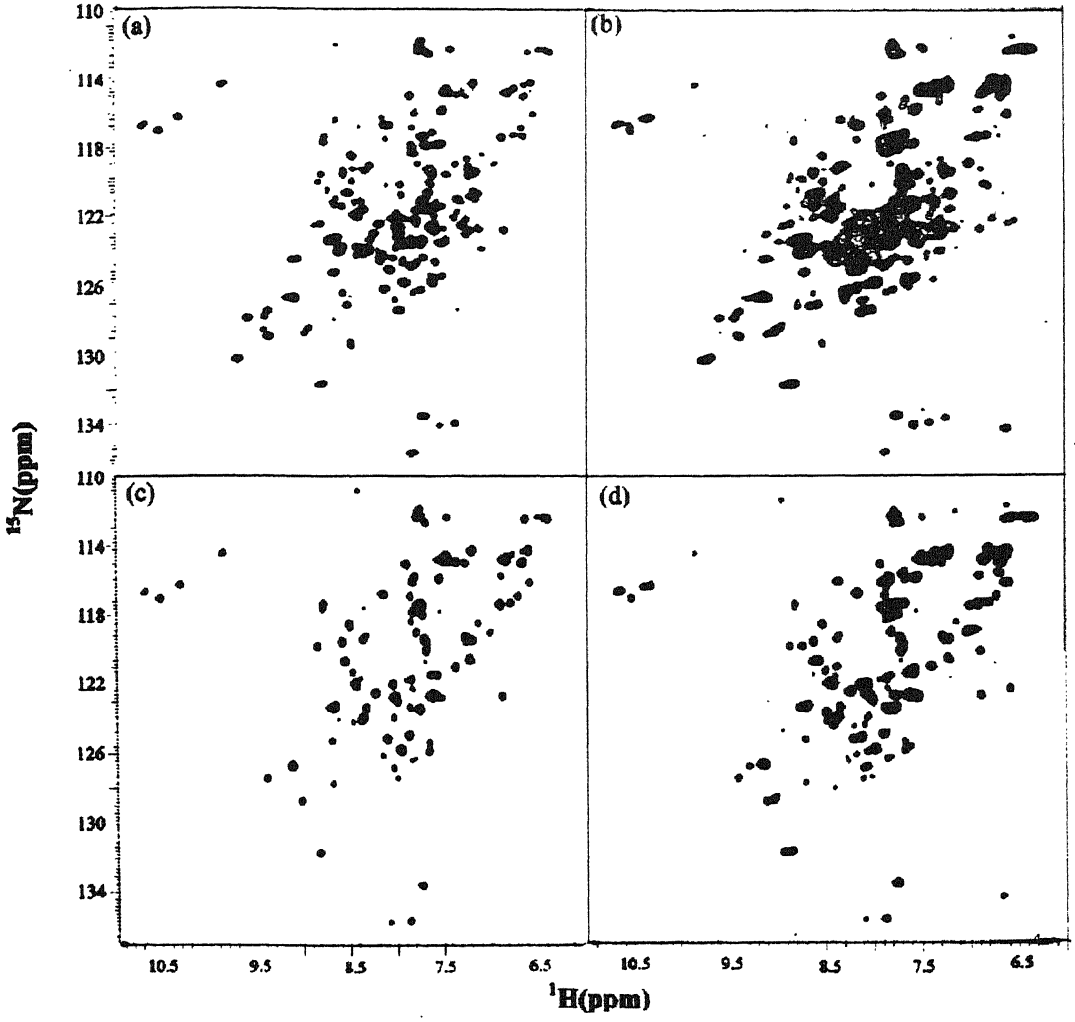


Fig. 1–2D sensitivity enhanced [^{15}N-^{1}H]HSQC spectrum of (a) uniformly ^{15}N-labeled $(Ca^{2+})_4$-*Eh*CaBP, (b) uniformly ^{15}N-labeled *Eh*CaBP at Dy^{3+} : protein ratio of 1 : 1, (c) Arg, Ile, Leu, Lys and Phe unlabeled-rest unlabeled ^{15}N labeled $(Ca^{2+})_4$- *Eh*CaBP and (d) Arg, Ile, Leu, Lys and Phe unlabeled-rest ^{15}N labeled *Eh*CaBP Dy^{3+} : protein ratio of 1:1.

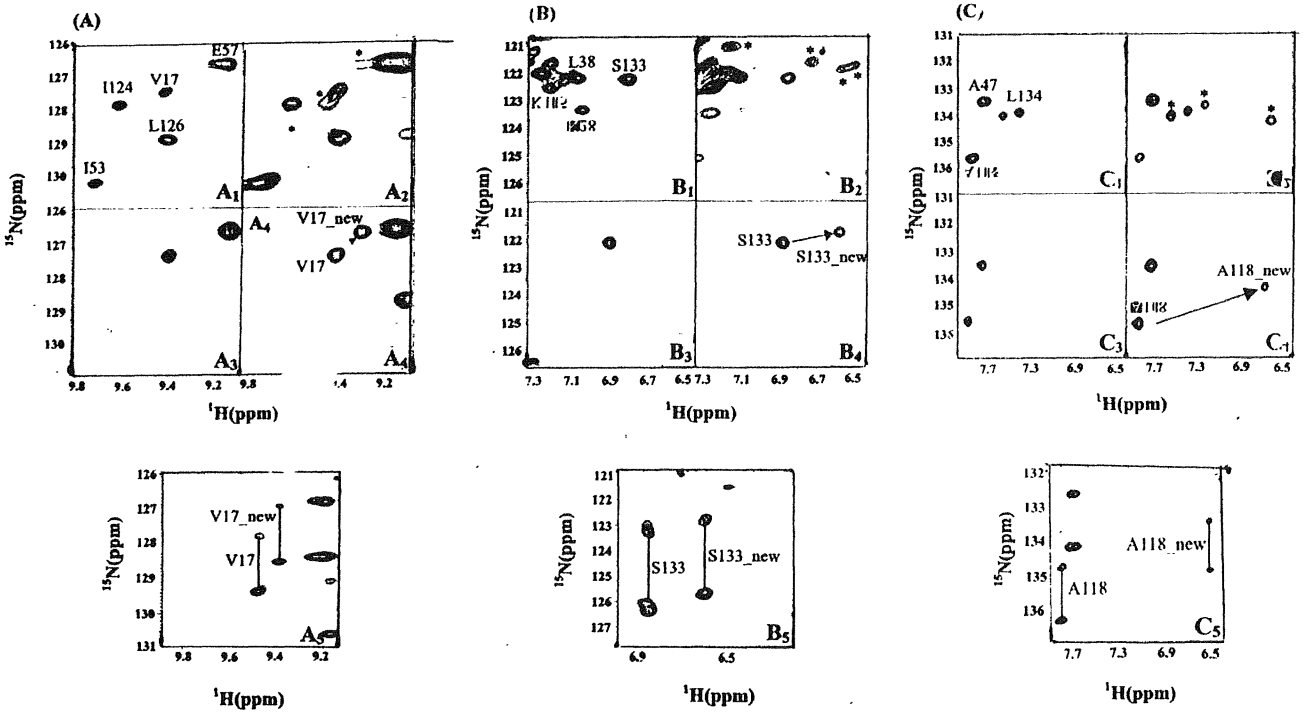


Fig. 2–Selected regions of 2D [^{15}N-^{1}H]HSQC spectrum of *Eh*CaBP. Fig. A-C is divided into five panels each (A_i, B_i and C_i, where i = 1-5). Panels 1 and 2 show a selected region of spectrum of Sample 1 at 0:1 and 1:1 Dy^{3+} : protein ratio, respectively, while panels 3 and 4 show the same region for sample 2. Panel 5, extracted from a ω_1-coupled HSQC spectrum corresponds, in each case, to the region shown in panel 4 and is used in measuring RDCs. Cross peaks shown with an asterix in A_2, B_2 and C_2 correspond to new PCS peaks arising due to addition of Dy^{3+}.

(i) Assignment of pseudo-contact shifted peak of V17 :

As shown in Fig. A_2 there are three new peaks (each marked by an asterix) compared to A_1, which arise due to PCS. It is impossible to assign these new peaks to any of the residues in *Eh*CaBP. For example, all these peaks serve as possible candidates for pseudo-contact shifted peaks of V17. This ambiguity is overcome by selective unlabeling of Ile and Leu as shown in A_3 and A_4. The spectral region is now simplified as selectively unlabeled amino acids don't show up their original and pseudo-contact shifted cross peaks. Thus, one is left with only cross peaks of V17, which can be unambiguously assigned to a lone pseudo-contact shifted cross peak seen in A_4. Further, such spectral simplification helps in measuring the corresponding RDC (if any)as shown in A_5.

(ii) Assignment of pseudo-contact shifted peak of S133 (Fig. 2B) :

As evident in Fig. 2B, simultaneous presence of cross peaks belonging to residues K28, K102, L38 and S133, result in ambiguity for the assignments of newly appeared pseudo-contact shifted peaks (each marked by an asterix in B_2). On selective unlabeling of Lys and Leu residues, cross peaks due to these residues are not seen in B_3 and B_4. Thus, the new pseudo-contact shifted peak in B_4 can be unambiguously assigned to S133. The corresponding RDC for this residue is measured as shown in B_5.

(iii) Assignment of pseudo-contact shifted peak of A118 :

In this case, two new peaks appear as a result of pseudo-contact shifted (each marked with an asterisk in C_2). However, from C_1 and C_2, it is not clear as to which of the new peaks correspond to the parent residue. However, removal of cross peaks belonging to L134 by selective unlabeling results in simplification of the spectra. From the earlier two cases shown in Fig. 2A and 2B, it is clear that new pseudo-contact peaks seem to appear with both ^1H and ^{15}N chemical shifts up field shifted as compared to the parent cross peak. Thus, the new pseudo-contact shifted cross peak in C_4 can be unambiguously assigned to A118 and the corresponding RDC is measured as shown in C_5.

Conclusion

Although NMR spectroscopy is relatively a young technique compared to X-ray crystallography for structure determination of biomolecules, during the last decade it

has emerged as a powerful technique for structural studies of large proteins and protein complexes in solution. With significant recent improvements in techniques for over expressing isotope labeled proteins, which have taken place contemporaneously with the sophistication in spectrometer hardware and developments in new methodologies for improving spectral resolution and sensitivity, it is now possible to determine structures of bio-macromolecules more rapidly than ever before. In this direction amino acid selective "unlabeling" provides a useful methodology for structural studies of large proteins in solution. Significant simplification of the spectra is achieved using this approach, resulting in unambiguous resonance assignments. Further, this technique uniquely provides information in all the stages of structure determination of proteins by NMR.

Acknowledgments

The facilities provided by the National Facility for High Field NMR, supported by Department of Science and Technology (DST), Department of Biotechnology (DBT), Council of Scientific and Industrial Research (CSIR), and Tata Institute of Fundamental Research, Mumbai, are gratefully acknowledged. We are grateful to Prof. Alok Bhattachaya (JNU, New Delhi) for providing the *Eh*CaBP clone. We dedicate this paper in the memory of late Prof. G. N. Ramachandran (1922-2001).

References

1. Wüthrich, K. (1986) *NMR of Proteins and Nucleic Acids*, Wiley Pulishers, New York.
2. Wagner, G. (1997) *Nat. Struc. Biol.* **4** : 841.
3. Bax, A. & Brzesiek, S. (1993) *Acc. Chem. Res.* **26** : 131.
4. Salzmann, M., Pervushin, K., Wider, G., Senn, H. & Wüthrich, K. (2000) *J. Am. Chem. Soc.* **122** : 7543.
5. Atreya, H. S. & Chary, K. V. R. (2000) *Current Science* **79** : 504.
6. Atreya, H. S. & Chary, K. V. R. (2001) *J. Biomol NMR* **19** : 267.
7. Atreya, H. S., Sahu, S. C., Chary, K. V. R. & Govil, G. (2000) *J. Biolmol NMR* **17(2)** : 125.
8. Neri, D., Szyperski, T., Otting G., Senn, H. & Wuthrich, K. (1989) *Biochemistry* **28** : 7510.
9. Bertini, I. & Luchinat, C. (1996) *Coord. Chem. Rev.* **150** : 1.
10. Muchmore, D. C., McIntosh, L. P., Russel, C. B., Anderson, D. E. & Dahlquist, F. W. (1989) *Methods in Enzymology* **177 (B)** : 44.
11. Kay, L. E., Keifer, P. & Saarinen, T. (1992) *J. Am. Chem. Soc.* **114** : 10663.
12. Sahu, S. C., Atreya, H. S., Chauhan, S., Bhattacharya, A., Chary, K. V. R. & Govil G. (1999) *J. Biomol. NMR* **14** : 93.

Topological modelling of binding affinity of 1-phenyl-3-amino-1,2,3, 4-tetrahydronaphthalenes as ligands for histamine H_1 receptors[#]

VIJAY K. AGRAWAL*, SHAILJA, SACHAN*, SANJEEV CHATURVEDI and PADMAKAR V. KHADIKAR**

**Department of Chemistry, A.P.S. University, Rewa-486003, India.*

e-mail : vijay-agrawal@lycos.com

***Research Division, Laxmi Fumigation and Pest Control Pvt. Ltd. 3, Khatipurra, Indore-452007, India*

Received Nov. 17, 2000; Revised June 28, 2001; Re-Revised January 1, 2002; Accepted August 27, 2002

Abstract

The binding affinity of various ligands that bind to the histamine H_1 receptor (PAT analogues) has been investigated using topological descriptors *viz.*, negentropy (*N*), molecular redundancy index (MRI), first-order molecular connectivity index ($^1\chi^v$), Wiener index (*W*), and Szeged index (Sz). The regression analysis gave a penta-parametric correlation involving N, MRI, Sz, IP_1 and IP_4 as the most significant QSAR model for modelling binding affinity of l-phenyl-3-amino-l,2,3,4-tetrahydronaphthalenes as ligands.

(Keywords : binding affinity / H_1 receptor / QSAR / Wiener index / Szeged index / regression analysis)

Introduction

Quantitative structure-activity relationship (QSAR) is a major factor in contemporary drug designing. Thus, it is quite clear why a large number of users of QSAR are located in industrial research units. The coupling of QSAR methodology to the experience and intuition of professional drug designer should result in a much more organized search for the novel drugs of human, animal, and plant therapy[1-4].

The molecular descriptors like geometric, electronic, information theoretic, topological, and their combinations have widely been employed in QSAR studies[5-10].

Paper presented at 70th Annual Session of the National Academy of Sciences, India and dedicated to Vijay on his 43rd birthday.

Booth *et. al.*[11] have shown that phenolamino tetralines (PATs) stimulate pyrosine hydroxylate activity and dopamine (DA) synthesis in rodent brain *in-vivo.* They have also shown[12] that this effect is medicated through interaction with a [N] binding site which was designated originally as the PAT-σ_3-receptor, because although it has low affinity for σ_1/σ_2 ligands, if incorporated a σ-like pharmacophore, it had a σ-like rodent brain distribution, and its functional effects on dopamine synthesis were blocked by the BMY -14802. These data suggested a dependence between chirality receptor interaction, and functional effect.

Recently, Bucholtz *et al*[13] have discussed that PATs also bind with high affinity to the [^{3}H]-mepyramine-labeled H_1 receptor in rat and guinea pig brain and also reported biological evaluation of additional PAT antagonists (Table 1, Fig. 1) to identify differences in binding at these sites *viz.* [^{3}H] -(-)- trans-H_2 -PAT sites versus [^{3}H] mepyramine-labeled H_1 σ-receptors. However, till date no quantitative structure-activity relationship (QSAR) was developed using topological indices.

In view of the above, the present paper deals with topological modelling of binding affinity of l-phenyl-3-amino-I,2,3,4-tetrahydronaphthalenes as ligands for histamine H_1-receptors (Table 1, Fig. 1).

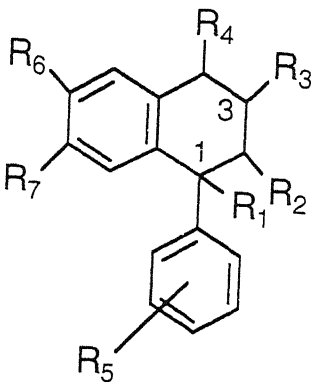


Fig. 1-1-phenyl-3-amino-l,2,3,4-tetrahydronaphthalenes used in the present study

The binding affinity expressed as $K_{0.5}$ (nm) are taken from the literature[13].

Table 1– Structural details and activity of compounds used in the present study.

Compd. No.	Config.	R_1	R_2	R_3	R_5	R_6	R_7	R_4	$K_{0.5}$
1.	(±)–trans	H	H	$N(CH_3)_2$	H	Cl	OH	CH_2	0.63
2.	(±)–trans	H	H	$N(CH_3)_2$	H	H	H	CH_2	35.00
3.	(±)–trans	H	H	NCH_3 (C_3H_5)	H	H	H	CH_2	3.40
4.	(±)–trans	H	H	$N(C_3H_5)_2$	H	H	H	CH_2	10.20
5.	(±)–cis	H	$N(CH_3)_2$	H	H	H	H	CH_2	1200.00
6.	(±)–trans	H	$N(CH_3)_2$	H	H	H	H	CH_2	940.00
7.	(±)–cis	H	H	$N(CH_3)_2$	H	H	H	C_2H_4	109.00
8.	(±)–trans	H	H	$N(CH_3)_2$	H	H	H	C_2H_4	20.90
9.	(±)–trans	H	H	$N(CH_3)_2$	H	OH	OH	CH_2	60.00
10.	(±)–cis	H	H	$N(CH_3)_2$	H	OH	OH	CH_2	9.60
11.	(±)–trans	CH_3	H	$N(CH_3)_2$	H	H	H	CH_2	18.30
12.	(±)–cis	CH_3	H	$N(CH_3)_2$	H	H	H	CH_2	1.90
13.	(±)–trans	H	H	NCH_3 $(CH_2)_2C_6H_5$	H	H	H	CH_2	140.00
14.	(±)–trans	H	H	NCH_3 $(CH_2)_3C_6H_5$	H	H	H	CH_2	333.00
15.	(±)–trans	H	H	NCH_3 $(CH_2)_4C_6H_5$	H	H	H	CH_2	212.00
16.	(±)–trans	H	H	$N(CH_3)_2$	o–Cl	H	H	CH_2	53.00
17.	(±)–trans	H	H	$N(CH_3)_2$	o–CH_3	H	H	CH_2	10.20
18.	(±)–trans	H	H	$N(CH_3)_2$	p–Cl	H	H	CH_2	9.00
19.	(±)–trans	H	H	$N(CH_3)_2$	p–CH_3	H	H	CH_2	2.47
20.	(±)–trans	H	H	$N(CH_3)_2$	p–F	H	H	CH_2	1.53
21.	(±)–cis	H	H	$N(CH_3)_2$	H	Cl	OH	CH_2	0.54

Contd..

Table 1 Contd..

22.	(±)–trans	H	H	$NH(CH_3)$	H	Cl	OH	CH_2	8.10
23.	(±)–trans	H	H	$NH(C_3H_5)$	H	H	H	CH_2	45.00
24.	(±)–trans	H	H	$N(CH_2)_4C_6H_5$	H	H	H	CH_2	1500.00
25.	(±)–trans	H	H	NH_2	H	H	H	CH_2	1270.00

Methodology of Modelling Activity

Pharmacology :

In the present study we have adopted $K_{0.5}$ (nm) from the literature[13].

Non-linear regression analysis of inhibition data was used to determine IC_{50} values using prism 2.0 (Graph Pat San Francisco, CA). IC_{50} values were converted to $K_{0.5}$ based upon the Cheng Prussof equation[14], where $K_{0.5} = IC_{50}/(1 + L^* / KD)$.

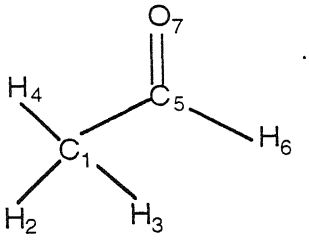
Experiments were repeated at least three times to determine mean $K_{0.5} \pm$ SEM.

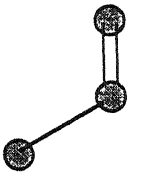
Molecular Descriptors :

Molecular descriptors are calculated using the information given in the following Table:

Molecular descriptors	Abbreviation Formula (e)	Basis	Ref.
Wiener index	$W = 1/2\sum_{i=1}^{n}\sum_{j=1}^{n} d(v_i, v_i \mid G)$	Vertex distance in molecular graph	8
Szeged index	$Sz = \sum_{e} n_1(e \mid G)\, n_2(e \mid G)$	Vertex distance (near to edge ends) in molecular graph	9,10
Negentropy index	$N = (i).(n)$ where $i = -K \Sigma P_i \log P_i$ (j)	Information theory	15
Molecular redundancy index	$MRI = \dfrac{\sum n_i \log n_i}{N \log N}$	Information theory	15
First order valence connectively index	${}^1\chi^{v} \sum_{ij} [\delta_i \delta_i]^{-0.5}$	Valence delta values	1,2,16

The aforementioned topological indices are calculated from adjacency and distance matrices. The adjacency matrix, M, of a chemical structure is defined by the elements $[M_{ij}]$ where M_{ij} is 1 if atoms i and j are bonded and zero otherwise. The distance matrix, D, of a chemical structure is defined by the elements $[D_{ij}]$ where D_{ij} is the length of the shortest path from atom i to j ; zero is used if atoms i and j are not part of the same connected component. The adjacency matrix of $CH_3CH{=}O$ is displayed on the left and its distance matrix is displayed on the right (below).





Structural graph of $CH_3CH{=}O$

C_1	0	1	1	1	1	0	0
H_2	1	0	0	0	0	0	0
H_3	1	0	0	0	0	0	0
H_4	1	0	0	0	0	0	0
C_5	0	0	0	0	1	0	0
H_6	0	0	0	0	1	0	0
O_7	1	0	0	0	1	0	0

Hydrogen suppressed molecular graph of $CH_3CH{=}O$

0	1	1	1	2	2	
1	0	2	2	3	3	
1	2	0	2	3	3	
1	2	2	2	3	3	
1	2	2	0	1	1	
2	3	3	1	0	2	
2	3	3	1	2	0	

The adjacency matrix and distance matrices of chemical structures are promising techniques in molecular modelling. In graph theory the molecular structure is transformed into molecular graph by depleting all the carbon and hetero-atoms hydrogen bonds. Hence, hydrogen suppressed molecular structure is defined as molecular graph.

A number of successful QSAR studies were made based on the Wiener index, however, very little is known on the use of Szeged index in developing quantitative structure-activity relationships.

Table 2– Calculated molecular descriptors and indicator parameters.

Compd. No.	*N*	$^{1}\chi^{v}$	MRI	Sz	*W*	Ip_1	Ip_2	Ip_3	Ip_4
1.	52.9074	0.224	8.2016	1960	1072	1	0	1	1
2.	50.7645	0.3176	7.7072	1524	826	1	0	0	1
3.	58.5225	0.2133	8.0286	1692	936	0	0	0	1
4.	64.4987	0.2212	8.6201	1911	1139	0	0	0	1
5.	47.2402	0.2856	7.1667	1466	730	0	0	0	0
6.	47.2402	0.2856	7.1667	1328	718	0	0	0	1
7.	50.1908	0.3059	7.6791	1434	798	1	0	0	0
8.	52.5976	0.2726	7.6892	1536	834	1	0	0	1
9.	53.1609	0.2431	6.7013	2183	1207	1	0	1	1
10.	50.7486	0.2771	7.4413	2159	1207	1	0	1	0
11.	51.9948	0.281	7.5446	1490	830	1	0	0	1
12.	51.9992	0.2809	7.5874	1360	792	1	0	0	0
13.	70.308	0.2484	9.81	2776	1852	0	0	0	1
14.	76.2432	0.2382	10.31	3454	2125	0	0	0	1
15.	80.442	0.246	10.81	3822	2426	0	0	0	1
16.	49.4132	0.2527	7.6952	1531	829	1	1	0	1
17.	54.1728	0.2502	7.5933	1531	829	1	1	0	1
18.	49.4132	02527	7.6893	1610	867	1	1	0	1
19.	54.1728	0.2502	7.5875	1610	867	1	1	0	1
20.	49.4132	0.2527	6.9756	1610	867	1	1	0	1
21.	50.5008	0.2593	7.8196	1942	1072	1	0	1	0
22.	50.6181	0.1843	7.8377	1960	1072	0	0	1	1
23.	53.1342	0.2206	7.5122	1732	976	0	0	0	1
24.	69.2493	0.3081	10.4306	3822	2426	0	0	0	1
25.	39.823	0.2631	6.3574	1274	733	0	0	0	1

Several computer programs are available for computing molecular descriptors including topological indices. Some of the popular packages in calculating molecular descriptors are: AHPAL, CODESSA, MOLCONN-X, HYPERCHM, DRAGON, POLLY, MOPAC, ALCHEMY III, TSAR, HASL, CAChe, Chem-3D, TOPMOST CLOGP. In addition, several softwares are available to carry out regression analysis: MSTAT, SPSS-X, BMD02R, BMLR, SPSS/PC, MINITAB, SAS etc.

Indicator parameters (Ip_1, Ip_2, IP_3, Ip_4) :

Indicator variables[17,26] (parameters), are some times used in linear multiple regression analysis to account for certain features which cannot be described by continuous variables. In QSAR equations they normally describe a certain structural element, be it a substituent or another molecular fragment. Thus, Free Wilson analysis may be interpreted as a regression analysis approach using only indicator variables.

The disadvantage of indicator variables are that they are dummy variables and that too many of them increases the possibility of chance correlation as well as collinearity defect[18,21-26].

In the present case the indicator parameter Ip_1 was taken as unity when $-N(CH_3)_2$ group is present at R_3. Similarly, Ip_2 is used as unity when R_5 is other than H. When R_6 and R_7 are other than H the indicator parameter taken is Ip_3 and its value is taken as unity. Ip_4 is taken as one when the compound is trans.

Regression Analysis :

We have used the maximum R_2 improvement method to identify prediction models[17-26]. This method finds the "best" one variable model, the "best" two variable model and so forth for the prediction of property/activity. Several models (combinations of variables) were examined to identify combinations of variables with good prediction capabilities. In all regression models developed we have examined a number of statistical parameters associated with residues, i.e. the Wilks-Shapiro test for normality and Cooks D-statistics for outliers, to obtain the most reliable results[26].

Multiple regression analysis for correlating binding affinity ($K_{0.5}$ Value) of the present set of compounds with the aforementioned molecular descriptors were carried

out using Regress-l software as supplied by Professor I. Lukovits, Hungarian Academy of Sciences, Budapest, Hungary. Several multiple regressions were attempted using correlation matrix from this program and the best results were considered and discussed in developing QSAR.

Computations :

All the computations were carried out in Power Macintosh 9600/233.

In the present study, we have used Wiener-l and Regress-l programs for the calculation of W and Sz indices and for making regression analysis respectively. Other calculations are made for programmable calculators. These softwares were made available to us by Prof. I. Lukovits, Hungarian Academy of Sciences, Budapest, Hungary.

Results and Discussion

A perusal of Table 1 shows that no correlation exists between configuration and the inhibition constant (binding affinity constant), $K_{0.5}$ (nm). That is, we can not use this parameter for distinguishing between cis-and trans-configurations. Surprisingly enough, we observed that the topological indices used (N, MRI, $^1\chi^V$, Sz, and W) have different values for these conformations (Table 1). It is observed that the values of these topological indices are higher for trans-conformers compared to the cis-conformers. Hence, these indices are appropriate for modelling binding affinity of 1-phenyl-3-amino-l,2,3,4-tetrahydronaphthalenes as ligands for histamine H_1 -receptors.

In order to obtain statistically significant models, we have employed the multiple regression analysis technique and obtained the correlation matrix as shown in Table 3. The descriptors in the selected sub set are those which exhibit correlation coefficient below 0.5.

A perusal of Table 3 shows the existence of collinearity between: (i) N and $^1\chi^v$ (ii) N and Sz; (iii) N and W; (iv) $^1\chi^v$ and Sz; (v) $^1\chi^v$ and W; (vi) Sz and W. The QSAR models based on such combinations of topological indices will suffer from the defect of collinearity. None of the indicator parameters (Ip_1, Ip_2, Ip_3 and Ip_4) correlate mutually or with any of the topological indices (N, MRI , $^1\chi^v$, Sz and W) used.

Table 3– Correlation matrix for the intercorrelation of molecular description and correlation with the activity.

	$K_{0.5}$	N	$^1\chi^v$	MRI	Sz	W	Ip_1	Ip_2	Ip_3	Ip_4
$K_{0.5}$	1.0000									
N	–0.0202	1.0000								
MRI	0.4013	–0.1811	1.0000							
$^1\chi^v$	0.0976	0.9447	–0.0737	1.0000						
Sz	0.2097	0.8836	–0.0862	0.8974	1.0000					
W	0.2232	0.8990	–0.0654	0.9149	0.9948	1.0000				
Ip_1	–0.5478	–0.4335	0.3041	–0.4358	–0.4228	–0.4486	1.0000			
Ip_2	–0.2523	–0.2035	–0.0917	–0.2185	–0.2556	–0.2679	0.4432	1.0000		
Ip_3	–0.2517	–0.1892	–0.3203	–01775	0.0636	0.0048	0.2418	–0.2500	1.0000	
Ip_4	–0.0275	0.2662	–0.3941	0.2049	0.1908	0.2002	–0.2418	0.2500	–0.2500	1.0000

The values of correlation coefficient in Table 3 also show that none of the molecular descriptors correlate with the inhibition constant (affinity constant) $K_{0.5}$' (nm). However, marked relationship occurred between MRI, Ip_1 with the $K_{0.5}$ nm. This indicates that statistically significant multi-parametric model will contain two molecular descriptors.

Applying multiple linear regression technique we have obtained several regression models. Only those models wherein the standard deviation of the coefficient is smaller than the values of coefficient of the descriptors are considered as statistically significant models. Such models are only considered and discussed critically using the data presented in Table 4.

The data presented in Table 4 shows that :

Table 4– Quality of correlation and other statistical paparameters of significant correlations.

Model No.	Regression equation	SE	R	F-ratio	Q
1.	$K_{0.5}$ = (–14.99) N-(614.23) Ip_1+1410.24	372.85	0.6180	6.796	0.0017
2.	$K_{0.5}$ = (8998.06) MRI-(661.50) Ip_1–1705.69	278.37	0.8096	20.924	0.0029
3.	$K_{0.5}$ = (–13.24) N+(8779.16) MRI–(766.21) Ip_1–860.74	257.31	0.8479	17.909	0.0033
4.	$K_{0.5}$=(–87.52)$^1\chi^v$+(9203.65)MRI–(751.59) Ip_1–1008.11	268.20	0.8335	15.928	0.0031
5.	$K_{0.5}$=(9633.23)MRI–(743.83)Ip_1 + (196.81)Ip_2–1862.43	275.08	0.8239	14.795	0.0030
6.	$K_{0.5}$=(10027.19)MRI–(716.73)Ip_1+(183.42)Ip_3–1976.32	276.12	0.8224	14.631	0.0030
7.	$K_{0.5}$ = (–42.33) N – (7822.09) MRI + (0.44) Sz – (718.47) Ip_1 + 114.35	208.46	0.9079	23.463	0.0044
8.	$K_{0.5}$ = (–44.60) N + (7406.58) MRI + (0.67) W – (693.09) Ip_1 + 428.79	211.78	0.9048	22.579	0.0043
9.	$K_{0.5}$ = (–13.00) N + (9386.81) MRI – (842.62) Ip_1 + (187.09) IP_2 – 1024.61	253.56	0.8603	14.238	0.0034
10.	$K_{0.5}$ = (–42.33) N – (7822.09) MRI + (0.44) Sz – (718.47) Ip_1 – 35.68	193.99	0.9249	22.494	0.0048
11.	$K_{0.5}$ = (–57.41) N + (5788.88) MRI + (0.64) Sz – (624.63) Ip_1 – (278.45) Ip_3 + 1077.60	198.32	0.9214	21.259	0.0047
12.	$K_{0.5}$ = (–43.85) N + (8399.77) MRI + (0.44) Sz – (711.16) Ip_1 + (133.77) Ip_4 – 76.54	206.71	0.9143	19.359	0.0044

(1) No mono-parametric models are possible for modelling the activity ($K_{0.5}$ nm);

(2) Only two bi-parametric models are obtained and the one using MRI and Ip_1 gave better value for R (= 0.8096);

(3) All the four tri-parametric models are statistically significant and the triparametric correlations containing MRI, N and Ip_1 gave the highest value of R (= 0.8479).

Comparing this result with the bi-parametric correlations discussed above we observed that the introduction of N to MRI and Ip_1 resulted into improvement of quality of model such that R value changed from 0.8096 (bi-parametric) to 0.8479 (tri-parametric).

(4) Three tetra-parametric models are possible which are statistically significant and each gave improved R-values compared to the best triparametric model discussed above. The tetra-parametric models; (i)involving MRI, N, Sz and Ip_1 and (ii) involving MRI, N, W. and Ip_1 have similar quality as their R-values are identical (0.9079 and 0.9048). These identical . qualities may be attributed to strong inter-correlation between W and Sz. Because of this information content in W and Sz is same.

(5) Finally, step-wise regression resulted into three penta-parametric correlations. All these three models are statistically excellent. However, the model containing MRI, N, Sz, Ip_1 and Ip_2 has the highest value of R.Second best penta-parametric model is the one containing MRI, N, Sz, Ip_1 'and Ip_3, (R = 0.9214). It is worthy to record that none of these models contained W as one of correlating parameters. This indicates that Sz is a better topological index than W in proposing multi-parametric models.

It is interesting to record that all the proposed models contain invariably MRI and Ip_1 as one of the correlating parameters. Also that the coefficient of MRI is always positive and that of Ip_1 is always negative. Recall that Ip_1 is used for the presence or absence of $-N(CH)_2$ moiety at R_3. The results, therefore, indicate negative effect of this group on the activity ($K_{0.5}$, nm) of the compounds used in the present study.

In order to confirm our aforementioned findings we have calculated quality factor Q[27]. This quality factor, Q, is defined as the ratio of the correlation coefficient R to the standard error of estimation, SE (Q = R/SE).That is, now the quality of model is judged considering R and SE simultaneously. Hence, Q is a better parameter than R or SE to decide the quality of models. Such Q values are given in Table 4.

The Q-values presented in Table 4 indicate that the quality of models (7), (8) (10) (11) and (12) are similar. Hence, in the present case Q-value failed to give which model is most suitable for modelling the inhibitor binding affinity constant. Hence, one has to use cross-validation method for deciding predictive ability of the models.

Another alternative for obtaining the most suitable model is to estimate $K_{0.5}$ and compare them with its observed values and finally obtain predictive correlation coefficient (R^2) .by the regression analysis of correlation between observed and estimated $K_{0.5}$ from different proposed models.

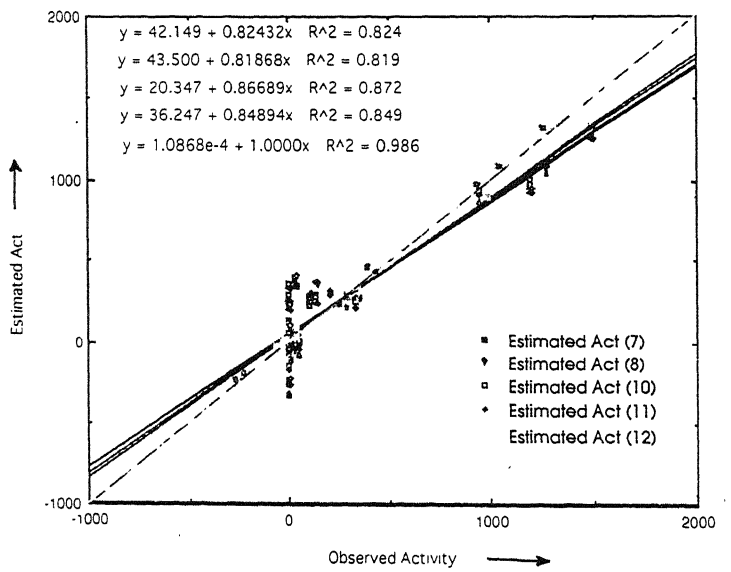


Fig. 2– Correlation between observed and estimated activity using various proposed models.

We have, therefore, calculated $K_{0.5}$ values using models (7), (8), (10), (11) and (12) and obtained R^2 values. highest R^2 (0.986) is observed for the model (12) indicating it to be the most appropriate model for modelling binding affinity ($K_{0.5}$, nm) of the series of compounds used in the present study.

Acknowledgments

Authors thank Prof. I. Lukovits for providing Regress-I software. One of the authors (VKA) thanks AICTE, New Delhi, India for financial support.

References

1. Kier, L.B. & Hall, L. H. (1976) *Molecular Connectivity in Chemistry & Drug Research,* Academic Press, New York.
2. Kier, L.B. & Hall, L.H. (1986) *Molecular Connectivity in Structure-Activity Relationship,* Wiley, New York.
3. Trinajstic, N.(1992) *Chemical Graph Theory,* 2nd Ed. CRC Press, Boca Raton Fl.
4. Gutman, I. & Cyvin, S.J. (1989) *Introduction to the Theory of Benzenoid Hydrocarbons,* Springer- Verlag, Berlin.
5. Gutman, I., Yeh, Y.N., Lee, S.L & Luo, Y. L. (1993) *Indian J. Chem.* **32A** : 651.
6. Trinajstic, N.(1983) *Chemical Graph Theory,* Vol. I, II, CRC Press: Boca Raton, Florida.
7. King R.B. (Ed.) (1983) *Chemical Applications of Topology & Graph Theory,* Elsevier, Amsterdam.
8. Wiener, H. (1947) *J. Am. Chem. Soc.* **69** :17.
9. Gutman, I.(1994) *Graph Theory Notes, New York,* **27** : 9.
10. Khadikar, P.V., Deshpande, N.V., Kale, P.P., Dobrynin, A., Gutman, I. & Domotor, G. (1995)*J. Chem. Inf Comput. Sci.* **35** : 547.
11. Booth, RG., Wyrick, S.D., Baldessarini, R.J., Kula, N.S., Myers, A.M. & Mailman, R.B. (1993) *Mol. Pharmacol.* **44** : 1232.
12. Wyric, S.D., Booth, R.G., Myers, A.M., Owens, C.E., Kula, N.S., Baldessarini, R.J., McPhail, A.T. & Mailman, R,B. (1993) *J. Med. Chem.* **36** :2542.
13. Bucholtz, E.C., Wyric, S.D., Brown, R.L., Tropsha, A., Booth, R.G.& Wyric, S.D.(1999) *J Med. Chem.,* **42** : 3041.
14. Cheng, Y.C. & Prusoff, W.H.(1973) *Biochem. Pharmacol.* **22** : 3099.
15. Kier, L.B. (1980) *J. Pharm. Sci.* **69** : 807.
16. Randic, M. (1975) *J. Am. Chem. Soc.* **97** : 6609.
17. Balaban, A.T., Motoc, I., Bonchev, D., Mekenyan, O., (1983) *Steric Effects in Drug Design,* Charton, M. & Motoc I, (eds.) Akademic-Verlag, Berlin.
18. Balaban A.T. (1982) *Chem. Phys. Lett.* **89** : 399.
19. Mezey, P.G. (1993) *Shape in Chemistry: An Introduction to Molecular Shape and Topology,* VCH Pub., New York.
20. Hall, L.H. & Kier, L.B. (1991) *The Molecular Connectivity Chi Indices and Kappa Shape Indices in Structure-Property Relations,* in *Reviews of Computational Chemistry,* Chap. 9, pp. 367-477, eds. Boyd, D. & Lipkovitz, K., VCH Pub. Inc.
21. Devillers, J. & Balaban, A.T. (eds) (1999) *Topological Indices and Related Descriptors in QSAR and QSPR,* Gorden and Breach, U.K.

22. Kier, L.B. & Hall, L.H. (1999) *Molecular Structure Description. The Electro Topological State,* Academic Press, San Diego.

23. Stuper, A.J., Brugger, W.C. & Jurs, P.C. (1979) *Computer-Assisted Studies of Chemical Structure and Biological Functions,* Wiley Interscience, New York

24. Todeschini, R. & Consonni, V. (2000) *Hand Book of Molecular Descriptors*, Wiley-VCH Weinheim (GER).

25. Karelson, M. (2000) *Molecular Descriptors in QSAR/ QSAR,* John Wiley & Sons, New York.

26. Chatterjee, S., Hodi, A. & Price, B. (2000) *Regression Analysis by Examples,* 3rd ed. Wiley, New York.

27. Pogliani, L. (1994 *)Amino Acids.* **6** : 141.

PROC. NAT. ACAD. SCI. INDIA, 73 (A), III, 2003

Vitamin B_{12} model compounds : Synthesis and characterization of trans-azido(pyridine) cobaloximes

N. RAVI KUMAR REDDY, D. SUDARSHAN REDDY, V. SRIDHAR and S. SATYANARAYANA*

Department of Chemistry, Osmania University, Hyderabad-500007, India.

E-mail : ssnsirasani@yahoo.com

Receives March 14, 2002; Revised November, 8, 2002; Accepted December 11, 2002

Abstract

A series of the complexes of the type $[Co(DH)_2(N_3)L]$ where DH = dimethyl glyoxime and L = pyridine or its derivatives have been synthesized and characterized on the basis of electronic, IR, NMR (^1H and ^{13}C) and FAB MS as well as thermal analysis. IR and NMR spectra indicate the trans configuration for the isolated complexes. The FAB MS shows molecular ion peak which corresponds to mono nuclear complex of the type $[Co(DH)_2N_3L]$.

(Keywords : azido cobaloximes/ dimethylglyoxime/ pyridine/ spectral studies/ trans configuration)

Introduction

The bis(dimethylglyoximato)cobalt(III) complexes, trivially known as cobaloximes in view of their resemblance to cobalamins. There has been growing interest in organo cobalt complexes which might serve as 'model compounds' for coenzyme B_{12}. These have been extensively studied in the last three decades[1-9] in view of their rich chemistry, both with respect to synthesis as well as catalysis[10-14]. Synthesis of organo cobaloximes with modified structural features continues to be a fascinating area in the chemistry of model compounds of coenzyme B_{12}. Recently, Gupta and Roy[15] reviewed the synthetic aspects of organo cobaloxime chemistry. Further, the X-ray crystal structure of alkyl cobaloximes suggests[16] that the Co atom in cobaloximes has a slightly greater positive charge, causing relatively stronger attachment of a base along axial directions. In addition to this the azido ligand present in cobaloximes shows many interesting chemical features[17,18]. All these considerations prompted us to synthesize a series of azido cobaloximes containing pyridine and substituted pyridines. We report here the synthesis, IR, electronic, NMR(^1H and ^{13}C), mass spectral data as well as thermal analysis of cobaloximes

containing pyridines as axial ligands and the linear tri-atomic azide ion (N_3^-) in the sixth coordination position.

Materials and Method

Cobalt(II)acetate , KN_3, dimethylglyoxime were obtained from BDH . Pyridine and substituted pyridines (4–aminopyridine, 4–picoline, 4–ethylpyridine, 4–bromo pyridine hydrochloride, 4–cyanopyridine, 4–vinylpyridine and isonicotinamide) were used as supplied by SD Fine chemicals.

Synthesis of [Co(DH)$_2$(N$_3$)L] complexes : Complexes of the type $[Co(DH)_2(N_3)L]$ (where L = pyridine and substituted pyridines) were prepared in 60–70% yield by bubbling air for a period varying from 2 to 6 h through an ethanolic solution of cobalt(II)acetate, KN_3, dimethylglyoxime and the ligand taken in a 1: 2: 2: 2 proportion. This was allowed to stand for to settle the micro crystalline solid at the bottom and collected on a frit, washed with small aliquots of EtOH, Et_2O and finally dried in a vacuum dessicator. The reaction presumably proceeds in the following manner.

$$2Co(CH_3COO)_2.4H_2O + 4MN_3 + 4DH_2 + 4L + \tfrac{1}{2}\ O_2 \longrightarrow$$

$$2[Co(DH)_2(N_3)L] + 4CH_3COOM + 2L.HN_3 + 9H_2O$$

Synthesis of [Co(DH)$_2$(N$_3$)(4-NH$_2$Py)] : 0.5g (2mmol) $Co(OAc)_2.4H_2O$ was dissolved in 25ml ethanol. 0.33g (4.1mmol) KN_3 was added to the above solution with constant stirring. Then 0.5g (4.3mmol) dimethylglyoxime was added to the mixture and heating and stirring continued for 30min till a deep brown solution was obtained. To the filtrate 0.395g (4.2mmol) of amino pyridine solution (dissolved in 5ml ethanol) was added and stirred for 5 more min and the solution allowed to cool at room temperature. A continuous stream of air was then bubbled through the solution for 2½ h when the reddish-brown micro crystalline solid was deposited at the bottom. After allowing the precipitate to settle, it was collected on a frit, washed with ethanol several times followed by dry ether. The product (73%) was finally dried *in vacuo*.

Cobalt was determined by the method of Laitenen and Burdett[19]. Micro analysis of complexes were performed on Perkin-Elmer 240C elemental analyzer. IR spectra were obtained on Perkin Elmer FTIR 1605 instrument using KBr pellets. ^1H and ^{13}C NMR spectra were recorded on Varian Gemini 200 NMR spectrometer and referenced to TMS in $CDCl_3$/DMSO-d_6. Mass spectra were recorded on Autospec mass

spectrometer and UV-Visible spectra of the complexes were recorded on Hitachi U-3410 spectrophotometer. Thermal analysis was obtained on Mettler Toledo Star system.

Results and Discussion

All these complexes have very low molar conductivity values which favour the neutral, non-ionic formulations and non-electrolytes in dilute solutions. The ligand-field spectra of the complexes in MeOH show a peak of weak to moderate intensity at around 18000–20000 cm^{-1} [20]. There are two other main bands centered at 40000–42500 cm^{-1} region attributable to the intra-ligand π–π^* transition of the coordinated oxime group, where as the band at 28000–30000 cm^{-1} may be due to the pyridine $\rightarrow$ cobalt transition. The strong band at around 47000 cm^{-1} due to the $d\pi(Co)$–$\pi^*(DH^-)$ transition[21,22]. The general features in the spectrum of these complexes are very similar to those observed for the corrins and other alkyl cobaloximes[23].

The IR spectra of the free ligands and the complexes have been carefully analysed since this technique serves as a probe to distinguish between the cis- and trans- forms in organo cobalt(III) compounds[24,25] and these are all shown to have indeed the trans configuration similar to the organo cobaloximes[26], which is further substantiated on the basis of NMR evidences. Most of the important bands of all these complexes appear in almost similar positions with identical intensity depicting the similarity in structure. The free uncoordinated DH_2 has no band at 1240 cm^{-1}, a strong band appears in the $Ni(DH)_2$ complex at 1240 cm^{-1} due to υ(N–O) of the ionised N–OH group of dimethylglyoxime[27]. In the present case, for all azido cobaloxime complexes, presence of two bands in the region 1230–1240 cm^{-1} and 1090–1095 cm^{-1} account for two non-identical linkages i.e. C=N–O–H and C=N–O···H in the complexes[4]. This observation is consistent with the X-ray diffractional analysis of the $Cu(DH)_2$ complexes in which two different Cu–N distances were observed[28,29]. The stretching vibration, υ(C=N), of the non-coordinated DH_2 appearing at 1620–1630cm^{-1} is consequently shifted in this azido cobaloximes to 1560–1570 cm^{-1}. A very weak intensity band observed in the region 1700–1750 cm^{-1} is attributed to the deformation of the strong intramolecular hydrogen bridge as it disappears on deuteration[30,31]. The characteristic υ(Co–N) (N of DH^-) appears at 510–515 cm^{-1} and υ(Co–N)(N of pyridine) at 420 cm^{-1} . The IR bands of the N_3^- ion , which is a linear symmetric tri atomic system with sixteen valency electrons, are of interest. The bending and strectching modes of the azide group[32,33] appearing at 640 and 2040 cm^{-1} are shifted to 660–680 cm^{-1} and 2015–2025 cm^{-1}, respectively. N_3^- stretching frequency confirms that the complex is mono nuclear and N_3^- coordinated to Co(III) in end on mode[34].

The characterstic absorption bands in dimethyl glyoximato ligands in these cobaloximes are also sensitive to the change of axial ligands. As the donating power of the base ligand increases the υO–H...O at 1770 cm^{-1} and υC=N at 1560 cm^{-1} shift to lower wave number region while υ(N–O) at 1230 cm^{-1} and 1085 cm^{-1} shift to higher one. These shifts can be interpreted as follows. The coordination of more electron donating base to Co(III) causes the increase in electron density in Co(III) which facilitates the back donation of Co(III) to the nitrogen atom of dimethyl glyoximato ligand, resulting in the increase in electron density in C=N and N–O bonds. The increase in electron density in N–O bonds causes the stronger hydrogen bridges O–H...O and higher frequency shift of N–O stretching vibration. The facilitated back donation from cobalt(III) to nitrogen atoms of dimethyl glyoxime means the increased metal donor π bond in the equatorial moiety of cobaloximes, which causes the stronger interaction of Co with equatorial 'N' atoms resulting in higher frequency shifts of υ(Co–N) vibration and causes more conjugation in the five membered chelate ring including Co(III) which effects the υ(C=N) vibrations to shift to lower frequency.

The NMR (^1H and ^{13}C) spectra have also been used in elucidating the stereo chemistry and in assessing the interaction of ligands coordinated to the same metal ion[35]. The ^1H NMR spectra of the azido cobaloxime complexes clearly show that on coordination, the signal due to CH_3 group of DH_2 at 1.98 ppm undergoes a clear down field shift by around 0.40 ppm to 2.36-2.42 ppm. In all these complexes, this signal appears as a singlet indicating the equivalence of four methyl groups and presence of trans structure[9]. The NMR spectra of simple free ligand of pyridine and other derivatives have been assigned. The aromatic protons of pyridine compounds absorb in the aromatic region. In free pyridine the C_4–H proton to the hetero atom observed at 7.75 ppm as triplet, the C_2–H(C_6–H) protons and C_3–H(C_5–H) protons observed at 7.60 ppm and 7.25 ppm respectively as multiplets. On coordination, pyridine to Co(III) in metal complex, these protons signals observed at 7.82 ppm, 8.18 ppm and 7.39 ppm for C_4–H, C_2–H(C_6–H) and C_3–H(C_5–H) respectively. The more down field shift of C_2–H(C_6–H) protons clearly shows the coordination of N atom of pyridine to the Co atom. 4-Bromo pyridine free ligand proton chemical shifts observed at 7.80 ppm and 7.30 ppm for C_2–H(C_6–H) and C_3–H(C_5–H) protons, respectively. On complexation, these protons undergo down field shift and observed at 8.16 ppm and 7.42 ppm, confirms the formation of the complex through N of pyridine ring. In all the other complexes the chemical shifts follow the same trend and the data are presented in Table 3.

Table 1– Analytical data of $[Co(DH)_2(N_3)L]$ complexes

S. No.	Complex $[Co(DH)_2(N_3)L]$ where L=	Formula (mol.wt)	Color	Yield (%)	Decomp. temp. (°C)	Found(Calc*)%			
						Co	C	H	N
1	C_5H_5N Pyridine	$CoC_{13}H_{19}N_8O_4$ (410)	Brown	72	210	14.12 (14.39)	37.54 (38.04)	4.22 (4.63)	27.24 (27.31)
2	H_2N-C_5H_4N 4-Amino pyridine	$CoC_{13}H_{20}N_9O_4$ (425)	Reddish brown	73	230	13.82 (13.88)	36.24 (36.70)	4.62 (4.70)	29.12 (29.64)
3	Br-C_5H_4N 4-Bromo pyridine	$CoC_{13}H_{18}N_8O_4Br$ (489)	Brown	60	205	11.64 (12.06)	31.25 (31.90)	3.62 (3.68)	22.52 (22.90)
4	NC-C_5H_4N 4-Cyano pyridine	$CoC_{14}H_{18}N_9O_4$ (435)	Brown	65	210	12.26 (13.56)	37.59 (38.62)	4.02 (4.13)	28.12 (28.96)
5	H_2NOC-C_5H_4N Isonicotinamide	$CoC_{14}H_{20}N_9O_5$ (453)	Brown	62	212	12.64 (13.02)	35.94 (37.08)	4.11 (4.41)	27.12 (27.81)
6	H_5C_2-C_5H_4N 4-Ethyl pyridine	$CoC_{15}H_{23}N_8O_4$ (438)	Dark brown	70	198	13.42 (13.47)	41.24 (41.09)	5.10 (5.25)	24.68 (25.57)
7	H_3C-C_5H_4N 4-Methyl pyridine	$CoC_{14}H_{21}N_8O_4$ (424)	Brown	68	194	13.24 (13.91)	38.63 (39.63)	4.56 (4.95)	25.93 (26.41)
8	H_2C=HC-C_5H_4N 4-Vinyl pyridine	$CoC_{15}H_{21}N_8O_4$ (436)	Brown	60	185	13.21 (13.53)	40.68 (41.28)	4.67 (4.81)	23.34 (25.68)

*Calculated values in parenthesis

Table 2– IR spectral data[$] of $[Co(DH)_2(N_3)L^*]$ complexes

S. No.	Complex	ν_2 (N_3)	ν_3 (N_3)	ν (N-O)	ν (C=N)	ν(CH_3)	ν (Co-N) (of DH)	ν(Co-N) (of L)
1	KN_3[#]	643.0	2041.0	–	–	–	–	–
2	NH_4N_3[#]	652.0	2030.0	–	–	–	–	–
3	$[Co(DH)_2(N_3)(C_5H_5N)]$	670.3	2022.6	1236.3 1091.4	1565.3	1365.0 1449.4	512.8	417.8
4	$[Co(DH)_2(N_3)(NH_2\text{-}C_5H_4N)]$	668.3	2019.0	1239.3 1093.8	1562.0	1369.5 1460.8	513.9	420.8
5	$[Co(DH)_2(N_3)(Br\text{-}C_5H_4N)]$	672.4	2023.2	1238.5 1093.1	1563.3	1366.1 1469.9	513.2	421.6
6	$[Co(DH)_2(N_3)(NC\text{-}C_5H_4N)]$	675.2	2024.4	1239.6 1092.0	1560.2	1375.1 1423.8	514.1	422.4
7	$[Co(DH)_2(N_3)(H_2NOC\text{-}C_5H_4N)]$	673.6	2023.8	1241.1 1094.2	1559.6	1377.9 1430.8	512.1	421.5
8	$[Co(DH)_2(N_3)(C_2H_5\text{-}C_5H_4N)]$	668.8	2021.2	1238.5 1092.4	1563.8	1366.7 1437.2	514.1	420.6
9	$[Co(DH)_2(N_3)(CH_3\text{-}C_5H_4N)]$	669.4	2021.8	1237.4 1091.8	1564.5	1360.8 1436.2	514.6	418.6
10	$[Co(DH)_2(N_3)(CH_2{=}CH\text{-}C_5H_4N)]$	670.1	2022.4	1236.2 1093.4	1562.1	1362.4 1438.2	512.6	421.2

: free ligands

$: Recorded as KBr discs and values in cm^{-1}

* : Pyridine, 4-amino pyridine, 4-bromo pyridine, 4-cyano pyridine, isonicotinamide, 4-ethyl pyridine, 4-methyl pyridine, 4-vinyl pyridine

Table 3–^{1}H NMR spectral data$^+$ of $[Co(DH)_2(N_3)L]$ complexes

S. No.	Ligand/Complex	eq CH_3*	Pyridine protons			
			H-2,H-6	H-3,H-5	H-4	R
1	Dimethylglyoxime	1.98	–	–	–	–
2	Pyridine	–	7.60	7.25	7.75	–
	$[Co(DH)_2(N_3)(C_5H_5N)]$	2.38s	8.18d	7.39m	7.82m	–
3	4-bromopyridine	–	7.80	7.30	–	–
	$[Co(DH)_2(N_3)(Br\text{-}C_5H_4N)]$	2.41s	8.16d	7.42d	–	–
4	4-aminopyridine	–	7.25	6.30	–	5.70 (NH_2)
	$[Co(DH)_2(N_3)(NH_2\text{-}C_5H_4N)]$	2.40s	7.45d	6.40d	–	6.05 (NH_2)
5	Isonicotinamide	–	8.15	7.55	–	8.35 ($CONH_2$)
	$[Co(DH)_2(N_3)(CONH_2\text{-}C_5H_4N)]$	2.36s	8.31d	7.88d	–	8.81 ($CONH_2$)
6	4-methyl pyridine	–	7.52	6.95	–	2.35 (CH_3)
	$[Co(DH)_2(N_3)(CH_3\text{-}C_5H_4N)]$	2.40s	8.22d	7.20d	–	2.80s (CH_3)
7	4-ethylpyridine	–	7.40	6.90	–	2.55 (CH_2) 1.10 (CH_3)
	$[Co(DH)_2(N_3)(C_2H_5\text{-}C_5H_4N)]$	2.37s	8.16d	7.10d	–	2.62q (CH_2) 1.20t (CH_3)
8	4-vinyl pyridine	–	7.55	7.10	–	2.60 (CH) 1.40 (CH_2)
	$[Co(DH)_2(N_3)(C_2H_3\text{-}C_5H_4N)]$	2.36s	8.25d	7.25d	–	2.85(CH) 1.82(CH_2)
9	4-cyano pyridine	–	8.50	7.60	–	–
	$[Co(DH)_2(N_3)(CN\text{-}C_5H_4N)]$	2.42s	8.92d	7.80d	–	–

+ : in ppm relative to TMS – solvent DMSO-d^6

* : equatorial methyl groups of dimethylglyoxime

Table 4–^{13}C [^{1}H]NMR spectral data* of $[Co(DH)_2(N_3)L]$ complexes

S. No.	Ligand/Complex	Dimethyl glyoxime Carbons		Pyridine Carbons			
		CH_3	C=N	C_3,C_5	C_2,C_6	C_4	R
1	Dimethylglyoxime	9.23	154.12	–	–	–	–
2	Pyridine	–	–	124.50	148.90	135.70	–
	$[Co(DH)_2(N_3)(C_5H_5N)]$	12.81	150.35	128.35	152.62	140.62	-
3	4-amino pyridine	–	–	111.40	151.30	156.80	–
	$[Co(DH)_2(N_3)(NH_2\text{-}C_5H_4N)]$	12.65	149.62	115.30	151.15	158.26	-
4	4-ethyl pyridine	–	–	123.30	149.80	152.80	27.10 CH_2 12.70 CH_3
	$[Co(DH)_2(N_3)(C_2H_5\text{-}C_5H_4N)]$	12.72	150.26	125.34	151.84	156.08	27.70 CH_2 13.35 CH_3
5	4-methyl pyridine	–	–	125.00	149.40	152.20	20.80 CH_3
	$[Co(DH)_2(N_3)(CH_3\text{-}C_5H_4N)]$	12.75	150.85	127.80	151.72	155.20	21.93 CH_3
6	4-vinyl pyridine	–	–	120.20	150.30	148.80	134.30 CH 117.70 CH_2
	$[Co(DH)_2(N_3)(C_2H_3\text{-}C_5H_4N)]$	12.79	150.92	128.12	152.05	154.12	135.20 CH 118.60 CH_2
7	4-bromo pyridine	–	–	127.60	152.60	133.20	–
	$[Co(DH)_2(N_3)(Br\text{-}C_5H_4N)]$	12.80	151.41	129.22	152.19	137.06	-
8	Isonicotinamide	–	–	122.70	150.20	142.00	162.70 $CONH_2$
	$[Co(DH)_2(N_3)(CONH_2\text{-}C_5H_4N)]$	12.86	151.65	125.56	152.34	146.60	166.30 $CONH_2$
9	4-cyano pyridine	–	–	127.50	152.10	121.80	116.80 CN
	$[Co(DH)_2(N_3)(CN\text{-}C_5H_4N)]$	12.91	151.82	130.65	152.85	154.62	146.32 CN

* : in ppm relative to TMS – solvent DMSO-d^6

^{13}C NMR spectroscopy has been recognised as one of the most promising tools for the study of vitamin-B_{12} and its model compounds[36-39]. A single peak was observed as expected for azido cobaloximes at 12.70–12.90 ppm and the imine carbon chemical shift at ~150.0 ppm. This confirms the trans configuration for these complexes. The ^{13}C signals of the free pyridine ligands undergo downfield shift on complexation. The $C_2(C_6)$,$C_3(C_5)$ and C_4 signals of pyridine ring resonating at 148.9 ppm, 124.5 ppm and 135.7 ppm respectively. In the $[Co(DH)_2(N_3)(Pyridine)]$ complex, these values are shifted downfield and observed at 152.62 ppm, 128.35 ppm and 140.62 ppm respectively. In free 4-ethyl pyridine, the CH_2 and CH_3 signals are observed at 27.10 ppm and 12.70 ppm. These signals in the complex appeared at 27.70 ppm and 13.35 ppm with slight down field. All these complexes presented in this work follow the same trend of down field shift. ^{13}C NMR chemical shifts for all the complexes studied are reported in Table 4.

The mass spectral studies of free DH_2, $Ni(DH)_2$ complexes reveal the formation of molecular ion peaks for both DH_2 and $Ni(DH)_2$[40,41]. The FAB MS studies of $[Co(DH)_2(N_3)(4\text{-}BrPy)]$ reveal the formation of molecular ion peak at 490. This corresponds to M^{+1} of $[Co(DH)_2(N_3)(4\text{-}BrPy)]$. Peak at 289 corresponds to the $Co(DH)_2$ moiety. FAB MS supports that complex is mono nuclear. The thermal decomposition studies indicate that thermal stability of all these cobaloximes is very high and with increase in temperature mass losses are seen corresponding to polymeric intermediates and the ultimate formation of Co_3O_4 as the end product[40-42].

References

1. Gupta, B. D., Qaungo, K., Veena Singh & Shobini (1998) *Ind. J. Chem.* **37(A)** : 707.
2. Randaccio, L., Bresciani-Pahar, N., Zangrando, E. & Marzilli, L. (1981) *Chem. Soc. Rev.* **18** : 225.
3. Bresciani-Pahar, N., Farcolin, M., Marzilli, L. G., Randaccio, L., Summers, M. F. & Toscano, P. J. (1989) *Coord. Chem. Rev.* **63** : 1.
4. Hussain Reddy, K., Radha Krishna Reddy, M., & Mohan Raju, K. (2000) *Ind. J. Chem.* **39(A)** : 1312.
5. Dreos, R., Felluga, A., Nardin, G., Randccio, L., Siega, P. & Tauzher, G. (2001) *Eur. J. Inorg. Chem.* 267.
6. Rajeshwar Rao, A., Sridhar V. & Satyanarayana, S. (1999) *Proc. Nat. Acad. Sci. India.* **69(A)** : 23.

7. Rajeshwar Rao, A. & Satayanarayana, S. (1998) *Proc. Indian Acad. Sci.(Chem Sci),* **110(1) :** 31.
8. Armugam, M.N. & Arunachalam, S. (1997) *Ind. J. Chem.* **36(A) :** 315.
9. Armugam, M. N. & Arunachalam, S. (1997) *Ind. J. Chem.* **36(A) :** 84
10. Marzilli, L. G. & Toscano, P. J., (1984) *Prog. Inorg. Chem.* **31 :** 104.
11. Tada, M. & Schimuzu, T. (1992) *Bull. Chem. Soc. Jpn.* **65 :** 1252.
12. Tada, M., Sugano, K. & Yoshihara, T. (1995) *Bull. Chem. Soc. Jpn.* **68 :** 2969.
13. Das, I., Chowdhury, S., Ravi Kumar, K., Roy, S. & Gupta, B. D. (1997) *J. Organo metal Chem.* **552 :** 101.
14. Gupta, B. D. & Das, I. (1996) *Ind.J.Chem.* **35A :** 1111.
15. Gupta, B.D. & Roy, S. (1988) *Inorg. Chim. Acta* **146 :** 209.
16. Lenhert, G. J.(1967) *Chem. Soc. Chem. Comm.* 980.
17. Kemmerich, T., Nelson, J., Takach, N. E., Bochme, H., Jablonski, B. & Beck, W. (1982) *Inorg. Chem.* **21 :** 1226.
18. Fehlhammer, W. P., Kemmerich, T. & Beck, W.(1979) *Chem . Ber.* **112 :** 468.
19. Laitenen, H. A. & Burdett, I. W. (1951) *Analyt. Chem.* **23 :** 1268.
20. Lever, A. B. P. (1968) *Inorganic electronic Spectroscopy,* (Elseiver,Amestardam).
21. Ablov, A. V., Filippov, M. P. & Samus, N. M. (1968) *Dokl Akad Nauk USSR.* **133 :** 575.
22. Yamano, Y., Masuda, I. & Shimura, K. (1977) *Bull. Chem. Soc. Jpn.* **44 :** 1581.
23. Giannothi, C. (1982) B_{12}, (Ed Dolphin, D.), Wiley New York **1 :** 393.
24. Dodd, D. & M. Johnson, M. (1973) *J. Organometal Chem.* **52 :** 1
25. Pratt, J. M. & Thorp, R. G.(1969) *Adv. Inorg. Chem. Radio Chem.* **12 :** 375.
26. Dodd, D. & Johnson, M.(1973) *J. Chem. Soc. Dalton Trans.* 1218.
27. Blinc, R. & Hadzi, D. (1958) *J. Chem. Soc.* 4536.
28. *Tables of Interatomic distances (Chemical Society, London),* 1958.
29. Frasson, E., Bardi, R. & Bezzi, S. (1959) *Acta Crystallogr.***12 :** 201.
30. Gillard, R. D. & Wilkinson, G. (1963) *J. Chem. Soc.* 6041.
31. Batyr, D. G., Starysh, M. P., Shafranskii, V. N. & Kharitonovo Yu Ya, (1974) *Russ. J. Inorg. Chem.***19 :** 417.
32. Gray, P. & Waddington, T. C. (1963) *Trans Faraday Soc.* 6041.
33. Dows, D. A., Whittle, E. & Pimental, G. C. (1955) *J. Chem. Phys.* **23 :** 1475.
34. Balch, A. L., Fossett, L. A., Guimerans, R. R., Olmstead, M. M., Reddy, P. E. & Wood, F. E. (1986) *Inorg. Chem.* **25 :** 1248.

35. Fay, R. C. & Piper, T. S. (1962) *J. Am. Chem. Soc.* **84 :** 2303.

36. Hogenkamp, H. P. C.(1975) *Cobalamin: Biochemistry and Pathophysiology,* Ed Babior, B. M., John Wiley, New York 61.

37. Bied-Charreton, C., Septe, B & Goudmer, A. (1975) *Org .mag.Res.* **7 :** 116.

34. Marzilli, L. G., Toscano, P. J., Randaccio, L., Bresciani-pahar, N. & Calligaris, M. (1979) *J. Am. Chem. Soc.* **101 :** 6754.

35. Silverman, R. B. & Dolphin, D. (1973) *J. Am. Chem. Soc.* **95 :** 1686.

36. Das, J. K. & Dash, K. C. (1985) *Polyhedron.* **4 :** 1109.

37. Das, J. K., Chakrovorthy, V. & Dash, K. C. (1986) *Thermochim. Acta* **97 :** 303.

38. Das, J. K. & Dash, K. C. (1986) *Polyhedron* **11 :** 1857.

PROC. NAT. ACAD. SCI. INDIA, 73 (A), III, 2003

Synthetic and structural studies of heterocyclic multidentate schiff base and its metal complexes with Co(II), Ni(II), Zn(II) and Cd(II)

R.C. SHARMA*, SHUBHRA SINGH, RITIKA VATS and SANDHYA AGARWAL

Department of Chemistry, Dr. B.R. Ambedkar University, Institute of Basic Sciences, Khandari Road, Agra-282002, India.

Received December 13, 2001; Revised September 24, 2002; Accepted January 3, 2003

Abstract

Four new complexes of bivalent transition metals Co, Ni, Zn and Cd with schiff base, 2-hydroxy-5-methyl benzene-l-carbalidene-2-aminothiazole-3-carbalidene-2-aminobenzothiazole (HMBCATCABT) having the stoichiometry ML_2, where M = Co (II), Ni (II), Zn (II) and Cd (II) and L= ligand have been synthesized. They have been characterized by their repeated melting point determination, T.L.C. for single spot, elemental analyses, conductance measurements, magnetic susceptibility, IR, NMR and UV/VIS spectral data.

(**Keywords** : heterocyclic schiff base/IR/NMR/UV/VIS spectra).

Introduction

The chemistry of metal complexes with schiff base ligands has gained much importance due to their diversified biological applications[1-5]. They are also found to have a number of pharmacological utilities[6]. This fact prompted us to synthesize some new schiff bases and their metal complexes to get better understanding in this field.

In continuation of our earlier work[7], we have prepared and characterized four complexes of different transition metals with the synthesized ligand (2-hydroxy-5-methyl benzene-1-carbalidene-2-aminothiazole-3-carbalidene-2-aminobenzothiazole).

Materials and Method

All chemicals used were of A.R. grade and the solvents were purified and distilled prior to their use.

1. *Synthesis of 2-hydroxy-5-methylbenzene-l ,3- dicarbaldehyde (HMBD)* : 2-Hydroxy-5-methylbenzene-1,3- dicarbaldehyde was prepared according to the procedure given by Gagne *et al.*[8] [Yield-4.5 g (28%)].

2. *Synthesis of 2-hydroxy-5-methylbenzene-1-carbalidene-2-amino thiazole-3-carbalidene-2-aminobenzothazole (HMBCA TCABT)* :To 15 ml methanolic solution of 0.16 g (1mM) of dicarbaldehyde, a mixture of 0.10 g (1mM) of 2-aminothiazole and 0.15 g (1mM) of 2-aminobenzothiazole in 30 mlmethanol was added. The resulting mixture was refluxed for 8-10 h. The excess of methanol was distilled off. On cooling, bright orange crystalline solid was isolated which was washed with alcohol, recrystallized from methanol and dried in vacuum desiccator over anhydrous $CaCl_2$ [Yield- 0.25 g (67%)].

3. *Synthesis of metal complexes* : To 20 ml methanolic solution of ligand (HMBCATCABT, 0.76 g, 2 mM), 15 ml aqueous solution of 1 mM of metal salt [0.25 g,$(CH_3COO)_2Co.4H_2O$/0.25g, $(CH_3COO)_2$ Ni.$4H_2O$/0.22 g, $(CH_3COO)_2$ Zn.$_2H_2O$/0.18 g, $CdCl_2$] was added and refluxed for 3 h. On cooling, coloured solid separated out. The resulting complex was filtered, washed with alcohol, ether and recrystallized from DMF. It was dried in vacuum desiccator over anhydrous $CaCl_2$

Physical and analytical measurements : Carbon, Hydrogen and Nitrogen analyses were carried out on Carlo Erba Micro Analyser (Model-1106) and Sulphur was estimated as $BaSO_4$ by standard procedure[9]. Metals were estimated by precipitating them as their pyridine complex[10]. Molecular weights of all the compounds were determined by Cryoscopic method[11]. IR spectra were recorded on a JASCO Spectrometer (Model IR-Report-100) in KBr medium. ^{1}H NMR spectra were carried out on NMR Brucker AC-300 MHz in $CDCl_3$. The UV/VIS spectra in DMSO were recorded on Shimadzu Digital Double Beam Spectrophotometer (Model UV 150-150.02). The conductance measurements were carried out on Toshniwal Conductivity Bridge using 10^{-3} M DMF solution. The magnetic susceptibility was determined at room temperature by Gouy's method.

Results and Discussion

The analytical data of complexes reveal their 1:2, (ML_2) stoichiometry and the conductivity measurements suggest their non-electrolytic nature.

In IR spectra of dicarbaldehyde, sharp bands in 1715-1695 cm^{-1} and at 2880 cm^{-1} were obtained due to the stretching vibrations of carobnyl[15] and -CH-(aldehyde)[13] groups respectively. The bands due to phenolic group[14] and -CH-(aromatic) were obtained at 3525 cm^{-1} and 3000 cm^{-1} respectively.

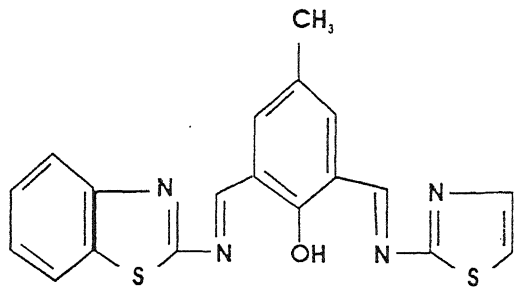
Table 1–Physical and analytical data.

S. No.	Compound	Molecular formula	Colour	M.P./ D.T. (°C)	% Analysis, Found/(Calculated)					Molecular weight F/(C)
					C	H	N	S	M	
1.	HMBD	$C_9H_8O_3$	Yellow	130	66.11 (65.85)	5.28 (4.88)	...	...	...	176 (164)
2.	HMBCATCABT	$C_{19}H_{14}H_4S_2O$	Yellowish orange	104	60.76 (60.32)	4.01 (3.70)	14.12 (14.81)	16.18 (16.81)	...	390
3.	[Co (II) (HMBCATCABT)$_2$]	[($C_{38}H_{26}N_8S_4O_2$) Co(II)]	Mustard	330	56.42 (56.09)	3.53 (3.19)	13.32 (13.78)	15.10 (15.74)	6.92 (7.24)	827.2 (812.9)
4.	[Ni (II) (HMBCATCABT)$_2$]	[($C_{38}H_{26}N_8S_4O_2$) Ni(II)]	Dark orange	230	56.34 (56.11)	3.62 (3.20)	13.34 (13.78)	14.99 (15.75)	6.34 (7.22)	824.3 (812.7)
5.	[Zn (II) (HMBCATCABT)$_2$]	[($C_{38}H_{26}N_8S_4O_2$) Zn(II)]	Bright orange	280	55.92 (55.65)	3.48 (3.17)	13.39 (13.67)	15.25 (15.62)	6.59 (7.98)	832 (819)
6.	[Cd (II) (HMBCATCABT)$_2$]	[($C_{38}H_{26}N_8S_4O_2$) Cd(II)]	Orangish yellow	240	52.86 (52.63)	3.36 (3.00)	12.37 (12.93)	13.63 (14.77)	11.64 (12.97)	891 (866)

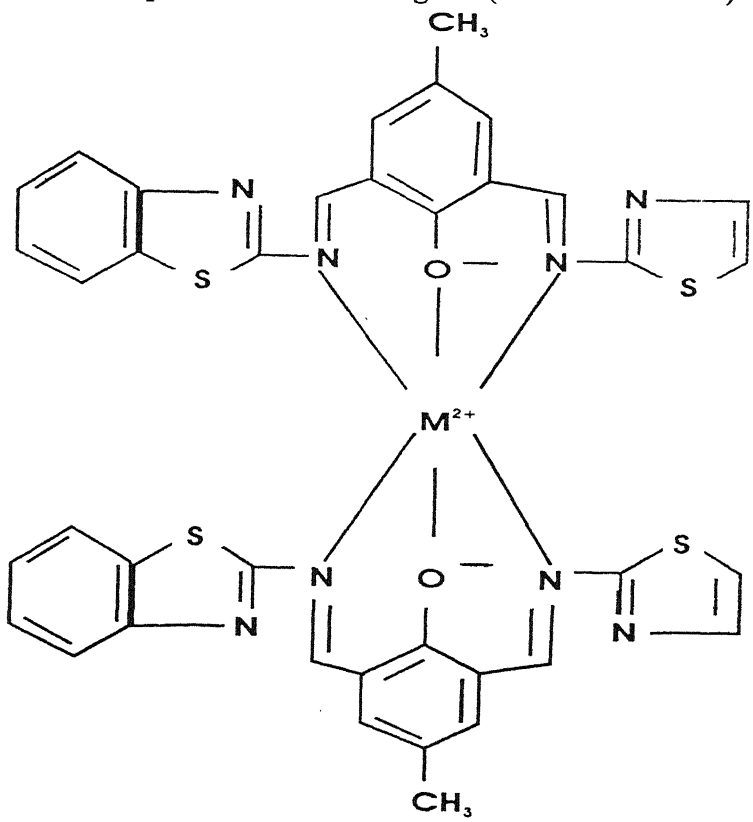
The infra-red spectra of schiff base (HMBCATCABT) show two bands in the region of 695-675 cm^{-1} and 650-630 cm^{-1} which may be due to symmetric and asymmetric vibrations of C-S stretching of thiazole or benzothiazole[15] while the C=N (cyclic) band has been observed in the region of 1485-1460 cm^{-1}. The sharp intensity bands at 1625 cm^{-1} and 3530 cm^{-1} due to stretching vibrations of azomethine group[16] and phenolic group were obtained. In the IR spectra of metal complexes, the shifting of azomethine band indicates the coordination of ligand to metal through nitrogen. The band due to phenolic group was absent in the complexes indicating the deprotonation of phenolic group. However, no shift in the band position due to sulphur (thiazole and benzothiazole ring) was observed which infers that the sulphur of the ligand does not coordinate.

^1H NMR spectra in $CDCl_3$, of the synthesized dicarbaldehyde show δ values at 2.2 (3H,s Me), 7.8 (2H,m, Ar-H)[17,18], 10.2 (2H,s, aldehydic-H)[19] and 11.4 (1 H,s, phenolic-H). In NMR spectra of ligand (HMBCATCABT), new δ value at 8.5 (2 H,s, azomethine-H)[20] was observed showing the condensation of dicarbaldehyde with ligand. A sharp signal characteristic of phenolic proton in ^1H NMR spectra of free ligand was found to be absent in their corresponding metal complexes. This observation confirms the deprotonation of phenolic group in the metal complexes and supports the formation of M-O bond.

In the electronic spectra of Co (II) complex, three bands were obtained at 8095 cm^{-1}, 15785 cm^{-1} and 18945 cm^{-1} corresponding to transitions $^4T_{1g} \rightarrow {}^4T_{2g} \rightarrow {}^4T_{1g} \rightarrow {}^4T_{2g} \rightarrow {}^4A_{2g}$ and $^4T_{1g}$ (*P*) respectively. The 10 Dq and β values were found at 7690 cm^{-1} and 696.3 cm^{-1} respectively. The UV/VIS data suggests an octahedral geometry[21] around the metal ion. The magnetic moment value at 4.14 B.M.[22] of the complex also supports the octahedral geometry. The appearance of three bands in the electronic spectra of Ni (II) complex at 11130 cm^{-1}, 17115 cm^{-1} and 26265 cm^{-1} correspond to transitions $^3A_{2g} \rightarrow {}^3T_{2g}$, $^3A_{2g} \rightarrow {}^3T_{1g}$ and $^3T_{1g}$ (P) respectively. These transitions suggest an octahedral geometry[23] around the central metal ion which is also supported by its effective magnetic moment value al 3.18 B.M. The 10 Dq and β values were obtained at 11130 cm^{-1} and 666 cm^{-1} respectively.



Proposed structure of ligand (HMBCATCABT)



[Where M^{2+} = Co^{2+}, Ni^{2+}, Zn^{2+} and Cd^{2+}]

Proposed structure of metal complex

References

1. Dass, B., Patra, M. & Mahapatra, P.K. (1983) *J. Indian Chem. Soc.* **60** : 772.
2. Nishide, Y. & Kida, S. (1977) *Bull. Chem. Soc. Japan* **50** : 759.
3. Kansagra, B.P., Bhatt, H.H. & Parikh, A.R. (2000) *J. Inst. Chemists (India)* **72**: 68.
4. Srivastava, S.K., Srivastava, S. & Srivastava, S.D. (2001)J. *Indian Chem. Soc.* **78** : 320.
5. Livingston, S.E. (1971) *Coord. Chem. Rev.* 7 : 59.
6. Mahindra, A., Fischer, I.M. & Rabinovitz, M. (1983) *Nature (London)* **303** : 64.
7. Sharma, R.C., Varshney, V.K. & Ambwani,.J. (1992) *J. Indian Chem. Soc.* **69** : 772.
8. Gagne, R.R., Spiro, C.L., Smith. T.J., Hainnan, C.A., Thies, W.R. & Shiemke, A.K. (1981) *J. Am. Chem. Soc.* **102** : 4073.
9. Vogel, A.I. (1964) *A Text Book of Quantitative Inorganic Analysis*, Green & Co. Ltd., London.
10. Trendwell, F.P. (1968) *Analytical Chemistry*, John Wiley & Sons. London.
11. Dean, .J.A. (1978) *Lange's Hand book of Chemistry,* 12th Ed., McGraw-Hill International Editions, p. 801.
12. Mathis, F. (1953) *Bull. Chem. Soc.* **9D**: 22.
13. Bellamy, J. (1968)*Advance in Infra Red Group Frequencies*, Methuen & Co. Ltd.
14. Basseler, G.C. & Silverstein. R.M. (1992) *Spectrophotometric Identification of Organic Compounds,* 3rd Ed., Wiley, New York.
15. Singh, P.P., Shukla, U.P. & Seth, I.N. (1976) *Indian J. Chem.* **14A** : 689.
16. Prasad, N., Sahay, A. & Srivastava, A.K. (1990) *Proc. Nat. Acad. Sci. India* **60A** : 147.
17. Shakir, M. & Varkey, S.P. (1994) *Polyhedron* 13 : 941.
18. Bhattacharjee, M.N. & Dutta, R.N. (1985) *Inorg. Chem.* **24** : 4.
19. Jayaram, B. & Mayanna, S.M. (1983) *Tetrahedron* **39**: 2271.
20. Shakir, M., Varkey, S.P. & Kumar, D. (1994) *Synth. React. Inorg. Met. Org. Chem.* **24** : 941.
21. Pappalardo, P. (1984) *Phill. Mag.* **4** : 219.
22. Martin, L.Y. (1977) *J. Am. Chem. Soc.* **99**: 2968.
23. Panda, A.K. (1994) *J. Indian Chem. Soc.* **71**. 89.

PROC. NAT. ACAD. SCI. INDIA, 73 (A), III, 2003

Surface wave propagation through a cylindrical bore in a micropolar generalized thermoelastic medium without energy dissipation

RAJNEESH KUMAR and SUNITA DESWAL

Department of Mathematics, Kurukshetra University, Kurukshetra-136119. India.

Received February 12, 2000; Revised April 16, 2000; Accepted October 30, 2000

Abstract

The propagation of surface waves in a cylindrical cavity embedded in a micropolar generalized thermoelastic medium is discussed in two cases (i) the cylindrical bore is empty (ii) the cylindrical bore is filled with homogeneous inviscid liquid. The dispersion equation appropriate to the surface wave propagation near the surface of the cylindrical bore is obtained, characterizing the dispersive nature of _ the wave. Some special cases have been deduced. The numerical results obtained have been illustrated graphically to understand the behaviour of phase velocity versus wave number of the wave. Significant thermal and microrotational effects are observed.

(**Keywords :** surface wave propagation/micropolar/ generalized thermoelasticity)

Introduction

The problem of surface wave propagation near the bore hole in elastic host medium is of great practical importance. Since valuable organic and inorganic deposits beneath the earth's surface are difficult to detect by drilling randomly, the wave propagation technique is the simplest and most economic and does not require any drilling through the earth. Thermoelasticity theories which admit a finite speed for thermal signals (second sound) have aroused much interest in the last three decades. Recently relevant theoretical developments in the theory of thermoelasticity on the subject of .finite velocity of heat propagation are due to Green an Naghde[1-3], which provide sufficient basic modifications in the constitutive equations that permit treatment of a much wider class of heat flow problems. An important feature of this theory, which is not present in other thermoelasticity theories is that this theory does not accommodate dissipation of thermal energy.

"Micropolar elasticity" termed by Eringen[4] is used to describe deformation of elastic media with oriented particles. A micropolar continuum is a collection of interconnected particles in the form of small rigid bodies undergoing both

translational and rotational motions. Typical examples of such materials are granular media and multimolecular bodies, whose microstructures act as an evident part in their macroscopic responses. The physical nature of these materials needs an asymmetric description of deformation, while theories for classical continua fail to accurately predict their physical and mechanical behaviour. For this reason, micropolar theories were developed by Eringen[4-6] for elastic solids, fluids and further for non-local polar fields and are now universally accepted.

The linear theory of micropolar thermoelasticity was developed by extending the theory of micropolar continua to include thermal effects by Eringen[7] and Nowacki[8]. Different authors[9-14] discussed different type of problems in elasticity/ micropolar elasticity/micropolar generalized thermoelasticity. The present study is concerned with the problem of surface wave propagation in a micropolar generalized thermoelastic solid containing a cylindrical bore.

Problem Formulation and Solution

Case I-Propagation of Waves in cylindrical empty bore : Consider a cylindrical empty bore of radius 'a' having a circular cross-section in a homogeneous, isotropic micropolar generalized thermoelastic medium of infinite extent. We are studying the propagation of axial symmetric waves which are pure sinusoidal along the axial direction. Cylindrical polar co-ordinates (r, θ, z) are considered with z-axis pointing upwards.

We are discussing two-dimensional problem with symmetry about z-axis. Therefore, we have

$$\vec{u} = (u_r, 0, u_z), \qquad \vec{\phi} = (0, \phi_\theta, 0), \qquad \text{and } \frac{\partial}{\partial \theta} = 0 \tag{1}$$

where u_r, u_z and ϕ_θ are related in terms of potential functions ϕ' ψ and Γ as

$$u_r = \frac{\partial \phi'}{\partial r} + \frac{\partial^2 \psi}{\partial r \partial z}, u_z = \frac{\partial \phi'}{\partial z} - \left(\nabla^2 - \frac{\partial^2}{\partial z^2}\right)\psi, \phi_\theta = -\frac{\partial \Gamma}{\partial r} \tag{2}$$

Making use of eqn. (2) in the field equations derived by Eringen[7] and Green Naghdi[3] and then eliminating T and Γ from the resulting expressions, we obtain

$$[\square_2 \square_3 + K^2\nabla^2]\,[\psi] = 0 \tag{3}$$

and $$[\square_1 \square_4 - \eta\frac{\partial}{\partial t^2}\nabla^2]\,[\phi'] = 0 \tag{4}$$

where

$$\nabla^2 = \frac{\partial^2}{\partial r^2} + \frac{1}{r}\frac{\partial}{\partial r} + \frac{\partial^2}{\partial z^2}, \qquad \square_1 = (\lambda + 2\mu + K)\nabla^2 - \rho\frac{\partial^2}{\partial t^2},$$

$$\square_2 = (\mu + K)\nabla^2 - \rho\frac{\partial^2}{\partial t^2}, \qquad \square_3 = \gamma\nabla^2 - 2K - \rho j\frac{\partial^2}{\partial t^2},$$

$$\square_4 = \nabla^2 - \eta\frac{\partial^2}{\partial t^2}, \qquad \eta = \frac{\rho C^*}{K^*},\ \eta_1 = \frac{\upsilon^2 T_o}{K^*} \tag{5}$$

The time harmonic wave solutions of eqn. (3) and (4) are given by

$$\chi = \left[A_i K_0(q_m r) + A_i' K_0(q_n r)\right] e^{i(kz-\omega t)} \tag{6}$$

where $i = 1, 2, \ldots..$; $m = 1$, $n = 2$ and $i = 3, 4, \ldots\ldots..$; $m = 3$, $n = 4$, χ stands for ψ, Γ, ϕ' T and corresponding to them $i = 1, 2, 3, 4\ldots\ldots$ respectively. A_i and A'_1 ($i = 1, \ldots.,4$) are constants and

$$q_{1,2}^2 = k^2 - \frac{1}{2}\left[\left(\sigma_1^2 + \sigma_2^2 + \eta_2^2 - \eta_3^2\right) \mp \left\{\left(\sigma_1^2 - \sigma_2^2 - \eta_3^2 + \eta_2^2\right)^2 + 4\eta_2^2\sigma_2^2\right\}^{1/2}\right],$$

$$q_{3,4}^2 = k^2 - \frac{1}{2}\omega^2\left[\left(\eta + \frac{1}{c_1^2} + \frac{\eta_1}{\rho c_1^2}\right) \mp \left\{\left(\eta - \frac{1}{c_1^2} + \frac{\eta_1}{\rho c_1^2}\right)^2 + \frac{4\eta\eta_1}{\rho c_1^2}\right\}^{1/2}\right] \tag{7}$$

where

$$\sigma_1^2 = \frac{\omega^2}{c_4^2}, \quad \sigma_2^2 = \frac{\omega^2}{c_2^2}, \quad \eta_2^2 = \frac{K^2}{(\mu + K)\gamma}, \quad \eta_3^2 = \frac{2K}{\gamma},$$

$$c_1^2 = \frac{\lambda + 2\mu + K}{\rho},\ c_2^2 = \frac{\mu + K}{\rho},\ c_4^2 = \frac{\gamma}{\rho j} \tag{8}$$

The phase velocity of waves in the z-direction is denoted by c ($=\omega/k$), k is the wave number and ω being the circular frequency $K_0(\)$ is the modified Bassel function of second kind and zero order.

A_i and A_i' (i = 1, ...,4), are related as

$$A_i = b_{i-1}A_{i-1},\qquad A_i' = b_i A_{i-1}',\ \ i = 2, 4,..... \tag{9}$$

where

$$b_i = \left(k^2 - \sigma_2^2 - q_i^2\right)/p^*,\ \ b_j = \frac{\rho c_1^2}{\nu}\left[\frac{\omega^2}{c_1^2} - k^2 + q_j^2\right],$$

$$p^* = \frac{K}{(\mu + K)},\ i = 1, 2,\qquad j = 3, 4, \tag{10}$$

Boundary Conditions

The boundary conditions are the vanishing of stresses and temperature on the surface of the cylindrical bore *i.e.* at $r = a$

$$t_{rr} = t_{rz} = m_{r\theta} = \frac{\partial T}{\partial r} = 0 \tag{11}$$

where t_{rr}, t_{rz}, *and* $m_{r\theta}$ have been borrowed from the constitutive relations derived by Eringen[7] and Naghdi[3] given as

$$t_{rr} = \lambda u_{k,k} + (2\mu + K)\, u_{r,r} - \nu T, \tag{12}$$

$$t_{rz} = \mu(u_{r,z} + u_{z,r}) + K(u_{z,r} + \phi\theta), \tag{13}$$

$$m_{r\theta} = -\frac{\beta\phi_{\phi}}{r} + \frac{\gamma\partial\phi_{\theta}}{\partial r}. \tag{14}$$

Using the expression (12) – (14) along with eqn. (2), (6) and (9) in the boundary conditions (11), we shall obtain four homogenous equations in four unknows namely A_1, A_1', A_3'. A non-trivial solution for these unknowns would give the following frequency equation

$$\left[D_3 b_4 \frac{K_0(q_4 a)}{K_1(q_4 a)} - D_4 b_3 \frac{K_0(q_3 a)}{K_1(q_3 a)}\right](a_1 D_2 - a_2 D_1) -$$
$$(2\mu + K)^2 k^2 \left[q_3 b_4 \frac{K_0(q_4 a)}{K_1(q_4 a)} - q_4 b_3 \frac{K_0(q_3 a)}{K_1(q_3 a)}\right] \tag{15}$$
$$\left[D_2 q_1 \left\{\frac{K_0(q_1 a)}{K_1(q_1 a)} + \frac{1}{q_1 a}\right\} - D_1 q_2 \left\{\frac{K_0(q_2 a)}{K_1(q_2 a)} + \frac{1}{q_2 a}\right\}\right] = 0$$

where

$$D_i = b_i q_i \left[\frac{(\beta + \gamma)}{q_i a} + \gamma \frac{K_0(q_i a)}{K_1(q_i a)}\right], i = 1, 2,$$

$$D_j = \left[(\lambda + 2\mu + K)q_j^2 - \lambda k^2 - \nu b_j\right] \frac{K_0(q_j a)}{K_1(q_j a)} + \frac{(2\mu + K)q_j^2}{(q_j a)}, j = 3, 4,$$

$$a_i = \mu(k^2 + q_i^2) + K(b_i + q_i^2), i = 1, 2, \tag{16}$$

Eqn. (15) determines the phase velocity of axial symmetric surface waves as a functions of dimentionless wave number *ka*, indicating that the waves are dispersive in nature.

Physically, it must be expected that for every short wave length *i.e.* for large values of *ka*, the dispersion eqn. (15) should coincide with the dispersion equation for the Rayleigh type waves at ta plane boundary of micropolar for the Rayleigh type waves at a plane boundary of a micropolar generalized theremoelastic half-space. This can be done by putting $ka = \infty$ in eqn. (15). For large value of the argument, the asymptotic value of modified Bessel functions[15] is

$$K_0(u) = K_1(u) = \sqrt{\frac{\pi}{2u}}e^{-u}, \ (u \to \infty) \tag{17}$$

Hence eqn. (15) reduces to

$$\left(D_3'b_4 - D_4'b_3\right)\left(a_1D_2' - a_2D_1'\right) - \left(2\mu + K\right)^2 k^2 \left(q_3b_4 - q_4b_3\right)\left(D_2'q_1 - D_1'q_2\right) = 0 \tag{18}$$

where

$$D_i' = b_iq_i\gamma, \qquad D_j' = \left(\lambda + 2\mu + K\right)q_j^2 - \lambda k^2 - \nu b_j, \ i = 1, 2; \ j = 3, 4, \tag{19}$$

Special Chases (I) : Neglecting thermal effect *i.e.* taking $\nu = C^* = K^* = 0$ in eqn. (15) and (18), we obtain the following dispersion equations

$$D_3^0\left(a_1D_2 - a_2D_1\right) - \left(2\mu + K\right)^2 k^2 q_3^0$$

$$\left[D_2q_1\left\{\frac{K_0\left(q_1a\right)}{K_1\left(q_1a\right)} + \frac{1}{q_1a}\right\} - D_1q_2\left\{\frac{K_0\left(q_2a\right)}{K_1\left(q_2a\right)} + \frac{1}{q_2a}\right\}\right] = 0 \tag{20}$$

and

$$D_3^0\left(a_1D_2' - a_2D_1'\right) - \left(2\mu + K\right)^2 k^2 q_3^0\left(D_2'q_1 - D_1'q_2\right) = 0 \tag{21}$$

where

$$D_3' = \left(2\mu + K\right)q_3^{0^2}\left[\frac{K_0\left(q_3^0a\right)}{K_1\left(q_3^0a\right)} + \frac{1}{q_1a}\right] + \lambda\left(q_3^{0^2} - k^2\right)\frac{K_0\left(q_3^0a\right)}{K_1\left(q_3^0a\right)},$$

and

$$D_3^0 = \left(2\mu + K\right)q_3^{0^2} + \lambda\left(q_3^{0^2} - k^2\right), \ q_3^{0^2} = k^2\left[1 - \frac{c^2}{c_1^2}\right], \tag{22}$$

Eqn. (20) is the dispersion equation for the propagation of elastic waves in a cylindrical bore, through micropolar elastic medium of infinite extent and coincides with the eqn. (2.24) of Banerji and Sengupta[10] with the appropriate change in notations, Eqn. (21) coincides with the equation of Rayleigh waves at a plane boundary of microporal medium obtaining by Kaliski *et al*[16].

(II) If we neglect micropolar effect ($\alpha = \beta = \gamma = K = j = 0$) in eqns. (15) and (18), we obtain the period equation for a generalized thermoelastic medium containing cylindrical bore as

$$\mu\left(k^2 - q_1'^2\right)q_1'\left[B_3 b_4' \frac{K_0(q_4 a)}{K_1(q_4 a)} - B_4 b_3' \frac{K_0(q_3 a)}{K_1(q_3 a)}\right] - 4\mu^2 k^2 q_1'^2\left[\frac{K_0(q_1' a)}{K_1(q_1' a)} + \frac{1}{q_1' a}\right]\left[q_3 b_4' \frac{K_0(q_4 a)}{K_1(q_4 a)} - q_4 b_3' \frac{K_0(q_3 a)}{K_1(q_3 a)}\right] = 0 \tag{23}$$

and

$$\mu\left(k^2 - q_1'^2\right)\left(B_3' b_4' - B_4' b_3'\right) - 4\mu^2 k^2 q_1'^2\left(q_3 b_4' - q_4 b_3'\right) = 0 \tag{24}$$

where

$$B_j = 2\mu q_j^2\left[\frac{K_0(q_j a)}{K_1(q_j a)} + \frac{1}{q_j a}\right] + \left[\lambda\left(q_j^2 - k^2\right) - \nu b_j'\right]\frac{K_0(q_j a)}{K_1(q_j a)}, \qquad j = 3, 4$$

$$B_j' = \left[2\mu q_j^2 + \lambda\left(q_j^2 - k^2\right) - \nu b_j'\right], \quad j = 3, 4,$$

$$b_j' = \frac{\rho c_1^*}{\nu}\left[\frac{\omega^2}{c_1^*} - k^2 + q_j^2\right], \quad j = 3, 4, \; c_1^* = \frac{\lambda + 2\mu}{\rho}$$

$$q_1'^2 = k^2\left(1 - \frac{c^2}{c_2^*}\right), \qquad c_2^* = \frac{\mu}{\rho} \text{ and}$$

$q_{3,4}^2$ are again given by equation (7), only with replacement of c_1^2 by c_1^*.

(III) Neglecting micropolar and thermal effects together in the medium considered, one can obtain the eqn. (2.26) and (2.27) of Banerji and Sengupta[10] and represent the dispersion equation obtained by Biot[9] for the propagation of elastic waves in borehole.

Case II-Propagation of waves in a cylindrical bore filled with liquid : Here we consider that the cylindrical bore is filled with homogeneous inviscid liquid. For axially symmetric waves, the displacement potential ϕ_0 in the liquid satisfies the wave equation

$$\nabla^2\phi_0 = \frac{1}{c_3^2}\frac{\partial^2\phi_0}{\partial t^2}$$

where $c_3^2 = \lambda_0/\rho_0$ is the velocity of dilatational wave in liquid ; ρ_0, λ_0 are the density and bulk modulus of the liquid respectively. The solution of eqn. (26) corresponding to the surface wave may be written as

$$\phi_0 = A_5 I_0(r\xi)e^{i(kz-\omega t)}, \text{ for } c < c_3 \tag{27}$$

where $\xi^2 = k^2 - \frac{\omega^2}{c_3^2}$ and I_0 () is the modified Bessel function of first kind and order zero. Notating $y=c/c_3$, the liquid pressure and radial displacement respectively are (for $y < 1$)

$$p = \rho_0\omega^2 A_5 I_0\left[rk\left(1-y^2\right)^{1/2}\right]e^{i(kz-\omega t)} \tag{28}$$

$$q_r = k\left(1-y^2\right)^{1/2} A_5 I_1\left[rk\left(1-y^2\right)^{1/2}\right]e^{i(kz-\omega t)} \tag{29}$$

Boundary conditions : The appropriate boundary conditions at the interferace $r = a$ between liquid and micropolar generalized thermoelastic medium are

$$q_r = u_r, \quad -p = t_{rr}, \quad t_{rz} = m_{r\theta} = \frac{\partial T}{\partial r} = 0 \tag{30}$$

The first two boundary conditions can be written as

$$\frac{-p}{q_r} = \frac{t_{rr}}{r_r},$$

which is a composite boundary condition to the matching of mechanical impedance. The last three boundary conditions are same as in Case I. These three boundary conditions and boundary condition (31) with the use of eqns. (6), (9), (12) – (14), (28), (29) give four equations in four unknowns namely A_1, A'_1, A_3 and A'_3. Fro non-trivial solution of these four homogenous equations, we must have the determinant of the co-efficient of the unknowns equal to zero, which yields (for $y < 1$).

$$\left[D_3^* b_4 \frac{K_0(q_4 a)}{K_1(q_4 a)} - D_4^* b_3 \frac{K_0(q_3 a)}{K_1(q_3 a)}\right](a_1 D_2 - a_2 D_1) - (2\mu + K)^2 k^2 \left[q_3 b_4 \frac{K_0(q_4 a)}{K_1(q_4 a)} - q_4 b_3 \frac{K_0(q_3 a)}{K_1(q_3 a)}\right] D_5 = 2 \tag{32}$$

where

$$D_j^* = D_j - mq_j \qquad j = 3, 4,$$

$$D_5 = \left[D_2 q_1 \left\{\frac{K_0(q_1 a)}{K_1(q_1 a)} + \frac{1}{q_1 a}\right\} - \frac{MD_2}{(2\mu + K)}\right] - \left[D_1 q_2 \left\{\frac{K_0(q_2 a)}{K_1(q_2 a)} + \frac{1}{q_2 a}\right\} - \frac{MD_1}{(2\mu + K)}\right]$$

$$M = \frac{\rho_0 \omega^2}{k(1 - y^2)^{1/2}} \frac{I_0\left[ak(1 - y^2)^{1/2}\right]}{I_1\left[ak(1 - y^2)^{1/2}\right]}. \tag{33}$$

If thermal effect is neglect then it can be verified that dispersion eqn. (32) recuces to that obtained by Banerje and Sengupta[10] for the relevant problem in micropolar elastic medium.

In the absence of microrotation effect , eqn. (32) reduces to the dispersion equation for surface wave propagation in a generalized thermoelastic medium containing a cylindrical bore hole (filled with inviscid liquid) as

$$\mu\left(k^2-q_1'^2\right)q_1'\left[B_3^*b_4'\frac{K_0(q_4a)}{K_1(q_4a)}-B_4^*b_3'\frac{K_0(q_3a)}{K_1(q_3a)}\right]-$$
$$4\mu^2k^2q_1'^2\left[\frac{K_0(q_1'a)}{K_1(q_1'a)}+\frac{1}{q_1'a}-Mq_1'\right]\left[q_3^*b_4'\frac{K_0(q_4a)}{K_1(q_4a)}-q_4^*b_3'\frac{K_0(q_3a)}{K_1(q_3a)}\right] \tag{34}$$

where

$$B_j^* = B_j - Mq_j \qquad j = 3, 4,$$

Numerical Results and Discussions

In order to study the problem numerically, frequency eqn. (15) and (32) are solved for phase velocity C_o = (c/c_1) by giving different values of wave number in non-dimensional form (ka) to study the thermal and microrotation effects on dispersion equation. we take the case of magnesium crystal[17] like material subject to thermal disturbance for numerical calculations. The physical constants used are

$\rho = 1.74$ g/cm^3, $j = 0.2 \times 10^{-15}$ cm^2, $\lambda = 9.4 \times 10^{11}$ dyne/cm^2

$\mu = 4.0 \times 10^{11}$ dyne/cm^2, $K = 1.0 \times 10^{11}$ dyne/cm^2

$\gamma = 0.779 \times 10^{-4}$ dyne, $K^* = 1.0005$ cal dyne/g °C cm^2

$C^* = 0.23$ cal/g °C, $\epsilon = 0.073$, $\nu = 0.89$ dyne/cm^2 °C,

$T_0 = 23$ °C.

The following values are taken from Ewing *et al.*[18] for inviscid liquid :

$\lambda_0 = .214 \times 10^{11}$ dyne , $\rho_0 = 1.0$ g/cm^3.

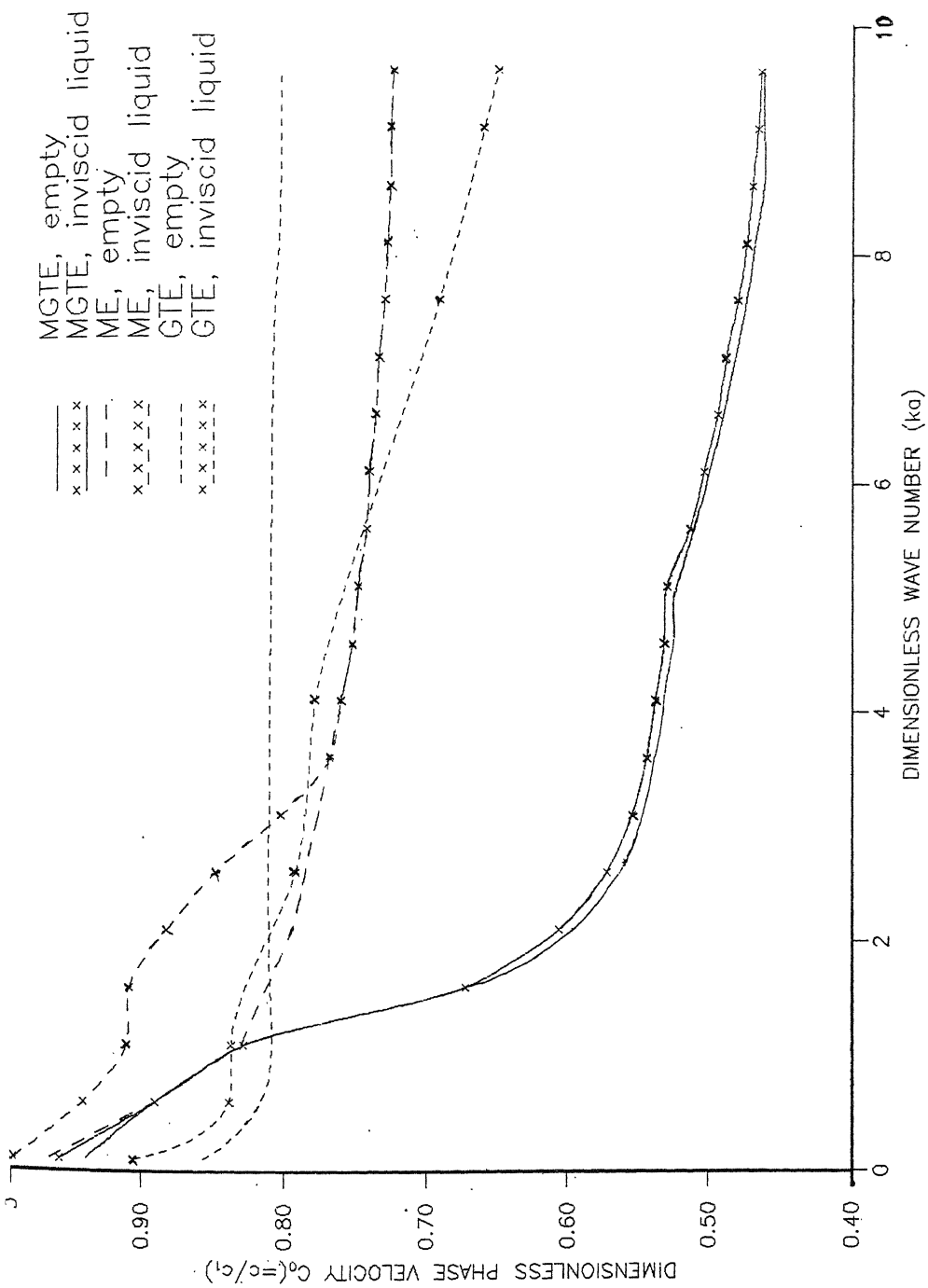


Fig. 1–variations of phase velocity with wave number.

For the above values of relevant parameters, we have calculated the normalized phase velocity C_0 against the values of normalized wave number ka, as depicted in Fig. 1. It is found that there exist infinite number of modes of propagation of surface waves for various values of wave numbers; the variations of only fundamental modes are presented graphically. These variations of phase velocity in micropolar generalized thermoelastic (MGTE) medium, generalized thermoelastic (GTE) medium and micropolar elastic (ME) medium are shown by (a) solid line (——), small dashed line (-----) and long dashed line (– – –) respectively in case of empty bore. (b) solid line with centre symbols (–×–×–×–), small dashed line with centre symbols (-× -× -×) and long dashed line with centre symbols (–× –× –×)respectively in case when bore is filled with inviscid liquid.

From Fig. 1, it is observed that in MGTE medium, the phase velocity decreases gradually with the increase in wave number as depicted by the two curves, one solid and other with centre symbols, also indicating that the effect of liquid is very small in this medium , If, micropolarity is neglected *i.e.* in GTE medium, the values of phase velocity are large but the variations lie in a very small range in comparison to MGTE medium as can be seen by the two curves; one small dashed and other with centre symbols, also characterising the significant effect of liquid in GTE medium. In the absence of thermal effect i.e. in ME medium, a similar trend i.e. decrease in phase velocity with the increase in wave number is observed and the values of phase velocity are large in comparison to MGTE medium. Since the difference in the values of phase velocity in ME medium for the cases of empty bore and liquid filled bore is very minute in the range $3.6 < ka < 9.6$, therefore the effect of liquid is not visible from Fig. 1 in this range.

One of the interesting phenomenon observed on comparison of the various curves in fig. 1 is that the values of phase velocity become large after the removal of microrotational or thermal effects from the medium, although the behaviour of variations is similar in all the curves. Also, the effect of inviscid liquid present in the bore hole on propagation of surface waves is more significant in ME and GTE medium in comparison to MGTE medium. This effect can be seen on comparing the three curves with centre symbols and the corresponding three curves without centre symbols in Fig. 1.

References

1. Green, A.E. & Naghdi, P.M. (1991) *Proc. Roy Soc. London Sere* A **32** : 171.
2. Green, A.E. & Naghdi, P.M. (1992) *J. of Thermal Stresses* **15** : 253.

3. Green, A.E. & Naghdi, P.M. (1993) *J. Elasticity* **31** : 189.
4. Eringen, A.C. (1966) *J. Math. Mech.* **15** : 909.
5. Eringen, A.C. (1966) *J. Math. Mech.* **16** : 1.
6. Eringen, A.C. (1976) *Non-local Polar Field Theories, in Continuum Physics,* Vol. IV, Academic Press, New York, p. 205.
7. Eringen, A.C. (1970) *Foundation of Micropolar Thermoelasticity,* Course of lectures No. 23, CISM Udine, Springer.
8. Nowacki, W. (1966) *Couple Stresses in thetheory of Thermoelasticity,* Proc. IUTAM Symposia, Vienna, Springer - Verlag, p. 259.
9. Biot, M.A. (1952) J. *Appl. Phys.* **23** : 997.
10. Banerji,. D.K. & Sengupta, P.R. (1977) *Bull. Acad. Polon. Sci.* Sere SC1. Techn. **25** : 257
11. Aron, M. & Chirita, S. (1997) *Arch. Mech.* **49** : 665.
12. Cheng, Z-Q. & He, L.-H. (1997) *Int. J. Eng. Sci.* 35 : 659.
13. Tomar, S.K. & Kumar, R. (1999) *Proc. Indian Acad. Sci. (Math. Sci.)* **109** : 425.
14. Singh, B. & Kumar, R. (1998) *Int. J Engng. Sci.* **36** : 865.
15. Andrews, L.C. (1992) *Special Functions of Mathematics for Engineers*; Mc-Graw Hill Inc., New York.
16. Kaliski, S., Kapelewski, J. & Rymarz, C. (1968) *Proc. Vib. prohL,* **9.** : 108.
17. Eringen, A.C. (1984) *Int. J. Engng. Sci.* **22** : 1113.
18. Ewing, W.M., Jardetzky, W.S. & Press, F. (1957) *Elastic Waves in Layered Media,* Mc-Graw Hill, New York.

PROC. NAT. ACAD. SCI. INDIA, 73 (A), III, 2003

A special type of topology in the plane

M.P. CHAUDHARY[1*], MOHAMMED ABDEL KARIM[1&2] and QAYS OMARI

[1]*Department of Mathematics, University of Delhi, Delhi-110007, India.*

[2]*Department of Mathematics, University of Delhi, Delhi-110007, India; and Ministry of Education, Ref. No. 76916, Amman Jordan*

[3]*Department of Physics & Astrophysics, University of Delhi, Delhi-110007, India.*

**Correspondence Address : 181, Jubilee Hall, University of Delhi, Delhi-110 007, India Email: mp_chaudhary2000@yahoo.co.in*

Received February 8, 2001; Accepted December 10, 2002

Abstract

In this paper we study a special type of topology and its property in the plane, called Sun Topology.

(**Keywords** : sun topology/density topology)

Introduction

We know that there are three well known topologies in the plane (Euclidean topology, Fine topology, Usual density topology) are linearly ordered. The fine topology is strictly finer than Euclidean topology, and has several useful geometric properties which disappear when use switch to the finer density topology.

Definition : The Lebesgue measurable set A in the complex plane is said to be sun open if every $x \in A$ for almost every $\alpha \in [0, 2\pi] \ni t_\alpha > 0 : \{z \in C : z = x + t(\cos\alpha + i \sin\alpha), |t| < t_\alpha\} \subset A$.

Lemma : The density topology is strictly finer than the sun topology.

Proof : Let a set A be sun open at x. For each $r > 0$ denoted by B_r the set of all $\beta \in [0, 2\pi]$ for which $\{z \in C : z = x + t(\cos\beta + i \sin\beta), |t| < r\} \subset A$. We see that $\lambda(B_r) \to 2\pi$ for $r \to 0$, hence

$$\frac{\lambda[(A\cap D)(x,r)]}{\lambda D(x,r)} \geq \frac{\lambda(B_r)}{2\pi} \to A \text{ for } r \to 0$$

Hence x is a point of density of A. The set A density open at x. Hence the density topology is finer than the sun topology. Again let the set $C - \{z \in C : 1/|z| \in N\}$ is density open at 0 and is not sun open at 0. Hence the density topology is strictly finer than the sun topology.

Result : Now we introduce the fine topology from potential theory in the plane. If we denote for an arbitrary point $x \in C$, a set $A \subset C$ and $n \in N$ then

$$A_n = \{z \in C\backslash A,\ 1/2^n \leq |z - x|,\ 2/2^n\}.$$

We can characterize points x at which a set is finely open as those for which the series

$$\sum_{n=1}^{\infty} \frac{-n}{\log \mathrm{Cap}\,[A_n(x)]}$$

converges (by Wierer's test), where Cap denotes the outer logarithmic Capacity [1, see theorem 9, 10].

Theorem : The sun topology is strictly finer than the fine topology.

Proof: Let us consider $0 \in A$ and A is finely open at 0. We now restrict to $K = \{z = x + iy \in C : x \geq 0, y \geq 0\}$ and we show that for almost every $\alpha \in [0, \pi/2]$ $\ni t_\alpha > 0 : \{z \in K : z = t(\cos\alpha + i \sin\alpha),\ 0 \leq t \leq t_\alpha\} \subset A$. for $n \in N$.

let

$$A_n = \{z \in K - A,\ 1/2^n \leq |z| < 2/2^n\}.$$

Let $B_n = p(A_n)$, where p is the projection from the origin on the line through the points $[1/2^n, 0]$ and $[0, 1/2^n]$ also let $C_n = R(A\text{-}n)$, where R is the projection from the origin on the circle $\{z \in C : |z| \in 1/2^n\}$, then the outer logarithmic capacity increases under contractions, now $\mathrm{Cap}(B_n) \leq \mathrm{Cap}(A_n)$ for the measurable liner set B_n we can use the estimate. The linear Lebague measure on the line through the points $[1/2^n, 0]$ and $[0,$

$1/2^n]$ by $\lambda(B_n) \leq 4\ \mathrm{Cap}(B_n)$ [2, see page 173]. There is a simple Lipschitz mapping from $B_n \to C_n$. Hence the linear Lebesgue measure of C_n on the circle $\{z \in C : |z| = 1/2^n\}$, is estimated by $\lambda(C_n) \leq 2\lambda(B_n)$. The set is finely open at 0, hence the series

$$\sum_{n=1}^{\infty} \frac{-n}{\log \mathrm{Cap}(A_n)} \text{ converges.}$$

Now we conclude that the series

$$\sum_{n=1}^{\infty} \frac{-n}{\log \lambda(C_n)} \text{ converges.}$$

We know that $\lambda(C_n) \in [0, \pi/2^{n+1}]$. Each point at C_N stops the radius from the origin at the distance $1/2^n$. The measure of the angles which stop at C_n is $q_n = 2^n\lambda(C_n)$. We show that $\Sigma_{n=1}^{\infty} q_n$ converges. We see that the measure of angles in $[0, 2/\pi]$ which stop at same distance due to C_n (Also $A_n\}$ for $n \geq m$ is smaller than $\Sigma_{n=1}^{\infty} q_n$. Hence arbitrarily small for m big enough. Hence almost every angle at $[0, 2/\pi]$ stops at same positive distance. The set A is sun open at 0. The set $C\text{-}R^+$ is obviously sun open at origin and is not finely open at the origin due to the fact that each finely open set contains with any point arbitrarily small circles centered at the point [3, see theorem 10.14]. The sun topology is strictly finer than the fine topology.

Remark : The sun topology under the name the core topology, almost everywhere, was already studied byHorbaczewska [4, see page 416], it has quite recently been proved by Wagner-Bojakowsak and Wilczynski [5, see theorem 2, page 363].

References

1. Brelot, M.(1971) *On Topologies and Boundries on Potential Theory*, Lecture Notes in Mathematics, No. 175, Springer, Berlin.
2. Landkof, N.S. (1972) *Fondation of Modern Potential Theory*, Springer-Verlag, Berlin.
3. Helms, L.L. (1969) *Introduction to Potential Theory*, Wiley Interscience pure and applied mathematics, 22, New York.
4. Horbaczewska, G. (1994/95) *Real Anal. Exchange* **20(2)** : 416.
5. Wagner-Bojakowsak, E. & Wilczynski, W. (1998) *Atti. Sem. Univ. Modena* **46** : 369.

PROC. NAT. ACAD. SCI. INDIA, 73 (A), III, 2003

A comparative study of the effects of anisotropy, blood flow and evaporation on temperature distribution in three dimensional regions of human skin and subcutaneous tissues with tetrahedral elements

D. S. PAL and SUSHMA PAL

Department of Mathematics and Statistics, Punjab Agricultural University, Ludhiana-141004, Punjab, India.

Received Sep. 21, 2000; Accepted May. 9, 2001

Abstract

A tetrahedral finite element based mathematical model has been developed to obtain the effects of anisotropy on the temperature distribution (TD) in three dimensional regions of human skin and subcutaneous tissues (SST). Galerkin's finite element technique has been used to compute steady state nodal temperatures for a comparative study of the effects of anisotropy, isotropy, blood flow, metabolic heat generation and evaporation by considering eleven different combinations of these parameters. It has been found that fall of temperature due to evaporation is more in isotropic medium than that of in an isotropic medium. The study also attributes that not only evaporation brings down the temperature of SST region, but similar role is also played by the components of thermal conductivity taken highest in the direction of width or length of SST. The study may be useful in formulating sophisticated mathematical models for the heat flow problems with tumours.

(**Keywords** : anisotropic skin/blood flow/tetrahedral element/Galerkin's finite element.)

Introduction

All animals/human beings live in variable thermal environment with varying internal metabolic heat generation. They are able to maintain a stable internal temperature at level which is generally above that of the environment. The thermal gains and losses vary with different parameters participating at different levels and times. Heat migration in human skin and subcutaneous tissues (SST) is the consequence of blood flow, metabolism and environmental conditions. Heat generation and its loss to the environment are the continuous processes in human body. Blood flow plays a vital role in carrying excessive heat from the body to the

skin surface where it is given off to keep the core temperature constant within narrow limits. The skin consists of two layers known as epidermis and dermis. The outer dead layer of epidermis, the stratum corneum, is composed of flattened cells. The dermis, which is the deeper and thicker of the two major layers of the skin, is composed of matted masses of connective tissues and elastic fibres through which pass numerous blood capillaries and nerves. The subcutaneous tissues, which attach the skin with the rest of the body, contain fat cells, connective tissues, larger blood vessels, lymph vessels and nerves. The thermal characteristic of tissues plays a very important role in heat regulation in SST subjected to external surrounding conditions and variable metabolic activity.

Various mathematical models for computing temperature distribution in SST regions have been developed by many investigators. Pennes[1] formulated an energy equation for living human tissues by idealizing the human forearm as a cylinder excluding the axial and angular effects. Gordon and Roemer[2] studied the effects of radial node spacing on finite difference calculations of temperature in living tissues. The thermal recovery of skin temperature after cooling has been studied by Stekette and Vender Hoek[3]. The SST was considered as a single region in these models with constant values of biophysical parameters like blood flow, metabolic heat generation and thermal conductivity. These models were oversimplified version of the multilayered nature of SST region with variable biophysical parameters. Saxena[4], Saxena and Pal[5], and Pal and Pal[6-8] developed improved multilayered one dimensional (1-D) mathematical models with heterogeneous variation of biophysical parameters and studied the temperature pattern in human SST under various environmental and physiological conditions. 2-D mathematical models for the steady state temperature distribution of SST region with triangular finite elements were developed by Arya and Saxena[9] and Pal and Pal[10]. The two dimensional mathematical model[10] revealed that the temperature profiles reflect the dependence of temperature distribution not only on the environmental conditions and biophysical parameters but also on the geometry of the SST region. Pardasani and Adlakha[11] investigated steady state temperature distribution in annular tissue layers of a human or animal body by applying cubic spline technique. In a later work, Pardasani and Adlakha[12] used coaxial elements to study radial and angular heat distribution problem in human limbs by considering core temperture variable in angular direction. It has been found that coaxial elements reduce computational work of the finite element technique in comparison to triangular elements. All these studies are confined to one and two dimensional models only. The difference between various multilayered mathematical models was of the number of layers and sublayers into which SST was divided according to the geometry and behaviour of biophysical parameters. Crisp[13] and Stolwijk[14] have discussed the

properties of SST region and suggested that it exhibits anisotropic behaviour. This aspect has not been addressed by the previous investigators. To understand the complete effect of anisotropy on temperature distribution, three dimensional mathematical models of SST region are required to be formulated.

In the present work, a 3-D mathematical model of anisotropic SST region has been developed by dividing the region into tetrahedral finite elements. Heterogeneous variation in biophysical parameters like blood flow, metabolic heat generation and thermal conductivity have been considered for computing the steady state nodal temperatures by Galerkin's finite element technique. Eleven different combinations of anisotropy, blood flow, metabolic heat generation and evaporation have been considered to study and compare their effects on temperature distribution in three dimensional SST. Such studies may be useful to medical scientists in formulating advanced mathematical models for the detection and diagnosis of tumours.

Mathematical Model

It T denotes the temperature at any point (x,y,z) of SST region which is assumed to be anisotropic, the governing bioheat equation for the steady state case is

$$k_x(\partial^2 T/\partial x^2)+k_y(\partial^2 T/\partial y^2)+k_z(\partial^2 T/\partial z^2)+w_b c_b(T_b-T)+Q=0 \qquad (1)$$

where k_x, k_y, k_z = thermal conductivities of the tissues in x(width), y(length) and z (thickness) directions respectively; w_b = rate of blood mass flow; c_b = specific heat of blood; Q = rate of metabolic heat generation and T_b = temperature of blood when it enters the tissue compartment. Let a and b the width and length respectively of SST under consideration. The thicknesses of epidermis, dermis and subcutaneous tissues are considered to be c_1, c_2, c_3 respectively. The total thickness 'c' of SST can be expressed as

$$c=\sum_{i=1}^{3} c_i \qquad (2)$$

If R, D and S_i (i=1-6) are the region, domain and the boundary respectively, then

$$R=D+\sum_{i=1}^{6} S_i \qquad (3)$$

where $S_1 : z = 0$; $S_2 : z = c$, $S_3 : y = 0$, $S_4 : y = b$, $S_5 : x = 0$; $S_6 : x = a$.

Each layer of SST has been divided into six, eight cornered, blocks by trisecting and bisecting its length and width respectively (Fig. 1). Each block is further divided into five tetrahedral elements[15] as shown in Fig. 2. Thus, whole of SST has been discretized into 90 tetrahedral elements which are connected to each other by forty eight nodes. Details of these blocks and their respective node and tetrahedral element numbers have been given in Table 1.

Table 1– Blocks, their respective node numbers and tetrahedral element numbers

Block Nos.	Node Nos.								Tetrahedral Element Nos.
1	1	2	5	4	7	8	11	10	1-5
2	4	5	14	13	10	11	20	19	6-10
3	13	14	17	16	19	20	23	22	11-15
4	2	3	6	5	8	9	12	11	16-20
5	5	6	15	14	11	12	21	20	21-25
6	14	15	18	17	20	21	24	23	26-30
7	7	8	11	10	25	26	29	28	31-35
8	10	11	20	19	28	29	38	37	36-40
9	19	20	23	22	37	38	41	40	41-45
10	8	9	12	11	26	27	30	29	46-50
11	11	12	21	20	29	30	39	38	51-55
12	20	21	24	23	38	39	42	41	56-60
13	25	26	29	28	31	32	35	34	61-65
14	28	29	38	37	34	35	44	43	66-70
15	37	38	41	40	43	44	47	46	71-75
16	26	27	30	29	32	33	36	35	76-80
17	29	30	39	38	35	36	45	44	81-85
18	38	39	42	41	44	45	48	47	86-90

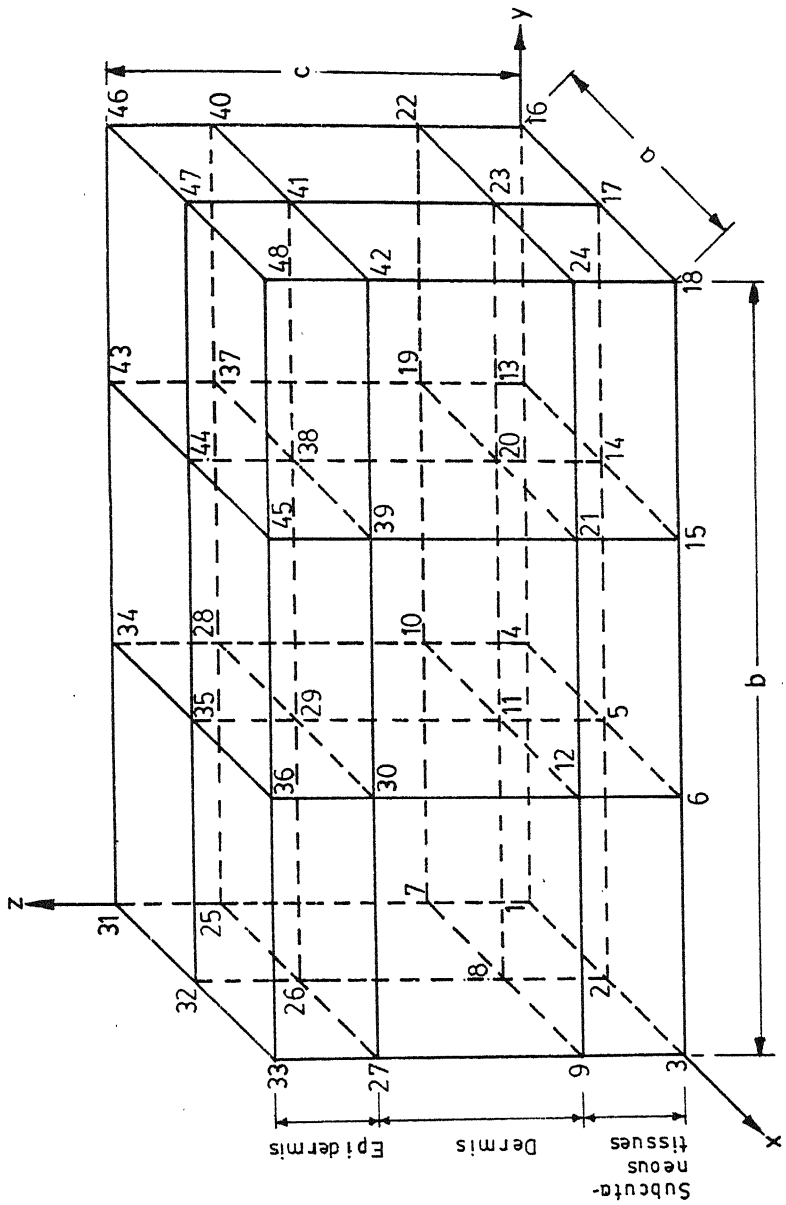


Fig. 1–Division of SST region into eighteen-eight cornered blocks.
Numbers indicate node numbers.

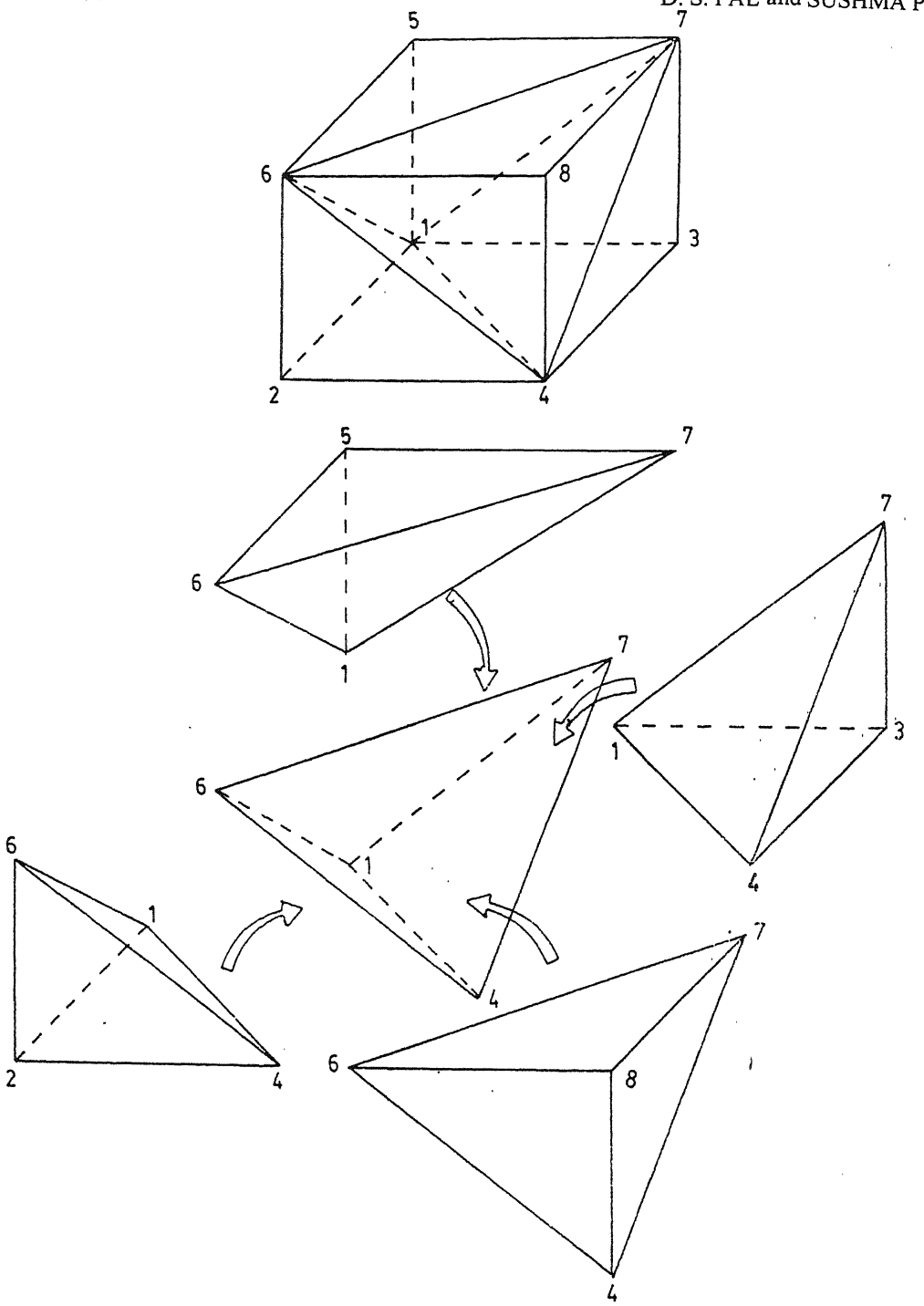


Fig. 2–Division of a master block into five tetrahedral elements

It is assumed that (i) S_1 coincides with the body core (ii) S_2 is exposed to the air environment and loss of heat is due to convection, radiation and evaporation of sweat (iii) surfaces S_i (i = 3-6) are insulated. Thus, we have

$$T(x, y, 0) = 37\ ^\circ\text{C}, \tag{4}$$

$$k_z(\partial T/\partial z)=h(T-T_a) + E, \text{ at } z = c, \tag{5}$$

where h = heat transfer coefficient, E = evaporative heat loss,

$$k_y(\partial T/\partial y) = 0 \text{ on } S_3 \text{ and } S_4, \tag{6}$$

$$k_x(\partial T/\partial x) = 0 \text{ on } S_5 \text{ and } S_6,$$

The evaporative heat loss E is calculated from the following equation :

$$E = \lambda. \text{ rate of evaporation of water}, \tag{7}$$

where λ = latent heat of vaporization of water.

The trial temperature $T^{(e)}$ within a typical tetrahedral element 'e', whose node identifiers $p(x_p, y_p, z_p)$, $q(x_q, y_q, z_q)$, $r(x_r, y_r, z_r)$ and $s(x_s, y_s, z_s)$, are taken in a counterclockwise direction, is assumed to be

$$T^{(e)} = \mathbf{N}^{(e)}(x,y,z)\ \mathbf{T}^{(e)}, \tag{8}$$

where

$$\mathbf{N}^{(e)}(x,y,z) = [N_p(x,y,z)\ N_q(x,y,z)\ N_r(x,y,z)\ N_s(x,y,z)], \tag{9}$$

$$\mathbf{T}^{(e)} = [\ T_p\ T_q\ T_r\ T_s] \tag{10}$$

$\mathbf{N}^{(e)}$ and $\mathbf{T}^{(e)}$ are shape function and nodal matrix respectively, Prime denotes the transpose of the vector.

Substitution of trial solution (8) into equation (1) (after rewriting it for the element 'e') results into a residual. The minimization of this residual with the help of

orthogonality conditions with respect to the basis function produces the following set of integrals. :

$$I^{(e)}=\left\langle k_x^{(e)}(\partial^2 T^{(e)}/\partial x^2)+k_y^{(e)}(\partial^2 T^{(e)}/\partial y^2)+k_z^{(e)}(\partial^2 T^{(e)}/\partial z^{(2)})\right.$$

$$\left.+w_b^{(e)}c_b^{(e)}(T_b-T^{(e)})+Q^{(e)},N_j\right\rangle=0 \tag{11}$$

where $j = p, q, r, s$. Green's theorem converts the equation (11) into the following form :

$$-\left\langle k_x^{(e)}(\partial T^{(e)}/\partial x),(\partial N_j/\partial x)\right\rangle-\left\langle k_y^{(e)}(\partial T^{(e)}/\partial y),(\partial N_j/\partial y)\right\rangle-$$

$$\left\langle k_z^{(e)}(\partial T^{(e)}/\partial z),(\partial N_j/\partial z)\right\rangle-\left\langle w^{(e)}T^{(e)},N_j\right\rangle+\int_{s^{(e)}}\int\left[k_x^{(e)}(\partial T^{(e)}/\partial x)+\right.$$

$$\left.k_y^{(e)}(\partial T^{(e)}/\partial y]+k_z^{(e)}(\partial T^{(e)}/\partial z)\right]N_j ds^{(e)}+\left\langle w^{(e)}T_b,N_j\right\rangle+\left\langle Q^{(e)},N_j\right\rangle=0 \tag{12}$$

where $w^{(e)} = w_b^{(e)}c_b^{(e)}$

Combining (8), (9) and (12) and imposing the Cauchy boundary conditions (5) and (6), we get

$$-\left\langle k_x^{(e)}\mathbf{T}^{(e)}(\partial N_i/\partial x),(\partial N_j/\partial x)\right\rangle-\left\langle k_y^{(e)}\mathbf{T}^{(e)}(\partial N_{(i)}/\partial y),(\partial N_j/\partial y)\right\rangle-$$

$$\left\langle k_z^{(e)}\mathbf{T}^{(e)})\partial N_i/\partial z),(\partial N_j/\partial z)\right\rangle+\left\langle w^{(e)}T_b,N_j\right\rangle-\left\langle w^{(e)}\mathrm{T}^{(e)}N_i,N_j\right\rangle+\left\langle Q^{(e)},N_j\right\rangle-$$

$$\int_{s_2^{(e)}}\int N_j[h(N_i\mathbf{T}^{(e)}-T_a)+E]ds_2^{(e)}=0;$$

$$i, j = p, q, r, s. \tag{13}$$

The above equation can be written in the matrix form as

$$\sum_{m=1}^{3}[\mathbf{K}_m^e]T^{(e)} = \sum_{m=1}^{3}\mathbf{P}_m^{(e)}, \tag{14}$$

where

$$\left[\mathbf{K}_1^{(e)}\right] = \left\langle k_x^{(e)}(\partial N_i/\partial x),(\partial N_j/\partial x)\right\rangle + \left\langle k_y^{(e)}(\partial N_i/\partial y),(\partial N_j/\partial y)\right\rangle +$$

$$\left\langle k_z^{(e)}(\partial N_i/\partial z),(\partial N_j/\partial z)\right\rangle;$$

$$\left[\mathbf{K}_2^{(e)}\right] = \left\langle w^{(e)}N_i, N_j\right\rangle; \quad \left[\mathbf{K}_3^{(e)}\right] = \int_{s_2^{(e)}} \int hN_iN_j\, ds_2^{(e)}; \mathbf{P}_1^{(e)} = \left\langle w^{(e)}T_b, N_j\right\rangle;$$

$$\mathbf{P}_2^{(e)} = \langle Q^{(e)}, N_j\rangle; \ \mathbf{P}_3^{(e)} = \int_{s_2^{(e)}} \int [hT_a - E]N_j ds_2^{(e)}; \ i, j=p, q, r, s. \tag{15}$$

The function N_j is unity at the no 'j' and zero at all the other nodes and can be expressed as

$$N_j(x,y,z)=(a_j+b_jx+c_jy+d_jz)/6V^{(e)}, \ j=p,q,r,s, \tag{16}$$

where

$$V^{(e)}=\begin{vmatrix} 1 & x_p & y_p & z_p \\ 1 & x_q & y_q & z_q \\ 1 & x_r & y_r & z_r \\ 1 & x_s & y_s & z_s \end{vmatrix} = \text{Volume of tetrahedron pqrs}, \tag{17}$$

$$a_p=\begin{vmatrix} x_q & y_q & z_q \\ x_r & y_r & z_r \\ x_s & y_s & z_s \end{vmatrix}, \qquad b_p=-\begin{vmatrix} 1 & y_q & z_q \\ 1 & y_r & z_r \\ 1 & y_s & z_s \end{vmatrix},$$

$$c_p=-\begin{vmatrix} x_q & 1 & z_q \\ x_r & 1 & z_r \\ x_s & 1 & z_s \end{vmatrix}, \qquad d_p=-\begin{vmatrix} x_q & y_q & 1 \\ x_r & y_r & 1 \\ x_s & y_s & 1 \end{vmatrix} \tag{18}$$

Other constants are obtained through a cyclic permutation of subscripts p,q,r and s. Equations (17)-(18) are valid only when the nodes p,q and r are numbered in a counterclockwise manner when viewed from the node 's'. The simplification of the above integrals yields the following matrices for the element 'e' :

$$\left[\mathbf{K}_1^{(e)}\right]=\left(1/36V^{(e)}\right)\begin{bmatrix} g_{11} & g_{12} & g_{13} & g_{14} \\ & g_{22} & g_{23} & g_{24} \\ & \text{symmetric} & g_{33} & g_{34} \\ & & & g_{44} \end{bmatrix};$$

$$\left[\mathbf{K}_2^{(e)}\right]=\left(w^{(e)}V^{(e)}/12\right)\begin{bmatrix} 2 & 1 & 1 & 1 \\ 1 & 2 & 1 & 1 \\ 1 & 1 & 2 & 1 \\ 1 & 1 & 1 & 2 \end{bmatrix};$$

$$\left[\mathbf{K}_3^{(e)}\right]=\left(hA_{pqr}^{(e)}/12\right)\begin{bmatrix} 2 & 1 & 1 & 0 \\ 1 & 2 & 1 & 0 \\ 1 & 1 & 2 & 0 \\ 0 & 0 & 0 & 0 \end{bmatrix}; \qquad \mathbf{P}_1^{(e)}=(w^{(e)}T_bV^{(e)}/4)[1\,1\,1\,1]';$$

$$\mathbf{P}_2^{(e)}=(Q^{(e)}V^{(e)}/4)[1\,1\,1\,1]'; \quad \mathbf{P}_3^{(e)}=\left[(hT_a-E)A_{pqr}^{(e)}/3\right][1\,1\,1\,0]';$$

$$g_{11}=(k_x^{(e)}b_p^2+K_y^{(e)}c_p^2+k_z^{(e)}d_p^2);$$

$$g_{12}=(k_x^{(e)}b_pb_q+k_y^{(e)}c_pc_q+k_z^{(e)}d_pd_q);$$

$$g_{13}=(k_x^{(e)}b_pb_r+k_y^{(e)}c_pc_r+k_z^{(e)}d_pd_r);$$

$$g_{14} = (k_x^{(e)} b_p b_s + k_y^{(e)} c_p c_s + k_z^{(e)} d_p d_s);$$

$$g_{22} = (k_x^{(e)} b_q^2 + k_y^{(e)} c_q^2 + k_z^{(e)} d_q^2); \quad g_{23} = (k_x^{(e)} b_q b_r + k_y^{(e)} c_q c_r + k_z^{(e)} d_q d_r);$$

$$g_{24} = (k_x^{(e)} b_q b_s + k_y^{(e)} c_q c_s + k_z^{(e)} d_q d_s); \; g_{33} = (k_x^{(e)} b_r^2 + k_y^{(e)} c_r^2 + k_z^{(e)} d_r^2);$$

$$g_{34} = (k_x^{(e)} b_r b_s + k_y^{(e)} c_r c_s + k_z^{(e)} d_r d_s); \; g_{44} = (k_x^{(e)} b_s^2 + k_y^{(e)} c_s^2 + k_z^{(e)} d_s^2);$$

(19)

and $A_{pqr}^{(e)}$ is the surface area of the face pqr. Each element contribution is computed by using element equation (14) and assembly of these contributions for all the ninety elements of the SST region gives the following system matrix equation :

$$\sum_{e=1}^{90} \sum_{m=1}^{3} \left[\mathbf{K}_m^{(e)}\right] \left[\mathbf{T}^{(e)}\right] = \sum_{e=1}^{90} \sum_{m=1}^{3} \mathbf{P}_m^{(e)} \tag{20}$$

Above equation is solved after the insertion of Dirichlet condition (4), to get the nodal temperatures.

Results, Discussion and Conclusions

The chief interest of the present investigation is the comparative study of the effects of anisotropy, rates of blood flow and evaporation on temperature distribution in three dimensional regions of human SST. The width, length and thickness of SST can be assigned any value depending on the sample under study. In the present case we have considered a=1.00 cm, b=0.9 cm, c=0.7 cm, c_1=0.15 cm, c_2=0.30 cm, c_3=0.25 cm. Eleven different combinations of biophysical parameters (elementwise) and evaporation denoted by C_i(i=1-11), given in Table 2, have been considered to compute the nodal temperatures at environmental temperature T_a=25 °C. Combinations C_i(i=1,2,3) are considered for isotropic medium. Evaporation rate is considered higher in C_2 than that of C_1. The rates of blood flow and metabolic heat generation have been considered to be double in C_3 than that of C_1 (or C_2). Combinations C_i(i=4-11) have been taken for anisotropic medium. C_4, C_5, C_6 incorporate anisotropy in epidermis, dermis and subcutaneous tissues respectively whereas C_i (i=7-11) consider anisotropy

Table 2–Eleven combinations of biophysical parameters (tetrahedral elementwise), rates of evaporation (ROE) and heat transfer coefficient (HTC).

Combs	Epidermis Finite Element Nos. (61-90)					Dermis Finite Element Nos. (31-60)					Subcutaneous Tissues Finite Element Nos. (1-30)					ROE	HTC
	$w(\alpha)$	$Q(\beta)$	$k_x(\gamma)$	$k_y(\gamma)$	$k_z(\gamma)$	$w(\alpha)$	$Q(\beta)$	$k_x(\gamma)$	$k_y(\gamma)$	$k_z(\gamma)$	$w(\alpha)$	$Q(\beta)$	$k_x(\gamma)$	$k_y(\gamma)$	$k_z(\gamma)$	$E(\delta)$	$h(\eta)$
C_1	0.0	0.0	0.50	0.50	0.50	0.275	0.725	0.75	0.75	0.75	0.495	1.305	1.00	1.00	1.00	0.0086	0.15
C_2	0.0	0.0	0.50	0.50	0.50	0.275	0.725	0.75	0.75	0.75	0.495	1.305	1.00	1.00	1.00	0.0180	0.75
C_3	0.0	0.0	0.50	0.50	0.50	0.550	1.450	0.75	0.75	0.75	0.990	2.610	1.00	1.00	1.00	0.0086	0.15
C_4	0.0	0.0	0.25	0.375	0.875	0.275	0.725	0.75	0.75	0.75	0.495	1.305	1.00	1.00	1.00	0.0086	0.15
C_5	0.0	0.0	0.50	0.50	0.50	0.275	0.725	0.375	0.5625	1.3125	0.495	1.305	1.00	1.00	1.00	0.0086	0.15
C_6	0.0	0.0	0.50	0.50	0.50	0.275	0.725	0.75	0.75	0.75	0.495	1.305	0.50	0.75	1.75	0.0086	0.15
C_7	0.0	0.0	025	0.375	0.875	0.275	0.725	0.375	0.5625	1.3125	0.495	1.305	0.50	0.75	1.75	0.0086	0.15
C_8	0.0	0.0	0.25	0.375	0.875	0.275	0.725	0.375	0.5625	1.3125	0.495	1.305	0.50	0.75	1.75	0.0180	0.75
C_9	0.0	0.0	0.875	0.375	0.25	0.275	0.725	1.3125	0.5625	0.375	0.495	1.305	1.75	0.75	0.50	0.0086	0.15
C_{10}	0.0	0.0	0.25	0.875	0.375	0.275	0.725	0.375	1.3125	0.5625	0.495	1.305	0.50	1.75	0.75	0.0086	0.15
C_{11}	0.0	0.0	0.25	0.375	0.875	0.550	1.450	0.375	0.5625	1.3125	0.990	2.610	0.50	0.75	1.75	0.0086	0.15

$\alpha = x\ 10^{-3}$ cal/cm^3 sec °C, $\beta = x\ 10^{-3}$ cal/cm^3 sec, $\gamma = x\ 10^{-3}$ cal/cm^3 sec °C, $\delta = x\ 10^{-3}$ gm/cm^2 sec, $\eta = x\ 10^{-3}$ cal/cm^2 sec °C,

Table 3– Computed nodal temperatures in three dimensional regions of human SST.

Node Nos.	C_1	C_2	C_3	C_4	C_5	C_6	C_7	C_8	C_9	C_{10}	C_{11}
1	37.00	37.00	37.00	37.00	37.00	37.00	37.00	37.00	37.00	37.00	37.00
2	37.00	37.00	37.00	37.00	37.00	37.00	37.00	37.00	37.00	37.00	37.00
3	37.00	37.00	37.00	37.00	37.00	37.00	37.00	37.00	37.00	37.00	37.00
4	37.00	37.00	37.00	37.00	37.00	37.00	37.00	37.00	37.00	37.00	37.00
5	37.00	37.00	37.00	37.00	37.00	37.00	37.00	37.00	37.00	37.00	37.00
6	37.00	37.00	37.00	37.00	37.00	37.00	37.00	37.00	37.00	37.00	37.00
7	35.13	33.35	35.30	35.09	34.97	35.74	35.59	33.85	34.25	34.85	35.68
8	35.66	34.37	35.81	35.64	35.63	36.22	36.18	35.16	34.74	35.32	36.26
9	36.11	35.21	36.23	36.09	36.13	36.60	36.62	36.10	35.18	35.71	36.67
10	35.57	34.19	35.72	35.54	35.50	36.14	36.07	34.92	34.67	35.21	36.15
11	35.66	34.37	35.80	35.64	35.62	36.20	36.16	35.11	34.74	35.33	36.23
12	35.77	34.57	35.91	35.75	35.75	36.30	36.27	35.33	34.82	35.44	36.34
13	37.00	37.00	37.00	37.00	37.00	37.00	37.00	37.00	37.00	37.00	37.00
14	37.00	37.00	37.00	37.00	37.00	37.00	37.00	37.00	37.00	37.00	37.00
15	37.00	37.00	37.00	37.00	37.00	37.00	37.00	37.00	37.00	37.00	37.00
16	37.00	37.00	37.00	37.00	37.00	37.00	37.00	37.00	37.00	37.00	37.00
17	37.00	37.00	37.00	37.00	37.00	37.00	37.00	37.00	37.00	37.00	37.00
18	37.00	37.00	37.00	37.00	37.00	37.00	37.00	37.00	37.00	37.00	37.00
19	35.78	34.58	35.91	35.75	35.76	36.30	36.28	35.36	34.83	35.44	36.35
20	35.67	34.39	35.81	35.65	35.63	36.20	36.17	35.15	34.74	35.34	36.24
21	35.57	34.20	35.72	35.54	35.50	36.15	36.08	34.93	34.67	35.21	36.15
22	36.11	35.22	36.23	36.09	36.14	36.60	36.62	36.10	35.18	35.71	36.68
23	35.67	34.40	35.81	35.65	35.64	36.22	36.19	35.20	34.75	35.32	36.27

Table 3 Cntd...

Table 3 Contd..

24	35.14	33.38	35.31	35.10	34.98	35.75	35.59	33.88	34.26	34.85	35.69
25	32.45	28.23	32.66	32.35	33.27	32.98	33.78	29.94	29.82	31.56	33.89
26	33.32	29.86	33.54	33.26	34.22	33.84	34.72	31.93	30.65	32.42	34.83
27	34.03	31.16	34.25	33.96	34.98	34.53	35.45	33.46	31.38	32.97	35.56
28	33.11	29.47	33.33	33.02	33.99	33.64	34.49	31.44	30.54	32.10	34.60
29	33.37	29.96	33.59	33.32	34.25	33.88	34.76	32.03	30.72	32.45	34.86
30	33.46	30.09	33.68	33.40	34.36	33.97	34.86	32.18	30.81	32.48	34.97
31	30.84	25.23	31.04	31.39	31.63	31.34	32.79	27.85	26.92	29.47	32.90
32	31.46	26.30	31.67	32.14	32.30	31.95	33.55	29.39	27.36	30.10	33.66
33	31.92	27.05	32.13	32.67	32.81	32.40	34.12	30.48	27.75	30.34	34.23
34	31.23	25.92	31.44	31.88	32.06	31.74	33.30	28.88	27.27	29.72	33.41
35	31.54	26.45	31.75	32.22	32.38	32.03	33.62	29.54	27.48	30.14	33.73
36	31.58	26.45	31.79	32.28	32.44	32.07	33.70	29.60	27.52	30.07	33.81
37	33.48	30.14	33.69	33.42	34.38	33.99	34.88	32.26	30.83	32.48	34.99
38	33.40	30.08	33.62	33.36	34.28	33.91	34.79	32.18	30.75	32.47	34.90
39	33.13	29.52	33.35	33.04	34.00	33.65	34.50	31.50	30.56	32.11	34.62
40	34.03	31.18	34.25	33.97	34.98	34.53	35.45	33.45	31.40	32.97	35.56
41	33.35	29.97	33.57	33.29	34.24	33.87	34.75	32.04	30.68	32.45	34.86
42	32.47	28.28	32.68	32.37	33.29	32.99	33.79	29.97	29.85	31.57	33.90
43	31.61	26.54	31.82	32.31	32.47	32.10	33.74	29.73	27.56	30.07	33.84
44	31.66	26.92	31.87	32.32	32.50	32.15	33.73	29.98	27.63	30.25	33.84
45	31.25	25.96	31.46	31.90	32.07	31.75	33.31	28.92	27.31	29.73	33.42
46	31.92	27.01	32.13	32.67	32.80	32.40	34.11	30.41	27.77	30.34	34.22
47	31.50	26.43	31.71	32.17	32.34	31.99	33.59	29.51	27.41	30.15	33.69
48	30.85	25.27	31.06	31.41	31.65	31.36	32.80	27.88	26.95	29.48	32.91

through out the region *i.e.* epidermis, dermis and subcutaneous tissues. The rate of evaporation in C_7 and C_8 have been taken equal to those of C_1 and C_2 respectively. In C_7 the component of thermal conductivity (CTC) is considered highest in z direction than that of x and y directions. C_9 considers CTC highest in x direction than that of y and z directions whereas C_{10} has CTC highest in y direction than that of x and z directions. In C_{11}, the rates of blood flow and metabolic heat generation have been assumed to be double of those of C_7. All the nodal temperatures computed for these eleven combinations have been listed tin Table 3.

Comparative study of cases C_1 with C_2 (isotropic medium) and C_7 with C_8 (fully anisotropic medium) reveals that higher rate of evaporation results in fall of the corresponding nodal temperatures (CNT) in both the media. It has been observed that the effect of evaporation is maximum at the skin surface and this effect decreases towards the body core (*i.e.* decreases with respect to depth). The difference between the CNT of C_1, C_2 is more than that of C_7, C_8 throughout the region. This depicts that the fall of temperature due to evaporation is more in isotropic medium than that of in anisotropic medium.

Comparisons of results of C_1 with C_3 and C_7 with C_{11} show that there is an increase in CNT due to increase in blood flow and metabolic heat generation in isotropic as well as in anisotropic media. The study implies that the heat carried by blood flow to the skin surface is reduced by the anisotropy of the region. The results also infers that the effect of evaporation on TD is more dominant than that of blood flow and metbolic heat generation in both types of media.

Comparisons of the results of C_7, C_9, C_{10} (fully anisotropic) with C_1 (isotropic) reveal that the CTC, taken highest in z direction (C_7) elevates the temperature throughout the SST region whereas the same taken highest in x direction (C_9) or in y direction (C_{10}) results in the fall of temperatures from that of C_1. The decrease in temperature is more in C_9 than that of in C_{10}. In all these cases the effect is maximum at the skin surface and their respective effect decreases with depth. It implies that there is a correlation between the variation of temperature and the CTC in the direction of length, width and depth of SST. This attributes that not only evaporation brings down the temperature of SST region, but similar role is also played by CTC when it is taken highest in the direction of width or length of SST.

Comparison of nodal temperatures for $C_i(i$=4-6) with C_1 reveals that the incorporation of anisotropy in epidermis, dermis and subcutaneous regions separately increases the skin surface temperatures in general, but the increases is highest in C_5, higher in C_4 and high in C_6 than that of C_1 (isotropic case). It is interesting to note that

the anisotropy of epidermis increases the skin surface temperatures only whereas the anisotropy of dermis increases the temperature of skin surface and of the interface of epidermis – dermis. The temperature of whole of SST region is elevated due to the anisotropy of subcutaneous tissues. However, their respective effects are nearly uniform at skin surface, interface between epidermis-dermis and interface between dermis-subcutaneous tissues. It is important to note that in all the three cases (C_4, C_5, C_6) the CTC has been taken highest in the direction of depth. These results are of interest and may be useful in the formulation of three dimensional sophisticated mathematical models for the heat flow problems with tumours in animal/human body.

Acknowledgement

The authors thank Dr.Rakesh Kumar Jindal, Senior Programmer, for his valuable help in the computer programming.

References

1. Pennes, H. H. (1948) *J. Appl. Physiol.* **1** : 93.
2. Gordon, R. G. & Roemer, R. B. (1975) *IEEE Trans on Biomedical Engg.* BME-**22** : 77.
3. Stekette, J. & Vander Hoek, H. J. (1979) *Phy. Med. Biol.* **24** : 583.
4. Saxena. V. P. (1983) *J. Theor. Biol.* **102** : 277.
5. Saxena. V. P. & Pal, D. S. (1984) *Indian J. Tech.* **22** : 16.
6. Pal, S. & Pal, D. S. (1986) *Bull Math. Biol.* **48** : 501.
7. Pal, D. S. & Pal, S. (1989) *Indian J. Tech.* **27** : 432.
8. Pal, D. S. & Pal, S. (1990) *J. Math. Biol.* **28** : 355
9. Arya, D. & Saxena, V. P. (1986) *J. Pure Appl. Math.* **17** : 84.
10. Pal, D. S. & Pal, S. (1993) *J. Math. Biol.* **32** : 17.
11. Pardasani, K. R. & Adlakha, N. (1993) *Indian J. Pure Appl. Math.* **24** : 721.
12. Pardasani, K. R. & Adlakha, N. (1998) *Proc. Nat. Acad. Sci.* **68(A) (1)** : 55.
13. Crisp, J. D. C. (1972) in *Properties of tendon and skin, in Biomechanics, Its Foundation and Objectives,* ed. Fung, Y. C. Perrone, N & Anilker, M., Prentice Hall, Inc. New Jersey, p. 164.
14. Stolwijk, J. A.J. (1980) *Annals of the New York Acad. Scien.* **335** : 98.
15. Norrie, D. H. & Derives, G. (1978) *An Introduction to Finite Element Analysis,* American Press New York, p. 194.

PROC. NAT. ACAD. SCI. INDIA, 73 (A), III, 2003

Fixed points of mappings satisfying a new condition

LJUBOMIR B. ĆIRIĆ

Faculty of Mechanical Engineering, 27 March 80, Belgrade, Serbia.

e-mail: edule@alfa.mas.bg.ac.yu

Received June 1, 2002; Revised December 31, 2001; Accepted July 19, 2002

Abstract

Let (X,d) be a metric space and $T : X \to X$ a self-mapping of X. In metric fixed point theory there are many fixed point theorems for contractive-type or expansive-type mappings. In this paper we define a new class of mappings which besides contractive mappings contains some expansive mappings. This class is defined by the following condition:

$$\min \{hd(Tx,Ty), (d(x,Tx)+d(y,Ty))\} \le (2k+a) \max \{d(x,y), \frac{1}{k} m(x,y)\}$$

where $k > 0$ is arbitrary and $0 \le a < 2$, $h > 2k + a$ and $m(x,y) = \min \{d(x,Ty), d(y,Tx)\}$. In complete metrically convex metric spaces these mappings have a fixed point.

(**Keywords :** metrically convex space/fixed point).

Introduction

Let (X,d) be a metric space and T a self-mapping on X. A solution of the equation $Tx = x$ is called a fixed point of T. A question when this equation has a solution generates a theory, which began in 1912 with the work of Brouwer[1] , who proved that any continuous mapping T of an n-ball into itself has a fixed point, and was followed in 1922 by Banach's Contraction Principle, already obtained in particular situation by Liouville, Picard and Goursat, which states that any mapping T of a com-plete metric space X into itself satisfying the inequality

$$d(Tx,Ty) \le \lambda d(x,y), \qquad 0 < \lambda < 1 \qquad (1)$$

for all x,y in X, has a unique fixed point. Schauder[2], Browder[3] and many others have added to and generalized these basic results for continuous mappings.

In 1973 Wong[4] proved some fixed point theorems for operators, not necessarily continuous. A class of contractive type mappings, not necessarily continuous, were significantly extended and generalized for single-valued mappings (5-15), as well as for multi-valued mappings (16-18).

One of the most general contractive-type definitions for which fixed point theorems have been proved, as pointed out by Rhoades[13], is introduced in (8) and states:

$$d(Tx,Ty) \leq \lambda \max \{d(x,y), d(x,Tx), d(y,Ty), d(x,Ty), d(y,Tx)\}, \ 0<\lambda<1 \qquad (2)$$

However, in many applications, the mapping involved is not of contractive type and does not satisfy anyone of the contractive type definitions.

The purpose of this short paper is to define and to study a class of mappings, not necessarily continuous, which on some parts of domain may be of contractive type, and on other parts may be of expansive type. For that class we shall prove fixed point and common fixed point theorems. One example is presented to show that this class contains mappings which are not necessarily contractive, nor expansive on a whole domain.

Main results

We need the following definition of metrically convex metric space due to Menger.

Definition 1 : (19, p.41) A metric space (X,d) is said to be metrically convex if for each x,y in X, $x \neq y$, there is a $z \neq x$, $z \neq y$ for which

$$d(x,y) = d(x,z) + d(z,y).$$

A subset $C \subseteq X$ is said to be metrically convex if subspace (C,d) is metrically convex.

Lemma 1 : (Menger) : If X is a complete metrically convex metric space, then for any $\lambda, 0 < \lambda < 1$ and any x,y in X, there exists z in X such that

$$d(x,z) = \lambda d(x,y) \text{ and } d(z,y) = (1-\lambda)\, d(x,y)$$

Proof: See (19, p.41, Theorem 14.1).

Now we shall prove the following result.

Theorem 1 : Let C be a nonempty closed and metrically convex subset of a complete metric space X and let $T: C \to C$ be a self-mapping on C satisfying

$$\min \{hd(Tx,Ty), (d(x,Tx) + d(y,Ty))\} \leq (2k+a) \max \{d(x,y), \frac{1}{k} m(x,y)\} \quad (3)$$

for all x, y in C, where $k > 0$ is arbitrary, a and h are such that

$$0 \leq a < 2, \; h > 2k + a \quad (4)$$

and

$$m(x,y), = \min \{d(x,Ty), \text{ d } d(y,Tx)\}.$$

Then T has at least one fixed point in C.

Proof: Let x_0 in C be arbitrary. Since C is convex, by Lemma 1 we may choose x_1 in C such that

$$d(x_0, x_1) = \frac{1}{k+1} d(x_0, Tx_0) \quad \text{and} \quad d(x_1, Tx_0) = \frac{k}{k+1} d(x_0, Tx_0),$$

or rewritten,

$$d(x_0, Tx_0) = (k+1) d(x_0, x_1), \qquad d(x_1, Tx_0) = k d(x_0, x_1).$$

Again by Lemma 1 we may choose x_2 in X such that

$$d(x_1, Tx_1) = (k+1) d(x_1, x_2), \qquad d(x_2, Tx_1) = k d(x_1, x_2).$$

Continuing in this fashion we can choose the sequence $\{x_n\}$ in X such that

$$d(x_{n-1}, Tx_{n-1}) = (k+1) d(x_{n-1}, x_n), \quad (5)$$

$$d(x_n, Tx_{n-1}) = kd(x_{n-1}, x_n).$$

We shall show that $\{x_n\}$ is a Cauchy sequence. Setting $x = x_{n-1}$, $y = x_n$ in the definition inequality (3) yields

$$\min\{hd(Tx_{n-1}, Tx_n), [d(x_{n-1}, Tx_{n-1}) + d(x_n, Tx_n)]\}$$

$$\leq (2k + a)\max\left\{d(x_{n-1}, x_n), \frac{1}{k}d(x_n, Tx_{n-1})\right\}.$$

Using (5) we get

$$\min\{hd(Tx_{n-1}, Tx_n), (k+1)[d(x_{n-1}, x_n) + d(x_n, x_{n+1})]\}$$

$$\leq (2k + a)\max\left\{d(x_{n-1}, x_n), \frac{k}{k}d(x_{n-1}, x_n)\right\} = (2k + a)d(x_{n-1}, x_n). \tag{6}$$

Suppose at first that from (6) we have

$$hd(Tx_{n-1}, Tx_n) \leq (2k + a)\, d(x_{n-1}, x_n). \tag{7}$$

By the triangle inequality we have

$$|d(x_n, Tx_n) - d(x_n, Tx_{n-1})| \leq d(Tx_{n-1}, Tx_n).$$

Hence, using (5), we get

$$|(k+1)d(x_n, x_{n+1}) - kd(x_{n-1}, x_n)| \leq d(Tx_{n-1}, Tx_n). \tag{8}$$

If $(k+1)\, d(x_n, x_{n+1}) \geq kd(x_{n-1}, x_n)$, then from (7) and (8)

$$h(k+1)d(x_n, x_{n+1}) - hkd(x_{n-1}, x_n) \leq (2k + a)d(x_{n-1}, x_n)$$

and hence

$$d(x_n, x_{n+1}) \le \frac{hk+2k+a}{h(k+1)} d(x_{n-1}, x_n). \tag{9}$$

If $(k+1)d(x_n, x_{n+1}) < kd(x_{n-1}, x_n)$, then this immediately implies

$$d(x_n, x_{n+1}) < \frac{k}{k+1} d(x_{n-1}, x_n). \tag{10}$$

Suppose now that from (6) we have

$$(k+1)[d(x_{n-1}, x_n) + d(x_n, x_{n+1})] \le (2k+a)d(x_{n-1}, x_n).$$

Then we get

$$d(x_n, x_{n+1}) \le \frac{k+a-1}{k+1} d(x_{n-1}, x_n). \tag{11}$$

Set

$$\lambda = \max\left\{\frac{k(2+h)+a}{h(k+1)}, \frac{k}{k+1}, \frac{k+a\text{-}1}{k+1}\right\} = \max\left\{1-\frac{h-(2k+a)}{h(k+1)}, 1\text{-}\frac{1}{k+1}, 1\text{-}\frac{2\text{-}a}{k+1}\right\}.$$

Then by (4), $\lambda < 1$ and so from (9), (10) and (11) in all cases we have

$$d(x_n, x_{n+1}) \le \lambda d(x_{n-1}, x_n), \quad 0 < \lambda < 1. \tag{12}$$

From (12), by induction, we get $d(x_n, x_{n+1}) \le \lambda^n d(x_0, x_1)$. Since

$$d(x_m, x_n) \le \sum_{i=m}^{n} d(x_i, x_{i+1}) \le \sum_{i=m}^{n} \lambda^i d(x_0, x_1) \le \lambda^n \frac{d(x_0, x_1)}{1-\lambda}$$

and $\lambda < 1$, we conclude that $\{x_n\}$ is the Cauchy sequence. Since X is complete, there exists some u in X such that

$$u = \lim_{n\to\infty} x_n .$$

From (5) we conclude that $\lim_{n\to\infty} Tx_n = u$, too.

Setting $x = u$, $y = x_n$ in (3) we obtain

$$\min\{hd(Tu, Tx_n), [d(u, Tu) + d(x_n, Tx_n)]\} \le (2k + a)\max\left\{d(u, x_n), \frac{1}{k} d(u, Tx_n)\right\}.$$

Taking the limit when n tends to infinity we get

$$\min\{hd(Tu, u), d(u, Tu)\} \le 0 . \tag{13}$$

Hence $Tu = u$ and the proof of the theorem is complete.

Now we shall prove a common fixed point theorem.

Theorem 2 : Let C be as in Theorem 1 and $S, T: C \to C$ a pair of selfmappings of C satisfying the following condition:

$$\min\{hd(Sx, Ty), [d(x, Sx) + d(y, Ty)]\} \le (2k + a)\max\left\{d(x, y), \frac{1}{k} m(x, y)\right\}$$

for all x,y in C, where $k > 0$ is arbitrary and a and h satisfy (4) and

$$m(x, y) = \min\{d(x, Ty), d(y, Sx)\}.$$

Then S and T have a common fixed point.

Proof: Similarly as in the proof of Theorem 1 we can choose a sequence $\{x_n\}$ in C such that

$$d(x_{2n}, x_{2n+1}) = \frac{1}{k+1} d(x_{2n}, Sx_{2n}); \quad d(x_{2n+1}, Sx_{2n}) = \frac{k}{k+1} d(x_{2n}, Sx_{2n})$$

and

$$d(x_{2n+1}, x_{2n+2}) = \frac{1}{k+1} d(x_{2n+1}, Tx_{2n+1}); \quad d(x_{2n+2}, Tx_{2n+1}) = \frac{k}{k+1} d(x_{2n+1}, Tx_{2n+1})$$

for $n = 0, 1, 2...$, where x_0 in C is arbitrary. Replacing x by x_{2n+2} and y by x_{2n+1} in the condition of Theorem 2, the reader may proceed on the lines of Theorem 1, to derive $d(x_{2n+2}, x_{2n+3}) \leq \lambda d(x_{2n+1}, x_{2n+2})$, where λ is the same as determined in the proof of Theorem 1. Thus, as in the proof of the above Theorem, it can be shown that $\{x_n\}$ is the Cauchy sequence and $u = \lim_{n\to\infty} x_n$ is such that $Su = u$ and $Tu = u$.

Remark 1: It is easy to see that a contraction mapping which satisfies (1) also satisfies (3) with any a, k and h with $a + 2k > \lambda h$. In this case assumption of metrically convexity of a space is supperfluous. The following example shows that also there are mappings which are expansive on some subsets and which satisfy (3).

Example :

Let X be the set of reals with usual metric and let $T : X \to X$ be defined as follows:

$$Tx = -2x, \qquad \text{if } x \geq 0$$

$$Tx = -\frac{3}{4}x, \quad \text{if } x \geq 0.$$

We show that T satisfies (3) on whole X with, for example, a= 1, $k = 2$ and $h = 6$.

Let x, y in X be such that $x < 0$ and $y < 0$. Then

$$hd(Tx, Ty) = \frac{9}{2}d(x, y) < 5d(x, y) = (2k + a)d(x, y).$$

Let now $x < 0$ and $y > 0$. Then

$$d(x, Tx) + d(y, Ty) = \frac{7}{4}|x| + 3y < 5(|x| + y) = (2k + a)d(x, y).$$

Similarly inequality holds for $x > 0$ and $y < 0$.

Let now $x > 0$ and $y > 0$. Then

$$d(x, Tx) + d(y, Ty) = 3(x + y).$$

Suppose that $x \le y$. Then

$$3(x + y) \le 5(y - x) = (2k + a)d(x, y), \quad if\ x \le y/4,$$

$$3(x + y) \le \frac{5}{2}(2x + y) = \frac{2k + a}{k}\min\{d(x, Ty), d(y, Tx)\}, \quad if\ y/4 \le x \le y.$$

Similarly, for $x \ge y$ we have two inequalities which correspond to the case $x \ge 4y$ and $y \le x \le 4y$, respectively. Therefore, T satisfies (3). Since Picard iterations $\{T^n x\}$ diverge for any $x \ne 0$, we conclude that T does not satisfy (2). T also does not satisfy any known contractive condition which implies convergence of Picard iterations.

Note that any expansive mapping T, defined on $X = (-\infty+\infty)$ by $Tx = -cx$ with $1 < c < 3$, satisfies (3) with $a = c-1$, where $k > 0$ is arbitrary and h satisfies (4).

References

1. Brouwer, L.E.J. (1910) *Math. Ann.* **71** : 97.
2. Schauder, J. (1930) *Studia Math.* **2** : 171.
3. Browder, F. E. (1968) *Math. Ann.* **177** : 283.
4. Wong, C.S. (1973) *Math. Ann.* **204** : 97.
5. Ćirić Lj., B. (1971) *Publ. Inst. Math. (Beograd)* **12 (26)** : 12.

6. Ćirić Lj., B. (1974) *Publ. Inst. Math. (Beograd)* **17**(31) : 52.
7. Ćirić Lj., B. (1990) *Proc. IV Meeting Inter. Work. Anal. Appl. (Kupari)* : 263.
8. Ćirić Lj., B. (1974) *Proc. Amer. Math. Soc.* **45** : 267.
9. Ćirić Lj., B. (1992) *Math. Pannonica* **3/2** : 51.
10. Ćirić Lj., B. (1995) *Rend. Accad. Naz. Sci. XL Mem. Math.* **19**(5) : 263.
11. Downing, D. & Kirk, W.A. (1977) *Pacific J. Math.* **69** : 339.
12. Pall, T.K. & Maiti, M. (1976) *Math. Balcanica* **6** : 152.
13. Rhoades, B.E. (1977) *Trans. Amer. Math. Soc.* **226** : 257.
14. Singh, S.L. (1986) *Punjab Univ. J. Math.* **19** : 83.
15. Singh, S.L. & Mishra, S.N., J. (1998) *J. Austral. Math. Soc. (Ser. A)* **65** : 1.
16. Assad, N.A. & Kirk, W.A. (1972) *Pacific J. Math* **43** : 553.
17. Khan, M.S. (1981) *Pacific J. Math.* **96** : 337.
18. Nadler, S.B. (1969) *Pacific J. Math.* **30** : 475.
19. Blumental, L.E., (1953) *Theory and application of distance geometry.* Clarendon Press, Oxford,.

PROC. NAT. ACAD. SCI. INDIA, 73 (A), III, 2003

Interaction of torsional waves with a penny-shaped crack situated in an infinitely long elastic cylinder

NAMITA SRIVASTAVA and SUJOY DAS

Department of Mathematics & Computer Applications, M. A. College of Technology, Bhopal - 462 007, India.

Received February 8, 2001; Revised August 14, 2002; Accepted November 9, 2002

Abstract

The diffraction of torsional waves by a penny-shaped crack situated in an infinitely long isotropic elastic cylinder is considered. Integral transform method is used for finding the solution of the equation of motion from the linear theory for homogeneous, isotropic elastic material. The problem is reduced to that of solving an integral equation. It is found that only torsional waves with frequencies less than a parameter-value, depending in the radius of the cylinder, can propagate. The associated integral equation is solved numerically for a range of wave frequency and the radius of the cylinder. The solutions are used for calculating the dynamic stress intensity factor, displacement on the surface of crack and crack energy. The results are presented graphically.

(Keywords : torsional waves/penny-shaped crack/Integral transform/dual integral equation/ stress intensity factor/crack energy.)

Introduction

Recently great interest has been shown in the problems of the interaction of elastic waves with cracks present in elastic solids. The study of these problems is motivated by their applications to seismology and exploration geophysics. Elastic waves propagating in a solid are modified by the presence of cracks / inclusions and a wave diffraction pattern can yield important information regarding the nature of the flow in the interior of the solids.

Due to this reason the problem of finding stress and strain fields in elastic solids containing cracks due to oscillatory loading have been extensively studied in recent years. Srivastava et al have studied the interaction of shear waves with Griffith cracks situated in an infinitely long elastic strip[1,2] and the interaction of longitudinal waves with penny-shaped cracks situated in an infinitely long elastic cylinder[3]. An interesting conclusion obtained in[1,2] was that only shear waves with frequencies less than a parameter-value depending on the width of the wave-guide can propagate in the

strip. In this paper we have studied the problem of the interaction of plane harmonic incident torsional waves with panny-shaped crack situated in an infinitely long homogenous, isotropic elastic cylinder.

With the help of Fourier sine and Hankel transform of order one a solution of the displacement equation appropriate to our problem has been obtained. The boundary value problem has been reduced to that of solving dual integral equations, which have finally been reduced to a Fredholm integral equation of the second kind. The Kernels of the integral equation have been written in the form suitable for numerical calculations. As in the case of interaction of shear waves with Griffith crack situated in an infinite strip, in this case also, the convergence of kernels of the integrals require to impose certain restriction on the frequency of the torsional waves, We have concluded that only torsional waves with frequencies less than a parameter value depending on the radius of the cylinder can propogate in the cylinder. The solution which we have derived are valid only for such frequencies. Numerical calculations have been made for a range of wave frequencies and the radius of the cylinder. Variation of important physical quantities like stress intensity factor, displacement on crack surface and crack energy has been illustrated graphically.

Formulation of the Problem

Consider an infinitely long, homogeneous, isotropic, elastic cylinder of radius h, containing a penny shaped crack of unit radius whose plane faces are stress free. Introduce cylindrical polar coordinates (ρ,θ, z) with the center and axis of the crack as origin and z-axis; the crack is then given by $z=0, 0 \le \rho \le 1$, and the infinitely long Cylinder is given by $0 \le \rho \le h$, $-\infty < z < \infty$ From Love[4] in torsion situation the only non-zero component of displacement is the θ-component which is denoted by $U_\theta(\rho,z)$ and the only non-zero stress components are $\sigma_{\theta z}(\rho, z)$ and $\sigma_{\rho\theta}(\rho, z)$ which are given in terms of U_θ by

$$\sigma_{\theta z} = \mu \frac{\partial U_\theta}{\partial z}, \quad \sigma_{\rho\theta} = \mu\left(\frac{\partial U_\theta}{\partial \rho} - \frac{U_\theta}{\rho}\right) \tag{1}$$

where μ is the shear modulus of the material. The equation of motion satisfied by U_θ is :

$$\frac{\partial^2 U_\theta}{\partial \rho^2} + \frac{1}{\rho}\frac{\partial U_\theta}{\partial \rho} - \frac{U_\theta}{\rho^2} + \frac{\partial^2 U_\theta}{\partial z^2} + k^2 U_\theta = 0 \tag{2}$$

where $k = \omega/c$. The speed of shear wave, $c = \left(\mu/\rho_0\right)^{1/2}$, ρ_0 being the density of the material. In what follows the time dependence of all field quantities assumed to be of the form $e^{i\omega t}$; the exponential is subsequently omitted in this paper. The plane harmonic incident torsional wave in given by the displacement vector (Mal[5])

$$U_\rho^0 = 0 = U_z^0 \tag{3}$$

$$U_\theta^0 = B_0 \rho e^{ikz} \tag{4}$$

where B_0 is constant .

Hence the boundary condition on $z = 0$ are

$$U_\theta(\rho,0) = 0, \quad \rho \geq \tag{5}$$

$$\sigma_{\theta z}(\rho,0) = -\sigma_{\theta z}^0(\rho,0) = -\mu\frac{\partial U_\theta^0}{\partial z} = -B_0 \rho \mu i k = -q_0 \rho, \quad 0 \leq \rho \leq 1 \tag{6}$$

If the boundary of the cylinder is stress free, then

$$\sigma_{\theta z}(h,z) \tag{7}$$

The problem of determining stress distribution reduces to that of obtaining solution of the displacement equation (2) subject to the above boundary conditions.

The solution of (2) for an elastic half-space obtained with the help of Hankel transform of order one, such that displacement at $z = \infty$ vanishes is given by

$$U_\theta(\rho,z) = (\operatorname{sgn} z)\int_0^\infty \xi A(\xi) e^{-\beta|z|} J_1(\xi\rho)\, d\xi \tag{8}$$

where $\beta^2 \xi^2 - k^2$.

Again the solution of (2) for an infinite elastic cylinder can be obtained with the help of Fourier sine transform. Let

$$\overline{U}_\theta(\rho,\zeta) = \int_0^\infty U_\theta(\rho,z)\sin\zeta z dz \tag{9}$$

By multiplying (2) by $\sin \zeta z$ and integrating with respect to z from 0 to ∞, we get

$$\rho^2\frac{\partial^2\overline{U}_\theta}{\partial\rho^2}+\rho\frac{\partial\overline{U}_\theta}{\partial\rho}-(g^2\rho^2+1)\overline{U}_\theta=0 \tag{10}$$

where $g^2\zeta^2 - k^2$. The solution of this equation is

$$\overline{U}_\theta = B(\zeta)I_1(g\rho)+C(\zeta)K_1(\rho g) \tag{11}$$

where $I_1(\rho)$ and $K_1(\rho)$ are modified Bessel functions of the first and third kind. Since $K_1(\rho)\to\infty$ as $\rho = 0$. Hence for a solution for cylinder containing origin $C = 0$ and the required solution is

$$\overline{U}\,\theta\,(\rho,\zeta) = \mathrm{B}\,(\zeta)I_1(g\rho) \tag{12}$$

By inversion theorem for Fourier sine transform we have

$$U_\theta(\rho,z)=\int_0^\infty B(\zeta)I_1(g\rho)\sin\zeta z d\zeta\,. \tag{13}$$

Thus the complete solution of (2) suitable for the problem stated above is obtained by superposing (8) and (13). It is given by

$$U_\theta(\rho,z)=(\operatorname{sgn} z)\int_0^\infty \xi A(\xi)e^{-\beta|z|}J_1(\xi\rho)d\xi+\int_0^\infty B(\zeta)I_1(g\rho)\sin\zeta z d\zeta \tag{14}$$

From stress and strain relation (1) we have

$$\sigma_{\theta z}(\rho,z)=-\mu(\operatorname{sgn} z)\int_0^\infty \xi\beta A(\xi)e^{-\beta|z|}J_1(\xi\rho)d\xi+\mu\int_0^\infty \zeta B(\zeta)I_1(g\rho)\cos\zeta z d\zeta \tag{15}$$

where

$$\text{sgn } z = -1, z < 0, \qquad \beta = \sqrt{\xi^2 - k^2}, \quad \xi > k \qquad g = \sqrt{\zeta^2 - k^2}, \qquad \zeta > k,$$

$$= 1, z > 0, \qquad = -i\sqrt{k^2 - \xi^2}, \quad \xi > k, \qquad = -i\sqrt{k^2 - \zeta^2}, \quad \zeta > k.$$

Derivation of the Integral Equation

The boundary conditions (5) and (6) are satisfied provided

$$\int_0^\infty \xi\beta A'(\xi) J_1(\xi\rho) d\xi - \int_0^\infty \zeta B(\zeta) I_1(g\rho) = p_0\rho, \quad 0 \le \rho \le 1 \tag{16}$$

$$\int_0^\infty A'(\xi) J_1(\xi\rho) d\xi \qquad\qquad 1 \le \rho \le 1 \tag{17}$$

where $A'(\xi) = \xi A(\xi)$ and $p_0 = q_0/\mu$.

From (7) after using inverse cosine transform, we have

$$\begin{aligned} \zeta B(\zeta) I_1(gh) &= \int_0^\infty \left[\int_0^\infty \beta A'(\xi) e^{-\beta z} J_1(\xi h) d\xi\right] \cos\zeta z dz \\ &= \int_0^\infty \beta A'(\xi) J_1(\xi h) \left[\int_0^\infty e^{-\beta z} \cos\zeta z dz\right] d\xi \\ &= \int_0^\infty \frac{\beta^2}{\beta^2 + \zeta^2} A'(\xi) J_1(\xi h) d\xi \end{aligned} \tag{18}$$

The equation (16) and (17) can be written as

$$\int_0^\infty \xi A'(\xi) J_1(\xi\rho) d\xi = P(\rho), \; 0 \le \rho \le 1 \tag{19}$$

$$\int_0^\infty A'(\xi) J_1(\xi\rho) d\xi = 0, \; \rho \ge 1 \tag{20}$$

where $H(\xi) = \dfrac{\sqrt{\xi^2 - k^2} - \xi}{\xi}$, $H(\xi) \to$ as $\xi \to \infty$ and

$$P(\rho) = p_0\rho + \int_0^\infty \zeta B(\zeta) I_1(g\rho)d\zeta - \int_0^\infty \xi H(\zeta) A'(\xi) J_1(\xi\rho)d\xi .$$

Let the solution of the above equation be

$$A'(\xi) = \int_0^t \sqrt{\xi t}\, q(t) J_{1/2}(\xi t)dt \tag{21a}$$

$$= \sqrt{\frac{2}{\pi}}\left\{ - q(1)\frac{\sin\xi}{\xi} + \frac{1}{\xi}\int_0^t \frac{[tq(t)]'}{t}\sin\xi t dt \right\} \tag{21b}$$

With this choice of $A'(\xi)$, (20) is satisfied and (19) gives

$$P(\rho) = \sqrt{\frac{2}{\pi}}\left\{\int_0^\rho + \int_\rho^t \right\}\left(\int_0^\infty J_1(\xi\rho)\sin\xi t d\xi\right)\frac{[tq(t)]'}{t}dt = \sqrt{\frac{2}{\pi}}\int_0^\rho \frac{[tq(t)]'}{\rho\sqrt{\rho^2 - t^2}}\, dt$$

since $\int_0^\infty J_1(\xi\rho)\sin\xi t d\xi = 0$, for $t \geq \rho$.

This is an Abel integral equation. Its solution is

$$[tq(t)]' = \sqrt{\frac{2}{\pi}}\cdot\frac{d}{dt}\int_0^t \frac{\rho^2 P(\rho)}{\sqrt{t^2 - \rho^2}}d\rho \tag{22}$$

By integrating the above equation, we get

$$tq(t) = \sqrt{\frac{2}{\pi}}\int_0^t \frac{\rho^2 P(\rho)}{\sqrt{t^2 - \rho^2}}d\rho \tag{23}$$

If we substitute the value of $P(\rho)$ from (19) in the above equation we get

$$tq(t)=\sqrt{\frac{2}{\pi}}\Big[\int_0\frac{p_0\rho^3}{\sqrt{t^2-\rho^2}}d\rho+\int_0\frac{\rho^2}{\sqrt{t^2-\rho^2}}\int_0^\infty\zeta B(\zeta)I_1(g\rho)d\zeta d\rho$$
$$-\int_0\frac{\rho^2}{\sqrt{t^2-\rho^2}}\int_0^\infty\xi H(\xi)A'(\xi)J_1(\xi\rho)d\xi d\rho\ \Big] \qquad (24)$$

By substituting the value of $A'(\xi)$ from (21a) in (18) after some manipulation we get

$$\zeta B(\zeta)I_1(gh)=\int_0\sqrt{t}q(t)\left[\int_0^\infty\frac{\beta^2}{\beta^2+\zeta^2}\sqrt{\xi}J_{1/2}(\xi t)J_1(\xi h)d\xi\right]dt$$
$$=\int_0\sqrt{t}q(t)\left[\int_0^\infty\sqrt{\xi}J_{1/2}(\xi t)J_1(\xi h)d\xi-\zeta^2\int_0^\infty\sqrt{\xi}\frac{J_{1/2}(\xi t)J_1(\xi h)}{\xi^2+g^2}d\xi\right]dt$$

since $\zeta^2+\beta^2=\zeta^2+\xi^2-k^2=\xi^2+g^2$.

By using the results given in Gradshten and Ryzhik[6] [pp 692, 694] we get

$$\zeta B(\zeta)=-\frac{\zeta^2}{\sqrt{g}}\frac{K_1(gh)}{I_1(gh)}\int_0\sqrt{t}q(t)I_{1/2}(gt)dt \qquad (25)$$

By changing the order of integration, (24) can be written as

$$tq(t)=\sqrt{\frac{2}{\pi}}\Big[\int_0\frac{p_0\rho^3}{\sqrt{t^2-\rho^2}}d\rho+\int_0^\infty\zeta B(\zeta)\left[\int_0\frac{\rho^2I_1(g\rho)}{\sqrt{t^2-\rho^2}}d\rho\right]d\zeta-$$
$$\int_0^\infty\xi H(\xi)A'(\xi)\left[\int_0\frac{\rho^2J_1(\xi\rho)}{\sqrt{t^2-\rho^2}}d\rho\right]d\xi\ \Big] \qquad (26)$$
$$tq(t)=\frac{2}{3}\sqrt{\frac{2}{\pi}}p_0t^3+\frac{1}{\sqrt{2}}\int_0^\infty\frac{t^2I_{1/2}(gt)}{\sqrt{gt}}\zeta B(\zeta)d\zeta-\frac{1}{\sqrt{2}}\int_0^\infty\frac{t^2J_{1/2}(\xi t)}{\sqrt{\xi t}}\xi H(\xi)A'(\xi)d\xi$$

For deriving the above equation we have used the results given in[6]. By substituting the values of $A'(\xi)$ and $\zeta B(\zeta)$ from (21) and (25), then by changing the order of integration we get the following integral equation for determining the unknown function$\chi(t)$.

$$\chi(t) + \int_0^t [L_1(t,m) + L_2(t,m)]\chi(t)dt = t^2 \tag{27}$$

where $q(t) = \frac{2}{3}\sqrt{\frac{2}{\pi}} p_o \chi(t)$,

$$L_1(t,m) = \sqrt{\frac{tm}{2}} \int_0^\infty \xi H(\xi) J_{1/4}(\xi t) J_{1/2}(\xi m) d\xi, \tag{28a}$$

and $$L_2(t,m) = \sqrt{\frac{tm}{2}} \int_0^\infty \frac{\zeta^2}{g} I_{1/2}(gt) I_{1/2}(gm) \frac{K_1(gh)}{I_1(gh)} d\zeta. \tag{28b}$$

Both the functions $L_1(t,m)$ and $L_2(t,m)$ are symmetric functions of t and m.

The integrand in $L_1(t,m)$ has no poles. It has only branch point at the point $\xi = k$. Following the procedure given in[5], the infinite integral in $L_1(t,m)$ can be converted in to the following integral with finite limits.

$$L_1(t,m) = -ik^2 \sqrt{\frac{tm}{2}} \int_0^t (1-\xi^2)^{1/2} J_{1/2}(\xi kt) H_{1/2}^{(1)}(\xi km) d\xi, \quad m > t \tag{29}$$

Since

$$L_2(t,m) = \sqrt{\frac{tm}{2}} \left[\int_0^t + \int_t^\infty \right] \frac{\zeta^2}{g} I_{1/2}(gt) I_{1/2}(gm) \frac{K_1(gh)}{I_1(gh)} d\zeta,$$

and

$$g = \sqrt{\zeta^2 - k^2}, \quad \zeta > k$$
$$= -i\sqrt{k^2 - \zeta^2} = -ig', \quad \zeta < k, \quad g' = \sqrt{k^2 - \zeta^2},$$

we have

$$L_2(t,m)=\sqrt{\frac{tm}{2}}\Big[\int_0^k \frac{\zeta^2}{-ig'}I_{1/2}(-ig't)I_{1/2}(-ig'm)\frac{K_1(-ig'h)}{I_1(-ig'h)}d\zeta+$$
$$\int_k^\infty \frac{\zeta^2}{g}I_{1/2}(gt)I_{1/2}(gm)\frac{K_1(gh)}{I_1(gh)}d\zeta\Big]$$
$$=\sqrt{\frac{tm}{2}}\Big[\frac{i\pi}{2}\int_0^k \frac{\zeta^2}{\sqrt{k^2-\zeta^2}}J_{1/2}(g't)J_{1/2}(g't)\frac{H_1^{(1)}(g'h)}{J_1(g'h)}d\zeta+$$
$$\int_k^\infty \frac{\zeta^2}{\sqrt{\zeta^2-k^2}}I_{1/2}(gt)I_{1/2}(gm)\frac{K_1(gh)}{I_1(gh)}d\zeta\Big]$$

By substituting $\zeta^2=k^2(1-y^2)$ in the first integral and $\zeta^2=k^2(1+y^2)$ in the second integral we get

$$L_2(t,m)=\sqrt{\frac{tm}{2}}k^2\Big[\frac{i\pi}{2}\int_0^1(1-y^2)^{1/2}J_{1/2}(kyt)J_{1/2}(kym)\frac{H_1^{(1)}(kyh)}{J_1(kyh)}dy$$
$$+\int_0^\infty(1+y^2)^{1/2}I_{1/2}(kyt)I_{1/2}(kym)\frac{K_1(kyh)}{I_1(kyh)}dy\Big] \qquad (30)$$

It may be noted that the first integral in (30) is convergent only when the dimensionless frequency k is such that $kh < j_{1,1}$, where $j_{1,1}$,=3.8317060, is the first finite zero of $J_1(x)$ when the zeros are arranged in ascending order. Hence it can be concluded that only the torsional waves with $k < j_{1,1}/h$ can propagate in an elastic cylinder of radius h. This fact is similar to the known result for the propagation of the shear waves in an infinitely long elastic strip containing a Griffith crack[1].

Quantities of Physical Interest

By using (15), (21b) and (32) it can be shown that the stress component $\sigma_{\theta z}(\rho,0)$ in the neighborhood of crack is given by

$$\sigma_{\theta z}(\rho,0)=-\mu\int_0^\infty \xi A'(\xi)J_1(\xi\rho)d\xi+O(1)=\frac{4q_0}{3\pi}\frac{\chi(1)}{\rho\sqrt{\rho^2-1}}+O(1),\quad \rho>1$$

Defining stress intensity factor by

$$N = \lim_{\rho \to 1+0} \sqrt{\rho - 1}\left|\sigma_{\theta z}(\rho,0)\right| = \frac{2\sqrt{2}q_0}{3\pi}\left|\chi(1)\right| \tag{31}$$

Another quantity of physical interest is the displacement on the crack surface. Using (14), (21a) and (21b) we get

$$\begin{aligned} U_\theta(\rho,0) &= \frac{4q_0}{3\pi\mu}\int_\rho^1 \frac{\rho\chi(t)}{t\sqrt{t^2-\rho^2}}dt = \frac{4q_0}{3\pi\mu}\rho\left[\sqrt{1-\rho^2}\chi(1) - \int_\rho^1 \sqrt{t^2-\rho^2}\,\frac{d}{dt}\left\{\frac{\chi(t)}{t^2}\right\}dt\right] \\ &= \frac{4q_0}{3\pi\mu}M(\rho), \quad 0 \le \rho \le 1 \end{aligned} \tag{32}$$

Crack energy can be calculated by using (35). Its value is

$$W = 2\pi q_0 \int_0^1 \rho U_\theta(\rho,0)d\rho = \frac{8q_0^2}{3\mu}\int_0^1 t\chi(t)dt = \frac{8q_0^2}{3\mu}W(k) \tag{33}$$

Numerical Calculations

The integral equation (27) has been solved numerically. Using the method of Fox and Goodwin[7] (27) has been converted into a system of linear algebraic equation. The second integral of $L_2(t,m)$ in (30) has been evaluated by using five point Gauss - Laguerre quadrature formula while the first integral of $L_2(t,m)$ and the kernel $L_1(t,m)$ in (29) have been evaluated by using Simpson's quadrature formula. A complex computer programme has been used to evaluate$\chi(t)$. These values have been used to calculate dynamic stress intensity factor; the displacement component U_θ and the crack energy. Calculations have been done for a range of dimensionless frequency k.

Since for $k = 0$, $g = \zeta$ the kernel $L_1(t,m)$ vanishes while $L_2(t,m)$ from (28b) reduces to the following form.

$$L_2(t,m) = \sqrt{\frac{tm}{2}}\int_0^\infty \zeta I_{1/2}(\zeta t) I_{1/2}(\zeta m)\frac{K_1(\zeta h)}{I_1(\zeta h)}d\zeta \tag{34}$$

Fig. 1–Stress Intensity Factor

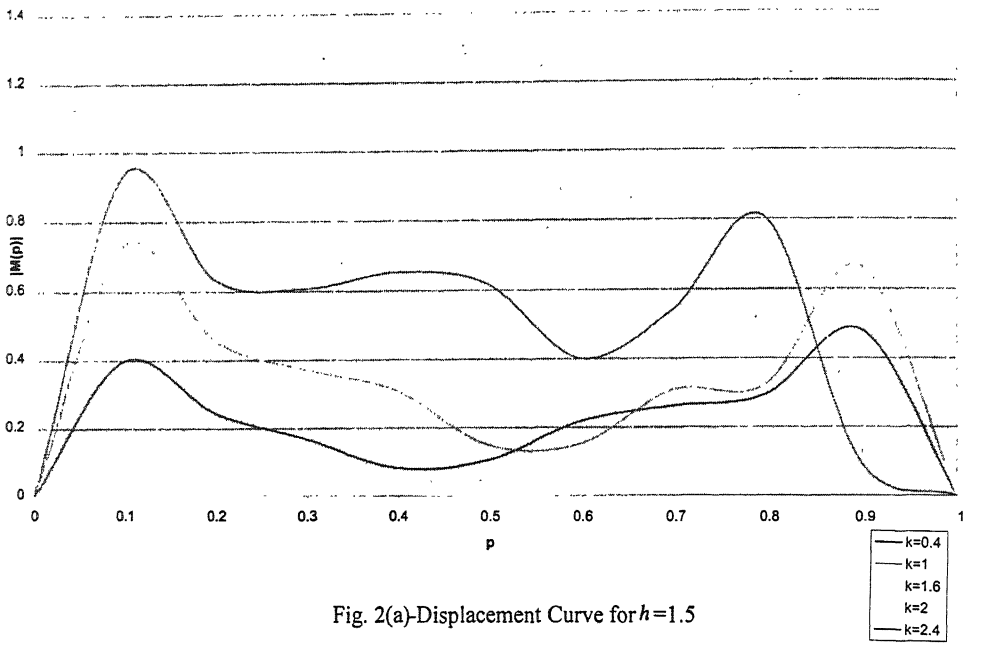


Fig. 2(a)-Displacement Curve for $h=1.5$

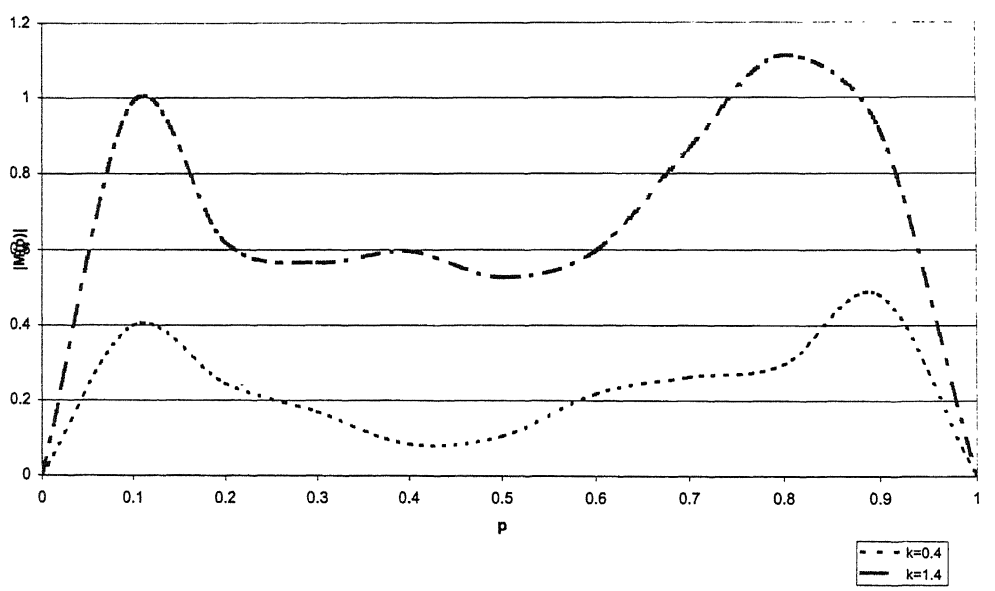


Fig. 2(b)– Displacement Curve for $h=2.5$

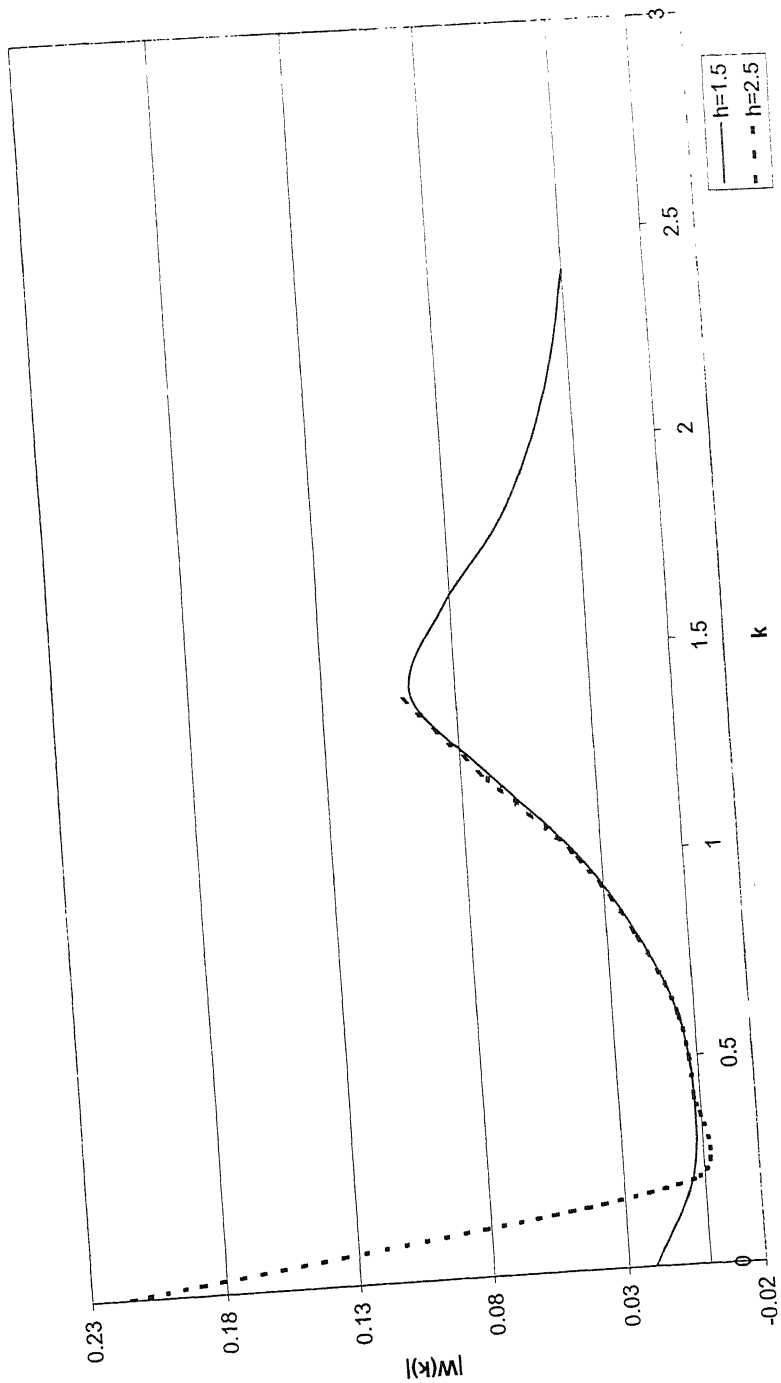


Fig. 3– Energy

Two different values of the radius of the cylinder viz. 1.5 and 2.5 have been chosen. Keeping the limiting condition $k < j_{1,1}/h$ in view, the values for k corresponding to $h = 1.5$ are from 0 to 2.5 in steps of 0.1. Similarly in the case $h = 2.5$, k has been taken from 0 to 1.5. The graphs shown in Fig: 1 represents the amplitude of $|\chi(1)|$ plotted against the dimensionless frequency k. It is evident from these graphs that for these values of the radius $h = 1.5$ and 2.5, $|\chi(1)|$ reaches minimum value for $k = 0.1$, then shows an oscillatory tendency.

In Fig. 2(a), displacement $|M(\rho)|$ has been plotted, for h=1.5 against frequencies $k = 0.4$, 1.0, 1.6, 2.0 and 2.4. In Fig. 2(b) displacement curve for $h = 2.5$ and $k = 0.4$ and 1.4 is plotted. These figures show that the multiple reflections inside the crack introduces oscillations in these curves.

Fig. 3 illustrate the variation of $|W(k)|$ the crack energy with the frequency k. For $h = 1.5$, $|W(k)|$ first decreases, has minimum value for $k = 0.6$ then increases and reaches maximum value for $k = 1.4$, then again decreases with increase in the values of the frequency k. While for h = 2.5, $|W(k)|$ first decreases to minimum value for $k = 0.4$ then increases with k.

Acknowledgments

We are grateful to Dr. K. N. Srivastava for suggesting this problem and his help and guidance in the preparation of this paper. The authors thank the referees for their valuable suggestions.

References

1. Srivastava, K.N., R.M., Palaiya & D.S., Karaulia (1983) *International Journal of Fracture* **21** : 39.
2. Srivastava, K.N., R.M., Palaiya & D.S., Karaulia (1983) *International Journal of Fracture* **23** : 3.
3. Srivastava, K.N., R.M., Palaiya & O.P. Gupta (1982) *Journal of Elasticity.* **12** : 143.
4. Love, A.E.H. (1952) *Mathematical Theory of Elasticity*, Cambridge University Press.
5. Mal, A.K. (1970) *International Journal of Engineering Sciences* **8** : 380.
6. Gradshteyn, I.S. & I.M. Ryzhik (1965) *Tables of Integrals, Series and Products*, Academic Press.
7. Fox, L. & E.T. Goodwin (1953) *Philosophical Transactions* **A.245** : 501.

PROC. NAT. ACAD. SCI. INDIA, 73 (A), III, 2003

Gravitational force as the inertial interaction of outermost electron of a molecule with its neighbour molecule in a gas

N. G. DONGRE*

Department of Physics, Harish Chandra P.G. College Varanasi-221 001, India.

**Present address : B-62, Brij Enclave, Varanasi 221 005, India.*

Received June 9, 2001; Accepted January 12, 2002

Abstract

(i) First we consider the structure of the electron. If an electron is a charged body - a sphere, the charge on its various parts should repel each other, and the sphere must expand till it blows off. To retain its shape, there must be some mechanism. It is the spin. Electrodynamics teaches us that a circulating. charge produces a magnetic field along its axis. Now a play between the spinning charge and this induced magnetic field may be imagined to provide a dynamic equilibrium between the opposing forces and hence the stability of the shape and size of electron. Therefore, intrinsically an electron is not only a charge but it is also a tiny magnetic dipole as well. For the electron to be dynamically stable it should posses spin angular momentum and contain certain amount of electromagnetic energy and that might be appearing as inertial mass.

(ii) In our view and according to Thomson[1] as well, an electron possesses mass solely by virtue of its electric charge and has no mass in the material sense it can be shown that the mass possessed by the electron in the frame of reference in which it is at rest gets increased in a natural way in the frame of reference in which the electron is moving with an uniform velocity, This relation is exactly the same as we get by the relativistic formula for the variation of mass.

(iii) If we generalize the view that the intrinsic mass is always by virtue of electric charge, as every material particle in the universe is composed of nuclear and electronic charges, it should vary with the velocity of the particle. Therefore it suggests that the mutual gravitational attraction of the masses must also be a kind of electromagnetic interaction since masses too have some kind of electrical origin, This view provides us a new way to picturise the planetary motion as well. Possibly it provides the answer to the problem that why is the elliptical path is acquired in general by a planet.

(iv) Now for a gas. a molecule is an entity which is blanketed by a dynamic electron in the outermost orbital of the molecule as a whole, The electronic charges. their orbital and spin angular momenta and the nuclei satisfies the valencies and keep up the molecule electrically

neutral in the dynamic equilibrium state, Except the outermost dynamic electron which envelopes the nuclei with the other satellite electrons within the molecule, offers itself as an enclosure to all confined nuclei and electrons and completely shields their electromagnetic interactions out side the enclosure and represents the only dynamic electron capable of influencing the similar electron of neighbour molecule by inertial interaction. Thus in a gas, every entity may be regarded as a mass Point of the rest mass. mass equivalent to that of the electromagnetic or electrical mass of an electron providing some sort of very weak. attractive force of electromagnetic or of electrical origin acting on its similar neighbor molecule / entity, which may not be other than the well known gravitational force.

(v) Along with this we may also consider one gm mole of a gas as a single whole of a bulk of material at a given temperature. which is under thermal equilibrium with the surrounding radiant energy in which the photons of, various frequencies following the temperature dependent statistical laws of distribution are under motion in all possible directions.

(vi) In this case there is very large empty space between the entities which may be regarded as free space provided for the motion of the photons and when they have occasional encounters with the outermost electrons. photons get absorbed by them followed by their release and so on. These consideration yield the formula for Universal Gravitational Constant, G in terms of standard values of velocity of light, rest mass of an electron, Stefan's constant; Avagadro's number, the volume and temperature of one gm mole of a gas at S.T.P. which is given bellow :

$$G = 21.493226\ \sigma.T_0^4 V_0^{4/3} / N_A^{8/3}.m_0^2.c$$

The values of G when calculated comes out to be 6.6627×10^{-8} c.g.s. which is strikingly very close to the standard value of gravitational constant G and just falls lower by 0.157 % only supporting its origin in the assumptions made earlier.

(**Keywords** : relativity/planetary motion/molecular gas/gravitation/electron).

1. Introduction

The Possible Structure of an Electron :

The set of equations of Lorenz transformation was used by Larmor to explain the null result of the Michelson - Morley experiment, in his Aether and Matter, pp. 174 - 176 (Cambridge University Press, New York 1900). Later the out come of the Michelson - Morley experiment as a new principle as that the speed of light (electromagnetic waves) is independent of the motion of. the light source or receiver formed the basis for the search of the equations of transformations for a frame of reference moving uniformly relative to other frame of reference. This lead scientists to consider it in two ways. (i) Lorenz considered a light wave spreading out from a point source at the origin in a reference frame. The space being attributed with the properties i.e.. it is isotropic and homogeneous in nature, the wavefront (surface of

qual phase) will be a sphere. But according to the new principle the wavefront must also be a sphere when viewed in an another reference. frame which is in uniform motion with respect to the source. (ii) While as the bodies are perceived in Nature by light signals Einstein tried to resolve the problem, adhering to the principle of equivalence and the constancy of the velocity of light resulting to the same Lorenz equations of transformations for a frame of reference moving uniformly relative to the other frame of reference. These equations do not concern with the intrinsic nature of the objects. Even an electron which has charge and the spin both-how does vary in mass while it is under relative motion? What happens to its structure? These are the questions which remain unsolved. If an electron is a charged body - a sphere, the charge on its various parts should repel each other and the sphere must expand till it blows off. To retain its shape, there must be some mechanism. It is the spin. Electrodynamics teaches us that a circulating charge produces a magnetic field along its, axis. Now 'a play between the spinning charge and this induced magnetic field may be imagined as to provide a dynamic equilibrium between the opposing forces and hence the stability of the shape and size.

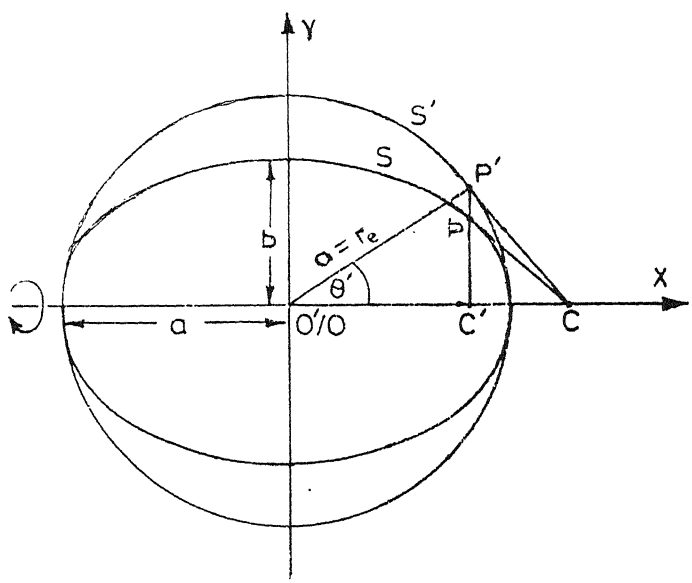


Fig. 1

2. The Spin Angular Momentum, the Mass of the Electron and its Variation with Velocity

Consider an electron of mass m_0 and as an electronic charge e smeared over on a spherical surface of radius r_e and say spinning with the average peripheral velocity $v_s = 2\pi r_e / T_s$ about X - axis as shown in the Fig. 1. The de Broglie wavelength λ associated with such an electron will be given by $\lambda = h/m_0 v_s$, where if $\lambda/2$ be equal to $2\pi r_e$, then obviously spin angular momentum will be given by

$$m_0 v_s r_e = h/4\pi = s.(h/2\pi)$$

where $s = 1/2$, a result used to detail the atomic and molecular physics. This spin motion of time period T_s will generate a magnetic field

$$H = \mu_0 (e / T_s) / 2 r_e = \left(\mu_0 e v_s / 4\pi r_e^2 \right)$$

along the X– axis which in turn (due to electromagnetic interactions of magnetic field with the charge will keep the electronic spin motion sustained. In this case the Lorenz force will act as the centripetal force equal to Hev_s which in turn must be equal to centrifugal force $m_0 v_s^2 / r_e$. Equating these two we get

$$Hev_s = m_0 v_s^2 / r_e \text{ or } \left(\mu_0 e v_s / 4\pi r_e^2\right) e v_s = m_0 v_s^2 / r_e .$$

substituting $\mu_0 = 1 / \varepsilon_0 c^2$, we get that the electrostatic energy,

$$E = e^2 / 4\pi \varepsilon_0 r_e = m_0 c^2$$

Obviously for this model the electronic mass appears as the equivalent mass to its net electrostatic energy, concluding that the electron the ultimate particle of electricity, has no mass in the material sense. Its mass is purely electrical.

Now let an electronic charge be smeared on a spherical surface of radius r_e and say spinning about X-axis as shown in the Fig. 1. Let O', the origin of S' frame of reference, be the centre as well of the charged spherical shell which is moving with uniform velocity v along X-axis with respect to another S frame of reference having the respective axes parallel to each other and being its origin O is just coinciding with O′ at the instant the figure has been drawn. This three dimensional spherical surface

may be generated by revolving a circle of radius r_e in the X'-Y' plane about the X-axis with its centre at O'. The equation of this plane of intersection of the spherical surface with the X'- Y' plane will be given by

$$x'^2 + y'^2 = r_e^2 \tag{1}$$

Let in the X'-Y' plane, $P'(x'. y', 0)$ be a point on the charged spherical shall having its foot of the perpendicular on the x-axis at C'. The circulating charge at P' and the magnetic field acting along the x-axis must be in conformity with each other, that is in the dynamic equilibrium the disturbances caused by them will travel with the velocity of light c and will be received in pace. Let δt be the time elapse in which a signal reaches from C' to P' then

$$\delta t = (C'P')/c$$

or $$y' = C'P' = c.\ \delta t = r_e \sin\theta' \tag{2}$$

where $$x' = r_e \cos\theta'$$

As this S' frame of reference is in relative uniform motion with S frame of reference the position of C' will appear at S further away from c by a distance

$$CC' = (v\ \delta t) = (C'P')\ v/c = r_e \sin\theta'.\ v/c \tag{3}$$

Now due to invariance of the speed of the light in uniformly moving frame of references with respect to one another, a result which is well confirmed by Michelson - Morley experiment, the point P' will appear at P so that .

$$CP = C'P' = y' = r_e \sin\theta'. \tag{4}$$

Therefore the ordinate y of the point P will appear into the S frame of reference of length $C'P$ and will be given by

$$y = \{(CP)^2 - (C'C)^2\}^{1/2} = \{(r_e sin\theta')^2 - (r_e \sin\theta'.v/c)^2\}^{1/2}$$

$$= r_e \sin\theta' \{1-(v/c)^2\}^{1/2}$$

$$= y'\{1-(v/c)^2\}^{1/2} \tag{5}$$

while the abscissa x of P will-remain the same as that of P' i.e.

$$x = OC' = x' = O'C' r_e \cos\theta' \tag{6}$$

The equation of the plane of intersection, of the Surface with the X-Y plane as observed in the S frame of reference will be had by substituting the values of. x' and y' in terms of x and y into the eqn. (1) then we have

$$x^2 + y^2 \{1-(v/c)^2\}^{1/2} = r_e^2$$

$$\text{or } x^2/\left[r_e^2\right] + y^2/\left[r_e^2\left\{1-(v/c)^2\right\}\right] = 1$$

$$\text{or } x^2/a^2 + y^2/b^2 = 1$$

where $a = r_e$ and $b = r_e\{1-(v/c)^2\}^{1/2}$.

When such an ellipse is rotated about x-axis it will generate an ellipsoid having its minor axis perpendicular to the direction of the motion. This gives us the structural change of a spherical shell of electronic charge which is at rest to an ellipsoidal shell of the same charge moving with an uniform velocity v. Thus the electronic charge smeared over the curved surface of the area $4\pi a^2$ of sphere of S' frame of reference will now appear as if it has smeared all over the curved surface of the area $4\pi ab$ of the ellipsoid in S frame of reference. Naturally the concentration of the charge will increase in the parts of the same quantum of charge. i.e. in the parts of the electron. This compression of the charge with in the body of the electron should increase the electrical energy stored in the surface possessed by the electron itself by the ratio of the curved surface area of the sphere to that of the ellipsoid. As the curved surfaces of the sphere and the ellipsoid are $4\pi a^2$ and $4\pi ab$ respectively. Therefore the ratio of the area of the sphere to that of the ellipsoid will be a/b. As the electric energy of the sphere of radius a is $e^2/4\pi\varepsilon_0 a$, the energy of the ellipsoid may be estimated as given below :

The energy of the ellipsoid = $(e^2/4\pi\varepsilon_0 a)\ a/b = e^2/4\pi\varepsilon_0 b$

= The electrical energy of a sphere of radius b.

Thus the electrical energy of a charged ellipsoid numerically is equal to $e^2/4\pi\varepsilon_0 b$ which is just the same as that of a charged sphere of radius b. Let us assume that the charge spherical shell of mass m_0 radius a being in the S' frame of reference and the charged elliptical shell of mass m_v in the S frame of reference, then their electrical energies will be

$$E_a = e^2/4\pi\varepsilon_0 a \text{ and } E_b = e^2/4\pi\varepsilon_0 b \text{ respectively}$$

The ratio $E_b : E_a$ will be given by

$$E_b/E_a = a/b = 1/(1-v^2/c^2)^{1/2},$$

where $a = r_e$ and $b = r_e \{1-v/c)^2\}^{/12}$.

Further as an electron possesses mass solely by virtue of its electric charge and has no mass in the material sense therefore the ratio $E_b : E_a$ must be equal to the ratio $m_v : m_0$, thus

$$m_v/m_0 = E_b/E_a = a/b = 1/(1-v^2/c^2)^{1/2}$$

or $m_v = m_0/(1-v^2/c^2)^{1/2}$.

This electron structure based formula ,tells us that the mass possessed by the electron in the frame of reference in which it is at, rest gets increased in a natural way in the frame of reference in which the electron is moving with an uniform velocity but so for the contraction in the radius of the charge sphere is concerned. it is perpendicular to the direction of motion. The theory of relativity derives the same relation for the variation of mass. In the relativistic formula the contraction takes place only in the direction of motion as in this case, a sphere is carried by an observer in motion it will appear as an ellipsoid for an observer at rest with its minor axis along the direction of the motion, where the structure of the particle is in no way considered.

3. The Planetary Elliptical Motion

As we have observed that the mass is purely electrical in nature and when this charge is in motion its mass increases. Every particle in the universe is composed of nuclear and of electronic charges having a mass and therefore it should vary with the velocity of the particle. This variation in mass must be numerically equal to that would

have obtained due to the application of the spatial theory of relativity. Further it suggests that the mutual gravitational attraction of the masses must have some kind of electromagnetic interaction since the mass itself have some kind of electrical origin. This view provides us a new way to picture the planetary motion.

A planet of mass m_p, in general moves on an ellipse around the Sun of mass M_s being at the focus Now whether the planet moves on a circular or an elliptical orbit the inverse square law of force will hold. The circular motion is more symmetric than the eccentric elliptical motion. It suggests that there must be one more condition which enables a circular motion to adopt the elliptical motion. In general a celestial body with initial velocity V_{ps}, with respect to Sun might have come from very remote place of the galaxy and entered into the gravitational field of the Sun which later on has appeared as a planet of mass m_p.

Let us consider first that a planet of mass m_p is moving on a circular orbit of radius around the Sun of mass M_s. For the dynamic equilibrium the centripetal force (GM_sm_p/a^2) must be equal to the centrifugal force $(m_pV_p^2/a)$ and the equation of the path will be

$$x^2 + y^2 = a^2.$$

If this has initial velocity V_{ps} with respect to Sun, the Sun will also has a relative velocity V_{sp} with respect to the planet equal and opposite to the velocity V_{ps} of the planet with respect to Sun. As we have considered that the gravitational interaction also being of some form of electromagnetic interaction. so every action acted by one on the other will also travel with the velocity of light c. The relative velocity V_{sp} of the Sun with respect to the planet will modify the equation of the path of the planet similar to the that which we have observed in the case of the electron. Considering the Sun at the origin let x', y' be the coordinates of the planet. Due to the relative motion the ordinate y will. get contracted to $y\ (1-V_{sp}^2/c^2)^{1/2}$ and will become y' while x will become x' that is

$$x = x' \text{ and } y = y'/\ (1-V_{sp}^2/c^2)^{1/2}$$

Substituting these values into the above-equation we get the equation of the path as

$$x'^2/[a^2] + y'^2/[a^2\{1-(V_{sp}/c)^2\}] = 1, \text{ or } x'^2/a^2 + y'^2/b^2 = 1,$$

which is an equation of ellipse with the major axis as a and the minor axis as $b = a\{1-(V_{sp}/c)^2\}^{1/2}$ The eccentricity ε will be given by $\varepsilon = V_{sp}/c$. Thus we find that the, orbits of the planets in general are elliptic where sun occupies a focus which is directed by the respective relative velocity V_{sp}.

As both the Sun and the planet are moving with velocity $|V_{sp}|$ relative to each other their respective masses will become $M_s/(1-V_{sp}^2/c^2)^{1/2}$ and $m_p/(1-V_{sp}^2/c^2)^{1/2}$ let at r distance apart, they settle in the mutual fields so that the planet continues to revolve round the Sun. Then the centripetal force must be equal to

$$G\{M_s/(1-V_{sp}^2/c^2)^{1/2}\}\ \{m_p/(1-V_{sp}^2/c^2)^{1/2}\}/r^2 = [GM_sm_p/r^2]\ (1+V_{sp}^2/c^2)$$

$$=[GM_sm_p/r^2]\ (1+\varepsilon^2).$$

When a body of mass m_p brought with infinitely slow motion from infinity to a distance r far from the Sun of mass M_s, there is a decrease in potential energy by $[GM_sm_p/r]$. The initial mass equivalent to the potential energy will be $\Delta M_{P,E} = [\{GM_sm_p/r\}/c^2]$.

The gravitational interactions have settled the body as a planet of mass m_p moving with an orbital velocity V_p, while in the, initial conditions the body was moving with the velocity V_{ps} hence the inertial mass equivalent to the potential energy $\Delta M_{P,E} = [\{GM_sm_p/r\}/c^2]$ will also continue orbiting with the same velocity V_{ps} with the planet. Allowing these considerations one can calculate the net centrifugal force as

$$[m_p]\ V_p^2/r + [\Delta M_{P,E}]\ V_{ps}^2/r = m_pV_p^2/r + [\{GM_sm_p/r\}/c^2]\ V_{ps}^2/r$$

$$= m_pV_p^2/r + [GM_sm_p/r^2]\ (V_{sp}^2/c^2)$$

$$= m_pV_p^2/r + [GM_sm_p/r^2]c^2$$

For equilibrium the centripetal force must be. equal to the centrifugal force, therefore

$$[GM_sm_p/r^2]\ (1+\varepsilon^2) = m_pV_p^2/r + [GM_sm_p/r^2]\ \varepsilon^2$$

or $$GM_s m_p/r^2 = m_p V_p^2/r$$

or $$V_p^2 = GM_s/r.$$

This equation shows that once the body is trapped as a planate its motion can be expressed in terms of the rest mass of the sun and the distance. The only clue regarding its initial relative velocity V_{ps}, which is just before appearing the scene. is given by tile eccentricity ε of the elliptical orbits. The elliptical orbit has more energy over and above than that of a circular orbits of radius a (the semi major axis) by a

value $\Delta M_{P,E} = V_{ps}^2/2$ where $\Delta M_{P,E.}$ is the inertial mass equivalent to the potential energy. Similarly the rosette shaped path of mercury about the sun that is the processional motion of the major axis of the orbit may be accounted by the variation of the inertial mass equivalent to its kinetic energy with its orbital velocity since the change in mass is greatest at the perihelion. it results in a precession of the orbit of the planet. The perihelion of the ellipse rotates as the time passes on i.e, the major axis of the ellipse turns about the sun in the plane of the ellipse and the resultant path of the planet is not a simple ellipse but a complicated curve known as rosette.

4. The Molecular Gas

Let us consider one gm mole of a gas as a single whole of a bulk of material at a given temperature which is under thermal equilibrium with the radiant energy all around specified to this temperature. Further an entity is defined by the volume $v_0=V_0/N_A$, where the volume V_0 at the standard temperature T_0 and pressure p_0 contains N_A the Avagadro's number of molecules. From the knowledge of quantum theory a molecule is an entity which has blanketed by a whirling electron in the outermost orbital of the molecule as a whole. The electronic charges, their orbital and spin angular moment in a molecule with the nuclei keep up it electrically neutral and satisfy the valances in the dynamic equilibrium states. The outermost dynamic electron which envelopes the nuclei with their other satellite electrons of the molecule offers itself as an enclosure to all confined nuclei and electrons as well as it completely shields their electromagnetic interactions outside the enclosure except the only outermost election is capable to influence the neighbor. Thus every molecule as an entity may be regarded as a mass point of the rest mass m_e equivalent to that of the electromagnetic or electrical mass of an electron providing some sort of very weak attractive force of electromagnetic or electrical origin on its similar neighbor

molecule/entity. Let thjs arisen force be the well known gravitational force T_0 effect this for a gas at any temperature T the following two assumptions are made *viz.*

(i) that (T/T_0) times an entity is the number of entities for. electromagnetic mass interaction.

(ii) that the number of entities present in a gas at any temperature T are defined by the ratio V_T/V_0, i.e. $V_T/V_0 = N_A(T/T_A)$ entities in all.

At the same time these entities may be considered as surrounded by the space, just like that of a black body, which is full of radiant energy in which the photons of various frequencies following the temperature dependent statistical laws of distribution are under motion in all possible directions. In our case there is very large empty space between and within the-entities as molecules being of very small, dimensions compared to that occupied by an entity, which may be regarded as free space provided for the motion of the photons and when they have occasionally encounters with the electrons get absorbed by the electrons of the outer most orbital and then followed-by. their release and so on. Consider the ideal gas at S.T.P. having Avagadro's number N_A (6.022169×10^{23}) of entities say primary molecules in volume V_0 (22410.656 cc) at temperature T_0 (273.l6 K). Further we may estimate the space volume V_0 provided for this single entity. For to evaluate this simply the volume has to be divided by the number of the molecules/entities present i.e. $V_0 = V_0/N_A = 3.7213595 \times 10^{-20}$ cc per entity be a constant quantity strictly for an entity at all temperatures. Let a_0 be the radius of average spherical confinement for this entity of volume equivalent to V_0 then $= 4\pi a_0^3/3$, therefore $a_0 = 20.711156 \times 10^{-8}$ cm.

As the size of a molecule is a few Angstrom (10^{-8} cm), the space in which an entity lies is thousand times larger than that of it. Therefore, one may picture this situation classically as every entity with regard the other entity is situated very far from one. another. The outermost dynamic electron which envelopes the nuclei with their other satellite electrons of a molecule. offers itself as an enclosure to all confined nuclei and the other electrons as well as it completely shields their electromagnetic interactions outside the enclosure. The only whirling electron is capable to in influence the neighbor. every entity may be regarded as a mass point (of the rest mass the equivalent to that of the electromagnetic mass of an electron) providing a some sort of very weak inertial attractive force on its neighbor molecule/entity arisen due to some kind of unknown electromagnetic interaction with similar entities at :S.T.P. Let this force be the well known universal gravitational force.

5. The-Molecule and Photon Interaction

The study of blackbody radiation has revealed that the space inside the black body is full of radiant energy in which the photons of, various frequencies following the temperature dependent statistical laws of distribution are under motion in all possible directions. In our case there is very large empty space between and within the entitles which may be regarded as free space provided for the motion of the photons and when they have occasionally encounters with the electrons get absorbed by the electrons of the outer most orbital and then followed by their release and so on :

6. Equilibrium between the Thermal Radiation and Potential Energy of Molecules

Combining the concepts of [4] and [5] together we may consider one gm mole of a gas as a single whole of a bulk of material at a given temperature which is under thermal equilibrium with the radiant energy all around specified to this temperature

To resolve this problem—

(a) we first calculate the lowering of potential energy of an entity as being under the action of a weak inertial attractive forces viz. universal gravitational forces of other entities

(b) Secondly we estimate the number of entities enveloping the appropriate shell which is holding one gm mole bulk.

(c) The net potential energy of these entities, which may be regarded as the ground state of the bulk, may be excited by the absorption of the incident radiant photons and be re-radiated out after the relaxation time. This released energy per unit cross section of the exposing surface of the bulk per unite time must be equal to the amount desired by Stefan's law for thermal equilibrium.

6 (a) The lowering of potential energy of an entity as being under the action of a weak attractive gravitational influences of the rest of entities

First we consider a gas at S.T.P. The volume V_0 at the standard temperature T_0 and pressure P_0 contains $.N_A$ number of entities. The volume $V_0 = .V_0 / N_A$ may be considered as a volume of a cell which is necessary to define one entity at temperature T_0. Now let us introduce two assumptions as follows :

(i) that T / T_0 times an entity is the number of entities for electromagnetic mass interaction,

(ii) that the number of entities present in a gas at any temperature are defined by the ratio V_T / T_0, i.e. $V_T / T_0 = N_A (T / T_0)$ entities in all.

Let a_T be radius of the spherical shell provided for a single molecule at temperature T then $V_T = V_0 T / T_0 = N_A V_0 T / N_A T_0 = (N_A T/T_0)(4\pi/3) a / a_0^3$, where $a_0 = (3 V_0/4\pi N_A)^{1/3}$. Further let us draw imaginary concentric spheres of "radii a_0, 3 a_0, 5 a_0,....., $(2r\text{-}1)\ a_0$, to $(2n_T\text{-}1)a_0$, so that the last sphere of radius $(2n_T\text{-}1)\ a_0$, includes the whole volume of 1 gm mole of the gas at temperature T, then N_A number of molecules which were the number of entities at temperature T_0 will now assume the number $N_A(T/T_0)$ then. $(4\pi/3)\ [(2n_T\text{-}1)\ a_0,]^3 = (N_A T/T_0).(4\pi/3)\ a_0^3$, or $(2n_T\text{-}1) = (N_A T/T_0)^{1/3}$. N_A being a large quantity.

$2n_T = (N_A T/T_0)^{1/3} + 1$ and will be approximately equal to $\sim (N_A T/T_0)^{1/3}$ or $n_T = (1/2)$ $(N_A T/T_0)^{1/3} = 42223509\ (T/T_0)^{1/3}$.

Thus the radii a_0, $3a_0$, $5a_0$, ..., $(2n_T\text{-}1)\ a_0$ will divide the whole space in $(n_T\text{-}1)$ concentric spherical annular zones z_0, z_1, z_2, etc. in which the rth zone (z_r) will be comprised of $\{2r+1)^3\text{-}\ (2r\text{-}1)^3\}$ entities. These entities will be equidistant from the centre of the central zone z_0 and the centre of this zone z_r will be at a distance $r.2a_0$ from the centre.

Now to visualize a spherical shell filled with one gm mole of the gas, we first assume that initially there is a single entity at the centre, then z_1 zone of which mid point is at $2a_0$, and continuing to say to rth zone z_r filling it with.$\{(2r+1)^3\text{-}(2r\text{-}1)^3\}$entities which will be at $2ra_0$ distance till r becomes n_T for the last zone.

To calculate the lowering of potential energy of an entity of this system, we assume first that up to z_{r-1} th zone have already been filled with $(2r\text{-}1)^3$ entities. Using the assumption (i) that (T / T_0) times an entity is a factor for electromagnetic inertial interaction and the only the rest mass of the outermost whirling electron of an entity is capable to influence the neighbor. the effective inertial mass of this core will become $[(2r\text{-}1)^3.\ T/\ T_0\ m_0]$. Further to fill the z_r th zone, we have to bring $\{(2r+1)^3\text{-}(2r\text{-}1)^3\}$ number of entities. in which every entity will be at a distance $2ra_0$ from the centre. The effective inertial mass of this core will become

$[\{(2r+1)^3\text{-}(2r\text{-}1)^3\}(T / T_0).\ m_0\]$.

The drop in potential energy ΔW_r will be given by

$$\Delta W_r = G[2r\text{-}1)^3 T/T_0.\ m_0]\ [\{2r+1)^3\text{-}(2r\text{-}1)^3\}\ T/T_0 m_0]/2r a_0.$$

$$= G m_0^2 (T/T_0)^2 (2r - 1)^3.\ (12r^2 + 1) / a_0.r$$

$$= G[m_0^2 (T/T_0)^2 / a_0]\ [96r^4 - 144r^3 + 80r^2 - 24r + 1 - 1/r]$$

Therefore the net potential energy of the entity at the center may be had by summing up the above expression for $r = 1$ to n_T, i.e. we have

$$W = \sum_{r=1}^{n_T} \Delta W_r = G[m_0^2 (T/T_0)^2/a_0] \sum_{r=1}^{n_T} [96r^4 - 144r^3 + 80r^2 - 24r + 1 - 1/r]$$

$$= G m_0^2 (T/T_0)^2 / a_0.] \quad [96/5]\ n_T^2$$

neglecting cubic and lower powers of r since $n_T = [1/2]\ ((N_A T/T_0)^{1/3})$ being a large quantity and $a_0 = (3\ V_0/4N_A)^{1/3}$ Therefore we have

$$W = [1/2^5][96/5]\ [G N_A^2 m_0^2 (T/T_0) 1^{1/3}]/(3V_0/4\pi)^{1/3}$$

The value of W so obtained for single entity may be generalized to every entity all being under the dynamic equilibrium.

6(b) Estimation of the number of entities per unit area of the enveloping surface of the appropriate shell which is holding 1 gm mole of the gas :

For the estimation of this number we divide the whole volume V_T of the spherical shell into tiny cubes having their faces normal to X, Y, Z axes. Let δ be the edge of cubical cell of volume V_0 at the temperature T_0 then $V_0 / N_A = \delta^3$, which confines a single molecule. Now as we know that

$$V_T = V_0 T/T_0 = N_A V_0 T / N_A T_0 = (N_A T / T_0)\ (V_0 / N_A)$$

$$= (N_A T / T_0)\delta^3 = (4\pi/3)[(3/4\pi)(N_A/8)\ (T/T_0)]\ (8\delta^3)$$

$$= \frac{4\pi}{3} n^{*3} (2\delta)^3$$

where $n^* = [(3/4\pi)\,(N_A/8)\,(T/T_0)]^{1/3}$

This gives us a clue and proposes how to construct a spherical shell of radius $n^*.2\delta$ having its volume V_T made by tiny cubical cells of edge 2δ arranged along the axes X, Y, Z. In this case we can calculate the number of the cells constituting the peripheral enveloping spherical surface similar to previous section and will be equal to

$$\{(2n^* + 1)^3 - (2n^*-1)^3\} = 24\,n^{*2} + 2 = 24\,n^{*2} \text{ approximately}$$

Using the assumption (i) that (T / T_0) times an entity is a factor for electromagnetic inertial interaction, the effective number of the cells constituting the peripheral enveloping spherical surface will become $.24n^{*2}\,(T / T_0)$.These peripheral enveloping cells being in thermal equilibrium with the outer radiation, they can casually absorb and permit the incident radiation to pass through to the interior to get absorbed by the other molecules during their passage through the bulk ,by which the gravitational state of these entities may get excited. As the exposed surface is $6(2\delta)^2$ of a tiny cell and $N_A\ T/\ T_0$, according to the assumption (ii), is the number of entities all over the volume, the net surface will be equal to $6N_A(T / T_0)\,(2\delta)^2$. The average number of entities per unit area of the exposed surface

$$= 24\,n^{*2}\,(T/\ T_0)/6N_A\,(T/\ T_0)\,(2\delta)^2 = n^{*2}\,/\,N_A\delta^2\ .$$

Therefore the potential energy of these entities is lowered by W $(n^{*2}/N_A\,\delta^2)$ per unit area normal to any of the axes where $n^* = [(3/4\pi)\,(N_A/8)\,(T / T_0)]^{1/3}$, $\delta = (V_0 / N_A)^{1/3}$ and $W = [1/2^5]\,[96/5]\,[G\,N_A^2 m_0^2 (T/T_0)^{11/3}] / (3V_0 / 4\pi)^{1/3}$.

6 (c) The relaxation time Δt and deduction of the formula for G :

This net potential energy per unit area normal to any of .the axes due to attractive actions of the entities, which restrict the free motion of the molecules, may be over come by absorbing the radiation in its course of passage through a cell and re-radiating out it after the relaxation, time Δt to maintain the thermal equilibrium. The relaxation time may be considered as the time required to travel a photon though the distance $2\delta_T$ where $2\delta_T = 2(V_0/N_A)^{1/3}\,(T/T_0)^{1/3}$ being the edge of an actual cubic cell at temperature T therefore $\Delta t = 2\delta_T/c$.

Therefore the energy released per unit cross-section per sec. will be given by

$$(n^{*2}/N_A\delta^2)W(c/2\delta_T)=(1/2)\, n^{*2}cW/N_A\delta^2\, \delta_T =(1/2)\, n^{*2}cW/V_0\, (T/T_0)^{1/3}$$

This released radiation energy amounting equal to potential energy per unit area per sec normal to any of the axes of 1 gm mole of the bulk must be equal to the amount received by the Stefan's law (the normal radiation per writ area per sec = σT^4) for thermal equilibrium. Therefore equating these two we get

$$\sigma T^4 = (1/2)\, n^{*2}cW/V_0\, (T/T_0)^{1/3}$$

$$= (1/2)\, [3/4\pi(N_A/8)\, (T/T_0)^{2/3}.c.[1/2^5]\, [96/5]$$

$$[\, GN_A^2 m_0^2 (T/T)^{11/3}\,]/(3V_0/4\pi)^{1/3}.\, V_0(T/T_0)^{1/3}$$

or $$\sigma = G\, [\{3/4\pi N_A\}^{2/3}/8V_0]\, [1/2^5]\, [96/5]\; N_A^2 m_0^2 (1/T_0)^4\,]/(3V_0/4\pi)^{1/3},$$

or $$G = \sigma/(3V_0/4\pi)^{1/3}/\, [\{(3/4\pi)N_A\}^{2/3}/8V_0]c\, [1/2^5]\, [96/5]\; N_A^2 m_0^2 (1/T_0)^4\,]$$

or $$G = 21.493226\, \sigma.T_0^4.V_0^{4/3}/N_A^{8/3}.m_0^2.c$$

The value of G may be calculated using the standard data[2] given below :

$c = 2.997925 \times 10^{10}$ cm/sec.		LT^1
$m_0 = 9.1095 \times 10^{-28}$ gm		M
$N_A = 6.022169 \times 10^{23}$		
$V_0 = 22410.656$	cc	L^3
$T_0 = 273.16$	K	K
$\sigma = 5.6697 \times 10^{-5}$	ergs per sec. per K^4	
$G = 6.6732 \times 10^{-8}$	c.g.s	$M^{-1}L^3T^{-2}$

The value of G when calculated comes out to be 6.6627×10^{-8} c.g.s. which is strikingly very close to the standard-value of gravitational constant G and just fails lower by 0.157 % only supporting its origin in the assumptions made earlier.

Conclusion

Considering the above said the mathematical calculations yield the formula for universal gravitational constant G in terms of standard values of velocity of light, rest mass of an electron, Stefan' constant and Avagadro's number of molecules, the volume and temperature of one gm mole of a gas at S.T.P. which as given below :

$$G = 21.493226\ \sigma\ T_0^4 . V_0^{4/3} / N_A^{8/3} . m_0^2 . c$$

The result is in fair agreement with the standard value of G.

References

1. Rajam, J.B. (1965) *Atomic Physics,* 17th Edition. Atmaram and Sons. New Delhi. p. 50.
2. Valerie, H. Pitt (1977) *The Penguin Dictionary of Physics*, Lawrence Urdang Associates Ltd. Penguin Books Ltd. Harmondsworth, England.

PROC. NAT. ACAD. SCI. INDIA, 73 (A), III, 2003

Dependence of rotational constants of diatomic oxides and chalcogenides on electronegativity

V. G. ASOLKAR* and C. MANDE

**L.A.D. College for Women, Shankar Nagar, Nagpur-440 010, India.*

Department of Physics, Nagpur University, Nagpur-440 0033, India.

Received Oct., 16, 2000; Revised June 27, 2001; Accepted December 11, 2002

Abstract

The dependence of the values of rotational constants B_e of the diatomic oxide and chalcogenide molecules of the elements of the groups IIA, IIIA, IVA, IVB and VA on electronegativity has been studied. The equation proposed by us earlier for the diatomic halides, in which the bonds exhibit predominant ionic character, is found to be valid for the IIA and IVB oxides and chalcogenides. For the rest of the oxides and chalcogenides, the equation proposed by us for the intragroup and homonuclear diatomic molecules is applicable indicating that the electronegativity equalization takes place in these molecules giving a covalent character to the bonds.

(**Keywords** : rotational constants/electronegativity/diatomic oxides/chalcogenides).

Introduction

The study of molecular spectra provides very useful information about the electronic structure as well as the vibration and rotation of the atoms in molecules[1]. Such studies in turn help in obtaining accurate information about geometrical arrangement of atoms in molecules, leading to the understanding of many of their physical and chemical properties.

Several properties of molecules depend upon the electronegativity values of their constituent atoms[2-6]. The equilibrium internuclear distance r_e in a diatomic molecule is decided by the force of attraction between the two atoms, which can be considered to be of related to the electronegatvities of the constituent atoms. The internuclear distance r_e is also related to the rotational constant B_e through the expression[7]

$$B_e = \frac{h}{8\pi^2 c\mu r_e^2}, \qquad (1)$$

where h is the Planck's constant, c is the speed of light and μ is the reduced mass of the diatomic molecule. In our earlier papers we have attempted to systematise the data on rotational constant B_e of some diatomic halides[8-9] and homonuclear and intragroup heteronuclear diatomic molecules[10] with the help of electronegativity. We have also been able to estimate the values of B_e in those cases in which the spectroscopic data on B_e were not available in literature. In the present paper, we have made an attempt to see if the available data on B_e in diatomic oxides and chalcogenides can be systematised in a similar fashion. We have considered only those molecules here, on which some work has been reported in literature, and which, therefore, seem to exist.

Rotational Constants and Electronegativity

Our earlier work shows that the rotational constant B_e of molecules exhibiting predominant ionic character can be correlated with the electronegativity difference $\Delta\chi$ of the constituent atoms A and B through the expression[8-9]

$$\log B_e = m \log \left(\frac{\Delta\chi}{\mu^2} \right) + C. \qquad (2)$$

We have tested this expression for the diatomic halides of the elements of the groups IA, IB, IIA, IIIA, IIIB, IVA and VA, in which the halogen atom is an electron acceptor. The values of the slope m and intercept C for the plots of log B_e versus log $(\Delta\chi/\mu^2)$ are found to be different for each of the groups.

For the intragroup and homonuclear diatomic molecules however, the situation is different. In the case of a homonuclear diatomic molecule AA, since the electronegativity difference is zero, equation (2) is not applicable. We have shown[10] that in the case of such molecules of group IA, VA, VIA and VIIA, the following equation

$$\log B_e = m \log \left(\frac{\chi}{\mu^2} \right) + C, \qquad (3)$$

is applicable. With the help of this equation we have estimated[10] the data on B_e in some homonuclear diatomic molecules, *viz.* Rb_2 and Te_2 which were not reported in literature[11].

The intragroup diatomic, molecules are strongly covalent because the constituent atoms have a strong tendency of sharing electrons rather than transferring them from the element of lower electronegativity value to the element with higher electronegativity value. In the case of a diatomic molecule held together by a single covalent bond, if the constituent atoms are different, then the polarity to the covalent bond is imparted to an extent and direction indicated by the initial electronegativity difference $\Delta\chi$. Sanderson[12] has suggested that to form a covalent bond, this must stop, and the electronegativities of the two atoms eventually become equal. Our earlier work has shown[10] that in intragroup heteronuclear diatomic molecules AB, the rotational constant B_e is related to the electronegativity values χ_A and χ_B of the constituent atoms through the relation

$$\log B_e = m \log \left(\frac{\sqrt{\chi_A \chi_B}}{\mu^2} \right) + C. \qquad (4)$$

It can be seen that equation (3) is just a special case of equation (4).

Rotational Constants of Diatomic Oxides and Chalcogenides, and Electronegativity

In the present paper, an effort is being made to see whether equations (2) and (4) can be extended to the diatomic molecules in which the acceptor atom B can accept two electrons. The diatomic oxide and chalcogenide molecules are expected to exhibit such behavior, and hence the present study has been undertaken. As a spin-off of this study, we have been able to estimate the values of B_e. for MgS, SrS, SrSe, TiS, InO, AlSe, GeSe, SiTe and SbO, for which data are not available in literature.

In Table 1 are given the values of the reduced mass μ as cited by Huber and Herzberg[13] and of the rotational constant B_e of the oxides and chalcogenides of the groups IIA, IIIA, IVA, IVB and VA, as cited in the CRC Handbook of Chemistry and Physics[11], 80th edition (1999-2000). The data on B_e on the molecules BiO, BiS, PS and HfO which are not given in the CRC Handbook are taken from reference 13. These values are reported to be either uncertain or of B_o, the lowest vibrational states, as cited by Huber and Herzberg. The data on the oxides and chalcogenides of other groups are too scanty. In this Table are also given the electronegativity values χ_A and χ_B (which are taken from the scale of Mande and coworkers[14-15], as was done in our

earlier papers[7-10]) along with the values of $\Delta\chi$ and $\sqrt{\chi_A\chi_B}$. We have plotted the values of B_e against the values of log $(\Delta\chi/\mu^2)$ for IIA, IIIA, IVA, IVB and VA oxides and chalcogenides. We obtain linear plots for IIA and IVB oxides and chalcogenides (Figs 1 and 2). However, the scatter in the plots for IIIA, IVA and VA chalcogenides is found to be large. Hence these curves are not shown in this paper.

Table 1–The values of electronegativity, reduced mass μ and rotational constant B_e of different molecules.

Molecules	χ_A	χ_B	$\Delta\chi$	$\sqrt{\chi_A\chi_B}$	μ(amu)	B_e(cm^{-1})
IIA oxides and chalcogenides						
BeO	2.11	3.71	1.60	2.80	5.7643286	1.6510
MgO	1.32		2.39	2.21	9.5957763	0.57470436
CaO	1.07		2.64	1.99	(11.4229222)	0.444441
SrO	0.73		2.98	1.65	13.5325857	0.33798
BaO	1.03		2.68	1.95	14.3325535	0.3126140
BeS	2.11	2.63	0.52	2.36	7.0304618	0.79059
MgS	1.32		1.31	1.86	(13.7042728)	0.2136*
CaS	1.07		1.56	1.68	17.7617688	0.1766757
SrS	0.73		1.90	1.39	(23.444936)	0.1328*
BaS	1.03		1.60	1.65	(25.954702)	0.10331
SrSe	0.73	2.57	1.84	1.37	(41.860451)	0.0592*
IIIA oxides and chalcogenides						
BO	2.23	3.71	1.48	2.88	6.52093998	1.7820
AlO	1.48		2.23	2.34	10.0419499	0.64136
GaO	1.77		1.94	2.56	12.982250	[(0.4271)]

Contd.. Table 1

Contd.. Table 1

InO	1.36		2.35	2.25	14.0404513	0.3296*
BS	2.23	2.63	0.40	2.42	8.1893677	0.79489
AlS	1.48		1.15	1.97	14.6327874	0.2799
AlSe	1.48	2.57	1.09	1.95	(20.171277_4)	0.1528*
IVA oxides and chalcogenides						
CO	2.73	3.71	0.98	3.18	6.58620870	1.93128075
SiO	1.87		1.84	2.63	10.1767074	0.7267521
GeO	2.01		1.70	2.73	13.1496247	0.4856981
SnO	1.59		2.12	2.43	14.112331	0.3557190
PbO	1.67		2.04	2.49	14.8526391	0.30730
CS	2.73	2.63	0.10	2.68	8.72519425	0.8200434
SiS	1.87		0.76	2.22	14.9206887	0.30352788
GeS	2.01		0.62	2.30	22.318826	0.1865676
SnS	1.59		1.04	2.04	25.241415	0.1368619
PbS	1.67		0.96	2.10	27.7119406	0.11632307
CSe	2.73	2.57	0.16	2.65	(10.43336091)	0.5750
SiSe	1.87		0.70	2.19	20.7224688	0.1920117
GeSe	2.01		0.56	2.27	(38.401003)	0.0899*#
SnSe	1.59		0.98	2.02	47.954285	0.06499776
PbSe	1.67		0.90	2.07	57.732418	0.05059953
SiTe	1.87	2.16	0.29	2.01	(23.019425)	0.16998*

Contd.. Table 1

Contd.. Table 1

GeTe	2.01		0.15	2.08	47.11256	0.06533821
SnTe	1.59		0.57	1.85	(62.351952_6)	0.4247917
PbTe	1.67		0.49	1.90	(79.961030_2)	0.03130774
IVB oxides and chalcogenides						
TiO	1.42	3.71	2.29	2.30	11.9938851	0.53541
ZrO	1.29		2.42	2.19	13.5790589	0.42263
HfO	1.58		2.13	2.42	(14.68922344)	[0.3860]
TiS	1.42	2.63	1.21	1.93	(19.1816180)	0.1823*
VA oxides and chalcogenides						
NO	3.26	3.71	0.45	3.48	7.46643320	1.67195
PO	2.21		1.50	2.86	10.5479381	0.7337
AsO	2.31		1.40	2.93	13.1809338	0.48482
SbO	1.79		1.92	2.58	(14.126107_1)	$0.3850^{*\#\#}$
BiO	1.77		1.94	2.56	14.8577	0.3034
NS	3.26	2.63	0.63	2.93	9.7380290	0.769602
PS	2.21		0.42	2.21	15.7325010	(0.29)
BiS	1.77		0.86	2.16	27.7296877	[0.112764]

Note :

1. Uncertain quantities in the data as mentioned in reference 10 are given in parentheses.
2. Quantities in square brackets [] in column 7 refer to B_o the value of the rotational constant for the lowest vibrational level.
3. We have considered only the magnitudes of $\Delta\chi$, the electronegativity difference.
4. The values of B_e indicated by *sign are obtained by us by extrapolation from the individual graphs.
5. $^{\#}$Value of B_e for GeSe reported as 0.09634051 cm^{-1} for $^1\Sigma^+$state in reference 11.
6. $^{\#\#}$Value of B_e for SbO reported as 0.3580 cm^{-1} for $^2\prod_{1/2}$ state in reference 11.

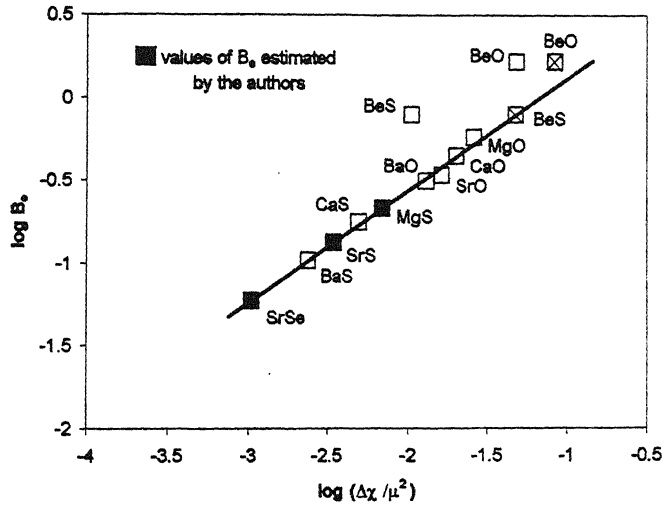


Fig. 1–Plot showing the variation between the values of log B_e and log ($\Delta\chi/\mu^2$) for IIA oxides and chalcogenides.

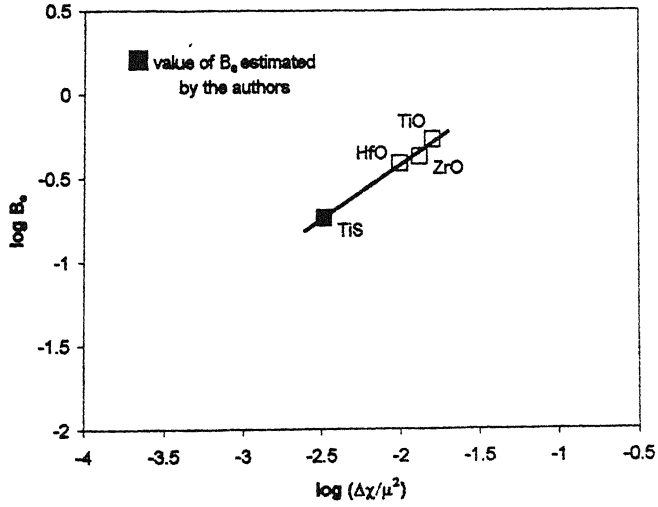


Fig. 2 –Plot showing the variation between the values of log B_e and log ($\Delta\chi/\mu^2$) for IVB oxides and chalcogenides.

Discussion

IIA and IVB oxides and chalcogenides

It can be seen from Fig. 1 that except for BeO and BeS, all other IIA oxides and chalcogenides fall on the straight line with $m = 0.68$ and $C = 0.79$, and the coefficient coefficient $R^2 = 0.9864$. This suggests that the chemical bonding in these molecules (except BeO and BeS) is more or less of the predominantly ionic type, since these molecules get systematised with the help of equation (2). The scatter in the case of BeO and BeS will be discussed later in this paper. We noticed that the data on rotational constant B_e of MgS, SrS and SrSe molecules are not available in literature. Hence we have used the curve in Fig. 1 to estimate the value of B_e in these molecules, which come out to be 0.2136 cm^{-1}, 0.1328 cm^{-1} and 0.0592 cm^{-1} respectively.

In the case of IVB oxides and chalcogenides (Fig. 2), the curve of log B_e versus log $(\Delta\chi/\mu^2)$ is found to be a straight line with $m = 0.66$, $C = 0.89$ and $R^2 = 0.8743$, passing through the points for TiO, ZrO and HfO. Although the point for TiS lies away from the points of the other three oxides, we have ventured to estimate the value of B_e of TiS from this curve by extrapolation which comes out to be 0.1823 cm^{-1}.

The other oxides and chalcogenides

The scatter in the plots of log B_e vs. log $(\Delta\chi/\mu^2)$ for IIIA, IV A and VA oxides and chalcogenides (plots not shown here, as mentioned earlier) indicates that the bonding character in these molecules is not predominantly ionic. Hence we thought it worthwhile to re-examine the bonding picture in these molecules. The bonding in the IV A oxides and chalcogenides may be considered as a very typical case where in the molecule AB, the atom A can be thought to be donating two electrons to the atom B belonging to VIA group of elements.

As shown in Fig. 3 (a) the outermost electronic configuration of group IV A elements (C, Si, Ge, Sn, Pb) is $ns^2\ np^2$ (atom A) and that for group VIA elements (S, Se, Te) is $ns^2\ np^4$ (atom B). In the ionic picture of the molecule (Fig. 3(b))one may expect that two p electrons from atom A are transferred to the p orbital of the atom B, thereby making the electronic configuration of A^{2+} as ns^2 and that of B^2 as $ns^2\ np^6$. But because of the large scatter in the log B_e *vs.* log $(\Delta\chi / \mu^2)$ plot for these molecules, we decided to look for an alternative bonding scheme.

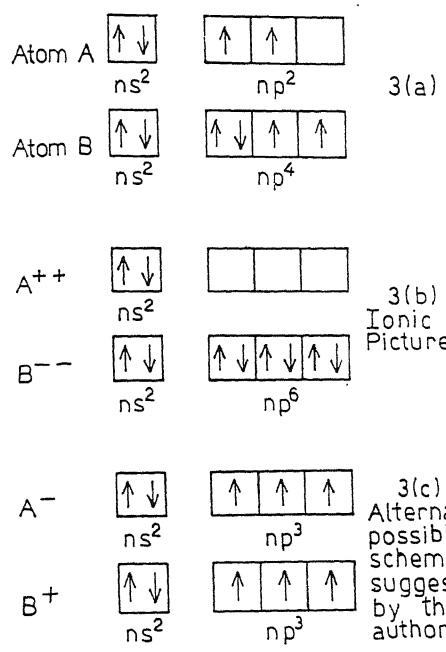


Fig. 3–Bonding schemes in IV A oxides and chalcogenides.

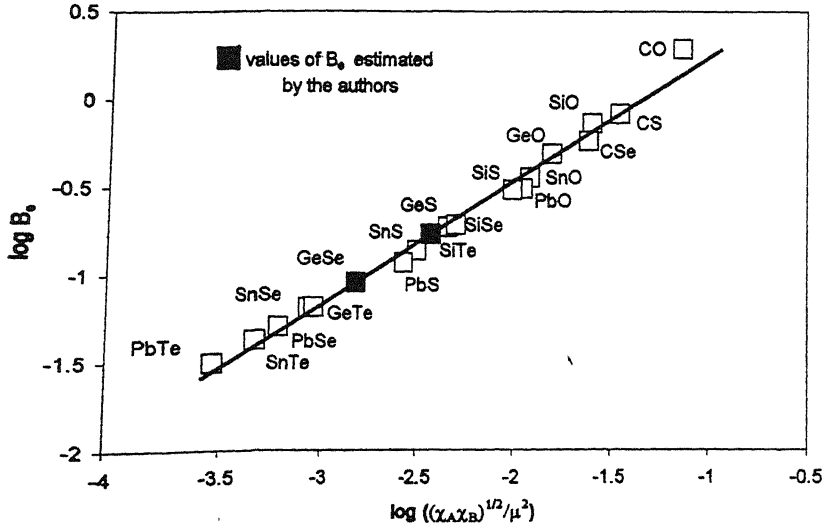


Fig. 4–Plot showing the variation between the values of log B_e and log $\left(\sqrt{\chi_A \chi_B}\,/\,\mu^2\right)$ for IV A oxides and chalcogenides.

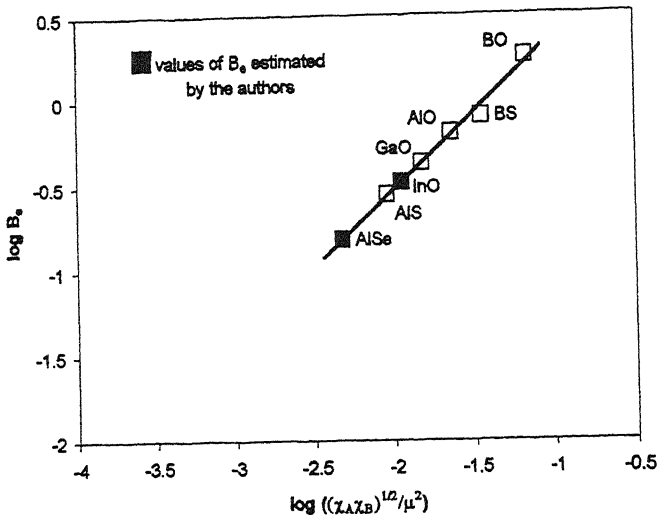


Fig. 5–Plot showing the variation between the values of log B_e and log $\left(\sqrt{\chi_A\chi_B}/\mu^2\right)$ for IIIA oxides and chalcogenides.

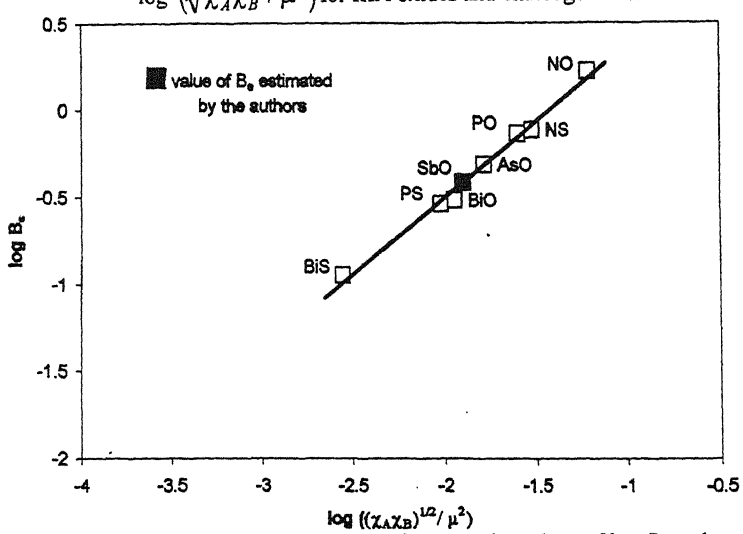


Fig. 6–Plot showing the variation between the values of log B_e and log $\left(\sqrt{\chi_A\chi_B}/\mu^2\right)$ for VA oxides and chalcogenides.

As shown in Fig. 3(c), it is possible that a p electron from the atom B is transferred to the p orbital of the atom A, thereby making the electronic configuration of A^- and B^+ similar ($ns^2\ np^3$), which may lead to electronegativity equalization and in turn to the formation of a covalent bond in the molecule. We have checked this idea by plotting log B_e *vs.* log $(\sqrt{\chi_A\chi_B}/\mu^2)$ for the IV A oxides and chalcogenides. The plot thus obtained is shown in Fig. 4 which is a good straight line with $m = 0.71$ and $C = 0.94$, and correlation coefficient $R^2 = 0.9884$. This confirms our idea of the bonding picture A^-B^+ arising out of electronegativity equalization leading to prominent covalent character of the bond instead of the ionic picture $A^{2+}B^{2-}$ in IV A oxides and chalcogenides. From the plot in Fig. 4 we have estimated the values of B_e for SiTe and GeSe which come out to be 0.16998 cm^{-1} and 0.0899 cm^{-1} respectively.

The log B_e vs. log $(\Delta\chi/\mu^2)$ plots for IIIA and VA oxides and chalcogenides also exhibit large scatter suggesting that the bonding in these molecules may not be predominantly ionic. We therefore decided to check whether the bonding in them is predominantly covalent. We have plotted the values of log B_e vs. log $(\sqrt{\chi_A\chi_B}/\mu^2)$ for IIIA and VA oxides and chalcogenides in Figs. 5 and 6 respectively. As can be seen, the plots are good straight lines with negligible scatter. From the plot in Fig. 5 which is a straight line with $m = 0.90$, $C = 1.26$ and $R^2 = 0.983$, we have estimated the values of B_e for InO and AlSe which come out to be 0.3296 cm^{-1} and 0.1528 cm^{-1} respectively. The plot for VA oxides and chalcogenides (Fig. 6) is a straight line with $m = 0.87$, $C = 1.23$ and $R^2 = 0.9893$. From this plot we have estimated the value of B_e for SbO which comes out to be 0.3850 cm^{-1}.

The case of B_eO and BeS

The case of BeO and BeS has been discussed in our recent paper[16]. The scatter for the points for BeO and BeS in the plot in Fig. 1 indicates that these molecules may have different bonding characteristics as compared to the other oxides and chalcogenides of the same group. In the latter molecules, the bonding seems to be predominantly ionic as they can be systematised very well with the help of equation (2). Hence we decided to check whether these two molecules exhibit covalent character. Shown in Fig. 1 by ⊠ are the values of log B_e plotted against log $(\sqrt{\chi_A\chi_B}/\mu^2)$ for BeO and BeS, which are seen to be better accommodated on the curve. This confirms our feeling that in BeO and BeS the bonds may have a large covalent character. The case of these two molecules is interesting and needs further investigation. The predominant covalence in these molecules may probably arise from the lightness and small size of the beryllium atom.

Support to the values of B_e estimated by us

We may mention here that no claim can be made about the accuracy of the values of B_e estimated by us since the values of the reduced mass in all these molecules (except for In O) are reported to be uncertain (see the footnote of Table 1) and also because the values of χ are known up to two places after the decimal point.

As is evident from equation (1), the value of the internuclear distance r_e can be calculated from the value of B_e. To check the correctness of the values of B_e estimated by us, we have calculated the values of r_e in all these nine molecules by using equation (1). Given in Table 2 are the values B_e estimated by us and those of r_e calculated from these values of B_e. In column 4 of this table are given the experimentally determined values of r_e in some of these molecules as reported in the CRC Handbook of Chemistry and Physics[11,17]. We find that the percentage error of the calculated values of r_e compared with the experimental values is about five percent. Thus, there appears to be a fair agreement between the values of r_e determined from the B_e values estimated by us and the experimental values. Our values of r_e can be considered to be accurate up to 0.01 A°. We may mention here that this much accuracy is considered sufficient for most physical and chemical work.

Table 2–Comparison between the values of internuclear distance r_e calculated by us, and the experimentally reported values of r_e.

Molecule	B_e (cm^{-1}) estimated by us	Value of r_e (in A°) from the value of B_e	Experimental value of r_e (in A°)
MgS	0.2136	2.40	...
SrS	0.1328	2.33	2.4405*
SrSe	0.0592	2.61	...
InO	0.3296	1.91	...
AlSe	0.1528	2.35	...
GeSe	0.0899	2.21	2.1346#
SiTe	0.16998	2.08	...
TiS	0.1823	2.20	2.0825*
SbO	0.3850	1.76	1.826##

*values from ultraviolet (UV) spectroscopy

values from microwave (MW) spectroscopy

Value for $^2\pi_{1/2}$ state as mentioned in reference 11.

Concluding Remarks

Our work has once again brought out the usefulness of electronegativity in the systematization of the rotational behaviour of molecules. We have been able to estimate the indicative values of rotational constant B_e for several molecules for which data are not available. Support for our values of B_e in three cases comes from experimental r_e values. It should be worthwhile to determine the values of B_e for all these molecules experimentally.

We have been able to suggest a bonding scheme in the case of IVA oxides and chalcogenides. More rigorous theoretical calculations for understanding the nature of bonding in these and other molecules seem to be necessary. In particular, it will be interesting to calculate the exact number of electrons transferred from the atom A to the atom B in the diatomic chalcogenides, as has been done for the IA halides by Ohwada[18].

Acknowledgement

One of us (VGA) is very grateful to the University Grants Commission, New Delhi, India for awarding her a fellowship under the College Faculty Development Programme during the period when this work was carried out.

References

1. Herzberg, G. (1950) *Molecular Spectra and Molecular Structure I. Spectra of Diatomic Molecules*, D. Van Nostrand, New York.
2. Pauling, L. (1960) *The Nature of the Chemical Bond,* Oxford & IBH Publishing Co.
3. Sanderson, R.T. (1960) *Chemical Periodicity,* Van Nostrand Reinhold Co.
4. Sen, K.D. & Jorgensen, C.K. (1987) *Structure and Bonding 66*, ed. Springer-Verlag Berlin Heidelberg.
5. Huheey, J.E., Keiter, E.A. & Keiter, R.L. (1993) *Inorganic Chemistry -Principles of Structure and Reactivity,* Addison-Wesley Pub. Co.
6. Asolkar, V..G. & Mande, C. (1997) *Indian J. Phys.* **71 A(1)** : 47.
7. Herzberg, G. (1950) *Molecular Spectra and Molecular Structure I. Spectra of Diatomic Molecules*, D. Van Nostrand, New York, p. 106.
8. Mande, C. & Asolkar, V.G. (1996) *Indian J. Pure Appl. Phys.* **34** : 47.
9. Asolkar, V.G. & Mande, C. (1997) *Indian J. Pure Appl. Phys.* **35** : 359.
10. Mande, C. & Asolkar, V.G. (1999) *Proc. Nat. Acad. Sci. India* **69(A)II** : 237.

11. *CRC Handbook of Chemistry and Physics* (1999-2000), 80th Ed., CRC Press, U.S.A., p. 9-81 - 9-86.

12. Sanderson, R.T. (1960) *Chemical Periodicity.* Van Nostrand Reinhold Co., p.37.

13. Huber, K.P. & Herzberg, G. (1979) *Molecular Spectra and Molecular Structure IV. Constants of Diatomic Molecules,* Van Nostrand Reinhold Co., New York.

14. Mande, C., Deshmukh, P. & Deshmukh, P. (1977) *J. Phys. B.* **10** : 2293.

15. Mande, C., Chattopadhyaya, S., Deshmukh, P.C., Padma, R. & Deshmukh, P.C. (1990) *Pramana 35* : 397

16. Asholkar, V.G. & Mande, C. (2001) *Indian J. Pure Appl. Phys.* **39** : 130.

17. *CRC Handbook of Chemistry and Physics* (1999-2000), 80th Ed., CRC Press, U.S.A., p. 9-15 - 9-41.

18. Ohwada, K. (1991) *Spectrochimica Acta* **47A (No. 12)** : 1751.

Interaction of torsional waves with a penny-shaped crack situated in an infinitely long elastic cylinder

Namita Srivastava and Sujoy Das ... 359

Physics

Gravitational force as the inertial interaction of outermost electron of a molecule with its neighbour molecule in a gas

N. G. Dongre ... 373

Dependence of rotational constants of diatomic oxides and chalcogenides on electronegativity

V. G. Asolkar and C. Mande ... 391

EDITORIAL BOARD

Chief Editor
Prof. H.C. Khare
Chairman, Board of Governors, Motilal Nehru National Institute of Technology,
(Deemed University, Formerly Motilal Nehru Regional Engineering College),
Former, Professor of Mathematics, University of Allahabad;
The National Academy of Sciences, India, 5, Lajpatrai Road.
Allahabad – 211 002
Fax : 91-532-2641183; E-mail : nasi@sancharnet.in

1. Prof. R.P. Agarwal
Former Vice-Chancellor,
Rajasthan & Lucknow Universities,
B1/201, Nirala Nagar,
Lucknow – 226 020
(Mathematics)

2. Prof. Suresh Chandra
Emeritus Scientist,
Department of Physics.
Banaras Hindu University,
Varanasi – 221 005
Fax : 91-542-2317040
E-mail : schandra@banaras.ernet.in
(Physics)

3. Dr. Anil Kumar
Scientist,
Physical Chemistry Division,
National Chemical Laboratory,
Pune – 411 008
Fax : 91-20-5893355;5893761;5893619;5893212
E-mail : prs@ems.ncl.res.in; rrh@ems.ncl.res.in
(Chemistry)

4. Prof. B.L. Khandelwal
Emeritus Scientist (CSIR),
Defence Materials and Stores Research
and Development Establishment.
DMSRDE Post Office, G.T. Road,
Kanpur – 208 013
Fax : 91-512-2450404
(Chemistry)

5. Dr. G.S. Lakhina
Director, Indian Institute of Geomagnetism,
Dr. Nanabhai Moos Marg,
R.C. Church, Colaba,
Mumbai – 400 005
Fax : 91-22-22189568
E-mail : lakhina@iig.iigm.res.in
(Geomagnetism/Atmospheric Sciences)

6. Prof. U.C. Mohanty
Professor & Head,
Centre for Atmospheric Science,
Indian Institute of Technology.
Hauz Khas,
New Delhi – 110 016
Fax : 91-11-26591386, 26862037
E-mail : mohanty@cas.iitd.ernet.in
(Climate Modeling)

7. Prof. K.S. Valdiya
Bhatnagar Research Professor,
Jawaharlal Nehru Centre for
Advanced Scientific Research,
Jakkur P.O.,
Bangalore – 560 064
Fax : 91-80-8462766
E-mail : nehrucen@jncasr.ac.in
(Environmental Geology/Neotectonics)

Managing Editor
Prof. S.L. Srivastava
Coordinator, K. Banerjee Centre of Atmospheric and Ocean Studies, Meghnad Saha
Centre for Space, University of Allahabad, Former Professor & Head, Department
of Physics, University of Allahabad; The National Academy of Sciences, India,
5, Lajpatrai Road, Allahabad – 211 002
Fax : 91-532-2641183
E-mail : nasi@sancharnet.in

EDITORIAL ADVISORY BOARD

1. Prof. Edwin D. Becker
Chief, Nuclear Magnetic Resonance Section,
Building 5, Room 124,
National Institute of Health,
Bethesda,
Maryland 20892-0520, U.S.A.
(Spectroscopy/NMR)

2. Prof. Sir Herman Bondi
Professor,
Churchill College,
Cambridge, CB3 ODS, U.K.
Fax : 01223-336180
(Mathematical Astronomy)

3. Prof. S. Chandrasekhar
Honorary Professor & Formerly Founder Director,
Centre for Liquid Crystal Research,
P.B. No. 1329, Jalahalli,
Bangalore – 560 013
Fax :91-80-8382044
E-mail : clcr@vsnl.com
(Condensed Matter)

4. Prof. S.K. Joshi
Hon. Vikram Sarabhai Professor,
National Physical Laboratory,
Dr. K.S. Krishnan Marg,
New Delhi – 110 012
Fax : 91-11-25726938. 25726952
E-mail : skjoshi@csnpl.ren.nic.in
(Solid State Physics)

5. Prof. M.G.K. Menon
Chairman, Board of Governors of
IIT (Delhi) and IIIT (Allahabad),
K-5 (Rear), Hauz Khas,
New Delhi – 110 016
Fax : 091-11-26510825
E-mail : mgkmenon@ren02.nic.in
(Physics)

6. Prof. A.P. Mitra.
Honorary Scientist of Eminence,
Former Director-General, CSIR and
Secretary to the Govt. of India,
National Physical Laboratory,
Dr. K.S. Krishnan Marg,
New Delhi – 110 016
Fax : 91-11-25752678; 25764189
E-mail : apmitra@doe.ernet.in;
apmitra@ndf.vsnl.net.in
(Ionospheric Physics/Radio Communication/Space Physics/Space Science)

7. Prof. Jai Pal Mittal
Director, Chemistry & Isotope Group,
Bhabha Atomic Research Centre,
Trombay, Mumbai – 400 085;
Mumbai – 400 085;
and Honorary Professor, JNCASR, Bangalore;
Fax : 91-22-25505151, 25505331
E-mail : mittaljp@magnum.barc.ernet.in
(Radiation and Photochemistry/Chemical Dynamics/Laser Chemistry)

8. Prof. C.K.N. Patel
Chairman & CEO,
Pranalytica, Inc.,
1101 Colorado Avenue,
Santa Monica, CA 90401-3009, U.S.A.,
Fax : 310-450171
E-mail : patel@pranalytica.com
(Physics)

9. Dr. B.L.S. Prakasa Rao
Distinguished Scientist,
Indian Statistical Institute,
7, S.J.S. Sansanwal Marg,
New Delhi – 110 016
Fax : 91-11-26856779
E-mail : blsp@isid.ac.in
(Mathematical Statistics)

10. Dr. P. Rama Rao
ISRO Dr. Brahm Prakash Distinguished
Professor, International Advanced Research
Centre for Powder Metallurgy and New
Materials (ARCI),
Balapur P.O.
Hyderabad – 500 005
Fax : 91-40-24441468, 24443168
E-mail : pallerama_rao@yahoo.co.in
(Physical & Mechanical Metallurgy/ Alloy Development)

11. Prof. M.M. Sharma
Kothari Research Professor (Hony.),
JNCASR, Bangalore;
Formerly Professor of Chemical Engineering
& Director, University Deptt. of Chemical Technology,
Matunga,
Mumbai – 400 019
E-mail : mmsharma@bom3.vsnl.net.in
(Mass Transfer with Chemical Reaction/ Catalysis with Ion Exchange Resins)

12. Prof. Govind Swarup
INSA Honorary Scientist,
Ex. Director, NCRA/GMRT,
National Centre for Radio Astrophysics,
Tata Institute of Fundamental Research,
NCRA, Post Bag 3, Ganeshkhind,
Pune – 411 007
Fax : 91-20-5692149/7257
E-mail : gswarup@ncra.tifr.res.in
(Radio Astronomy/Cosmology)

13. Prof. H.C. Khare
(Chief Editor)
Chairman, Board of Governors,
Motilal Nehru National Institute of Technology,
(Deemed University; Formerly Motilal Nehru
Regional Engineering College), Allahabad,
Former Professor of Mathematics,
University of Allahabad;
General Secretary, The National Academy of
Sciences, India,
5, Lajpatrai Road,
Allahabad – 211 002
Fax : 91-532-2641183
E-mail : nasi@sancharnet.in
(Applied Mathematics/Fluid Mechanics/ Magneto-hydrodynamcis/Theoretical Physics)

Regd. No. R.N. 35621/78

CONTENTS

Chemistry

Amino acid selective "unlabeling" : A new tool for structural studies of proteins in solution by NMR

H. S. Atreya, K. V. R. Chary and Girjesh Govil ... 273

Topological modelling of binding affinity of 1-phenyl-3-amino-1,2,3, 4-tetrahydronaphthalenes as ligands for histamine H_1 receptors

Vijay K. Agrawal, Shailja, Sachan, Sanjeev Chaturvedi and Padmakar V. Khadikar ... 283

Vitamin B_{12} model compounds : Synthesis and characterization of trans-azido(pyridine) cobaloximes

N. Ravi Kumar Reddy, D. Sudarshan Reddy, V. Sridhar and S. Satyanarayana ... 297

Synthetic and structural studies of heterocyclic multidentate schiff base and its metal complexes with Co(II), Ni(II), Zn(II) and Cd(II)

R.C. Sharma, Shubhra Singh, Ritika Vats and Sandhya Agarwal ... 309

Mathematics

Surface wave propagation through a cylindrical bore in a micropolar generalized thermoelastic medium without energy dissipation

Rajneesh Kumar and Sunita Deswal ... 315

A special type of topology in the plane

M.P. Chaudhary, Mohammed Abdel Karim and Qays Omari ... 329

A comparative study of the effects of anisotropy, blood flow and evaporation on temperature distribution in three dimensional regions of human skin and subcutaneous tissues with tetrahedral elements

D. S. Pal and Sushma Pal ... 333

Fixed points of mappings satisfying a new condition

Liubomir B. Ćirić ... 349

(Content Continued on p. (i)

Published by Professor H.C. Khare, General Secretary for the National Academy of Sciences, India, Allahabad and printed by National Graphics, Allahabad.
Managing Editor – Professor S.L. Srivastava